

# MEASURING BEARING CURRENTS

Master Thesis  
by

**PAVLIK MARINOV**  
**MOHAMMED MASUDUR RAHMAN**



Department of Energy and Environment  
Division of Electric Power Engineering  
Chalmers University of Technology  
Gothenburg, Sweden

ISSN

Examensarbete

Examiner: Torbjörn Thiringer



Industrial Division  
Prominent Needs Development  
Gothenburg, Sweden  
Supervisors: Olle Bankeström, Göran Lindsten, Linus Svensson



## **Abstract**

This thesis deals with bearing current detection. It focuses on electric motors driven by variable speed converters. Established techniques for bearing current detection were studied and modified to suit the investigated detecting requirement. Sensors with different characteristics were tested. The resulting equipment consisted of a mobile sensor, which allows remote detection of discharges taking place inside the motor bearings. The main benefit of using a remote diagnostic device is the removing the need of direct contact to the investigated object and the possible production process interruption. The new approach for discharge detection was validated performing different tests on motors with different power ratings driven by various frequency converters.

The obtained results confirm the possibility of using a universal sensor on motors in the power range from 5-130 kW. The sensor output data can be combined with the data obtained using other sensors, in order to improve the reliability of the results.

Two different examples of discharge detection and quantifying devices are presented in this thesis. For current detection a Rogowski coil, a coaxial shunt and current probes were used.

An early detection of bearing currents can have a substantial economical effect when used for early diagnostic and problem solving before the machine bearing has been seriously damaged. This means that the potential problem can be detected before any vibration in the bearing housing occurs.

Using advanced calculative methods and additional research, it is believed that the new technique will give satisfactory bearing currents detection.



## Acknowledgement

We would like to gratefully extend our sincere thanks to all the people who gave their time generously to the success of this thesis. Keeping all this in mind, our first and foremost gratefulness goes to Olle Bankeström and Göran Lindsten, our supervisors, for guidance, support, and encouragement. Thank you for providing us the invaluable opportunity of carrying out our master's thesis in SKF under yours supervision.

We would also like to thank to our examiner Torbjörn Thiringer for his inspiration and important tips. Special thanks to you for scheduling the meetings to the success of this thesis. Thanks also to Jörgen Blennew & Robert Karlsson for many useful inputs and discussions concerning the work.

We would also like to thank to SKF NOVA, Mr.Jhon and Mr.Lars for their constant technical support. We would also thanks the rest of the personal in SKF group for their support and for taking the time to answer our questions.

SKF Sverige AB is gratefully acknowledged for the financial support.



# Table of Contents

<b>ABSTRACT</b> .....	III
<b>ACKNOWLEDGEMENT</b> .....	VII
<b>1 INTRODUCTION</b> .....	1
1.1 BACKGROUND AND MOTIVATION .....	1
1.2 AIM OF THE THESIS.....	2
1.3 OVERVIEW OF THE THESIS.....	2
<b>2 LITERATURE REVIEW</b> .....	4
2.1 INTRODUCTION OF BEARING DISCHARGE PHENOMENON .....	4
2.2 SINE WAVE BEARING AND SHAFT CURRENTS .....	4
2.3 INVERTER DRIVEN MOTOR BEARING CURRENT.....	6
2.4 MAIN DAMAGE TYPES OF INDUCTION MOTOR.....	8
2.5 BEARING FAULTS.....	8
2.6 POTENTIAL SOURCES OF SHAFT VOLTAGES .....	9
2.6.1 Electromagnetic induction.....	9
2.6.2 External voltages supplied to the rotor windings .....	10
2.6.3 Magnetic Asymmetries in electrical windings .....	10
2.6.4 Electrostatic voltages .....	11
2.6.5 Other Causes.....	11
2.7 EFFECTS OF SHAFT VOLTAGES ON BEARINGS.....	11
2.7.1 Frosting/Fluting .....	12
2.7.2 Spark Tracks.....	14
2.7.3 Pitting.....	14
2.7.4 Welding.....	14
2.8 BEARINGS AND BEARING LUBRICANTS .....	14
2.9 BEARINGS AND THE EFFECT OF BEARING VOLTAGE AND CURRENT.....	15
<b>3 GENERATING BEARING CURRENTS</b> .....	17
3.1 HOW IS HIGH FREQUENCY BEARING CURRENTS GENERATED .....	17
3.1.1 Small capacitive currents.....	17
3.1.2 Electrical Discharge Machining (EDM) .....	17
3.1.3 High Frequency Circulating Current .....	22
<b>4 MEASUREMENT OF BEARING CURRENTS</b> .....	23
4.1 INTRODUCTION.....	23
4.2 ROGOWSKI COIL TECHNIQUE .....	23
4.2.1 Introduction .....	23
4.2.2 Background.....	24
4.2.3 Principle of Rogowski Coil .....	24
4.2.4 Rogowski coil basic equations .....	25
$Rd = \frac{\pi}{2} \sqrt{\frac{L}{C}}$ (4.9).....	26
4.2.5 Advantages of Rogowski transducers .....	26
4.2.6 Applications.....	26
4.3 CO-AXIAL SHUNT.....	27

4.4 CURRENT TRANSFORMER .....	28
4.5 OSCILLOSCOPE.....	29
<b>5 ANTENNAS .....</b>	<b>30</b>
5.1 INTRODUCTION.....	30
5.2 CHARACTERISTICS OF ANTENNAS .....	30
5.3 INDUCED VOLTAGE IN AN ANTENNA COIL .....	31
5.4 APPLICATIONS .....	32
5.10 ADVANTAGES AND DISADVANTAGES .....	35
<b>6 DESCRIPTION OF THE EXPERIMENTAL MODEL AND MEASUREMENT SETUP .....</b>	<b>36</b>
6.1 EXPERIMENTAL SETUP IN GENERAL.....	36
6.2 INVESTIGATION OF FEW ELEMENTS.....	36
6.3 DESIGN OF THE IMPULSE CIRCUIT FOR THE TEST/SYNTHETIC MOTOR 37	
6.4 ROGOWSKI COIL DESIGN.....	38
6.4.1 Measuring Rogowski coil inductance.....	40
6.4.2 Measuring coil self resonance .....	41
6.4.3 Measuring coil frequency response .....	41
6.5 SLIP RING .....	45
6.5.1 Slip ring investigation .....	45
6.5.2 Slip ring DC test .....	52
6.6 MACHINE SPECIFICATIONS.....	55
6.7 ANTENNA DESIGN.....	55
6.7.1 Antenna Matching .....	56
6.7.2 Building up .....	57
6.7.3 Measuring the Quality Factor (Q) .....	57
6.7.4 Test on a synthetic and a real motor .....	59
<b>7 BEARING CURRENT MEASUREMENTS.....</b>	<b>61</b>
7.1 BEARING CURRENT MEASUREMENT EQUIPMENT.....	61
7.2 SYNTHETIC TEST CONFIGURATION.....	61
7.2.1 Measuring system.....	62
7.2.2 Measuring Procedure.....	63
7.2.3 Obtained Results .....	63
7.3 7.5kW MOTOR TEST CONFIGURATION.....	65
7.3.1 Measuring Procedure.....	65
7.3.2 Obtained Results .....	66
7.4 CLOSED LOOP ANTENNA .....	69
7.4.1 Synthetic test configuration.....	69
7.4.2 7.5kW motor test configuration .....	73
7.5 MEASUREMENTS USING TEKTRONIX TDS 544A.....	78
7.5.1 Dipole antenna.....	78
7.5.2 7.5kW motor with Pearson current probe .....	79
7.5.3 Closed loop antenna .....	80
7.5.4 Fan motor ASEA MT100L28-2 3kW investigation .....	82
7.5.5 Fan motor ASEA MT100L28-2 3kW investigation with 16Mhz DA.....	89
7.5.6 7.5kW motor driven by Scandialogic SL 5500 frequency converter investigation using 16Mhz DA.....	93

7.5.7	7.5kW motor driven by ABB 5.5kW Sami GS ACS501 frequency converter investigation using 16Mhz DA.....	98
7.5.8	132kW motor driven by Siemens frequency converter investigation using 16Mhz DA 100	
<b>7.6 USING AT THE ROGOWSKI COIL CWT1 IN BEARING CURRENTS</b>		
<b>DETECTION.....</b>		<b>105</b>
7.6.1	Synthetic test configuration.....	105
7.6.2	7.5kW motor driven by Danffos converter .....	107
7.6.2.1	CWT1 around the power cable.....	107
7.6.2.2	CWT1 around the motor base.....	109
7.6.3	132kW motor driven by Siemens converter.....	114
7.6.3.1	CWT1 placed around the motor shaft.....	114
7.6.3.2	CWT1 placed around the motor power cables.....	119
7.7	<b>SUMMARY.....</b>	<b>121</b>
<b>8</b>	<b>SUGGESTED SET-UP .....</b>	<b>125</b>
<b>9</b>	<b>CHARACTERIZATION .....</b>	<b>126</b>
<b>10</b>	<b>CONCLUSION .....</b>	<b>129</b>
<b>11</b>	<b>FUTURE WORK.....</b>	<b>130</b>
<b>REFERENCES .....</b>		<b>131</b>
<b>LIST OF SYMBOLS .....</b>		<b>135</b>



# 1 INTRODUCTION

## 1.1 Background and Motivation

Bearing currents, or shaft currents, which usually flow from the shaft of an electric machine through its bearings, have existed ever since the invention of electric machines [34]. During recent years, an increase in bearing failures relatively soon after start-up, within one to six months has been noted in Adjustable Speed Drive (Fast Switching IGBT-inverter)-fed electric motors [2]. The recent advance in power electronics has widened the scope of application of induction motors dramatically. In particular, PWM inverters with their high switching frequencies have made it possible for variable frequency drive systems to possess good spectra, low acoustics noise and more efficient electromagnetic power conversion. PWM inverters have been associated with the generation of induction motor bearing currents [34].

ASDs / VFDs regulate the speed of a motor by converting sinusoidal line AC voltage to DC voltage, then back to a pulse width modulated (PWM) AC voltage of variable frequency. The switching frequency ranges 2 kHz to 20 kHz and is referred to as the carrier frequency, in principle creating a pulse train having such a frequency. The ratio of changes of the  $dv/dt$  creates a discharge of the parasitic capacitance located between the motor stator and the rotor, which induces a voltage on the rotor shaft. This voltage is referred to as common mode voltage/shaft voltage. If this voltage reaches a sufficient level, it can discharge to ground through the bearings. Currents that finds their way to ground through the motor bearings in this manner is called "bearing current". It has been found that the converter itself is a common mode voltage generator [11]. The common mode voltage is usually at a high voltage level and with a frequency equal to inverter switching frequency [11].

The frequencies of inverter-induced bearing currents are much higher than  $f = 50/60$  Hz, ranging from several 100 kHz of circulating bearing currents and bearing currents due to rotor ground currents to several MHz for EDM (Electric Discharge Machining) and  $dv/dt$  bearing currents. The high  $dv/dt$  common mode voltage excitation and the parasitic coupling capacitance in a drive system were found to account for the generation of these bearing currents [35].

## 1.2 Aim of the thesis

The primary goal of the thesis is understanding the discharging phenomenon of bearing currents and investigate the discharge characteristics, moreover, to create a roadmap of possible power electronics solutions in the test equipment and in a real application and finally to suggest a function for as instrument for the finding and the characterization of bearing currents for a machine. The possibility for remote sensing is highly desirable.

## 1.3 Overview of the Thesis

The contents are divided into 11 chapters. Besides this introductory chapter the following chapters are presented:

**Chapter 2:** This chapter contains a review and evaluation of related work on bearing current. It also describes the main damage types that occur in bearings and also describes the different kinds of shaft voltages and the effects of shaft voltages on bearing.

**Chapter 3:** This chapter describes how the high frequency bearing currents are generated in adjustable speed drive systems.

**Chapter 4:** Describes the commonly used techniques and devices that are used for detection and measurement of bearing currents.

**Chapter 5:** This chapter presents the possibilities of an antenna as a high frequency bearing discharge current detector and includes the principle of operation.

**Chapter 6:** One of the most commonly used methods for measuring shaft voltages is the Rogowski Coil Technique. In this chapter the design and calibration methods of a Rogowski coil. It also deals with antenna design consideration, construction and calibration.

**Chapter 7:** Results from experimental verifications of the motor bearing currents including analysis and summery are presented.

**Chapter 8:** Based on the practical experience, gained during the performed tests, some practical advices are given. It will help the technical staff to apply the antenna method in the field of bearing current measurements and early fault detection.

**Chapter 9:** This chapter deals with the possibility for EDM currents detection and characterization using the discovered antenna method. Two possible circuits for this purpose are proposed. They can be software or hardware implemented.

**Chapter 10 & 11:** Contain the conclusions of this work and proposal for future work.

## 2 LITERATURE REVIEW

### 2.1 Introduction of Bearing Discharge Phenomenon

Some new drive installations can have a motor bearing failure only a few months after start-up. This can be caused by bearing currents induced in the motor shaft and discharged over the bearings. Modern motor design and manufacturing practices have nearly eliminated bearing failures under normal circumstances, but the rapid switching in modern drive systems generate high frequency voltages that can damage the bearings. When the resulting currents find the path to earth over the bearings, metal transfer between the ball and races occurs. This is known as electric discharge machining or EDM.

### 2.2 Sine wave bearing and shaft currents

Electric motor bearing and shaft currents are not new; in fact, they have been around since electric motors were invented. The most common underlying causes of unwanted bearing and shaft currents for sine wave driven motors is a lack of motor symmetry. In 1927 one Electric Journal, said of the subject: "If it were possible to design a perfectly balanced and symmetrical machine, both theory and practice indicate that no bearing current could exist". The two primary causes of shaft and bearing currents in sine wave driven motors are

- 1) Homo polar flux, i.e. flux flowing down the center of the motor shaft and
- 2) Alternating flux linking the motor shaft.

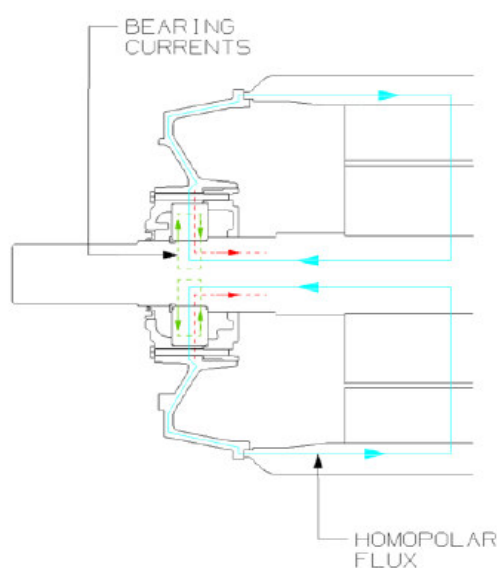


Figure 2.1: Homo polar fluxes around stator, rotor and shaft [12]



The resulting current is not localized within the bearing. Its driving voltage can be measured on motors with at least one bearing that is electrically insulated from the motor frame. When both bearings in the current path are conducting, the impedance of this path is small; therefore, an axial shaft voltage as little as 500milli volts rms can create a current of up to 20 amps rms through the bearing and can cause significant bearing damage, particularly in larger machines. Remedial action entails employing an electrical insulator outside the bearing outer race to break the current path.

Bearing currents in sine wave driven motors can be reduced or eliminated through current or flux barriers. This is because the bearing currents are internally sourced. Note that these types of bearing currents are not dependent upon system installation issues, such as grounding [15].

### 2.3 Inverter driven motor bearing current

The most common form of inverter for variable speed drives on the market place is the voltage source PWM inverter. In order to achieve the desired variable speed output from a motor, power electronics is used to rectify the incoming mains supply to a smooth dc voltage in an intermediate link, which will incorporate some capacitive energy storage. The inverter will then create an alternating voltage of a desired fundamental frequency.

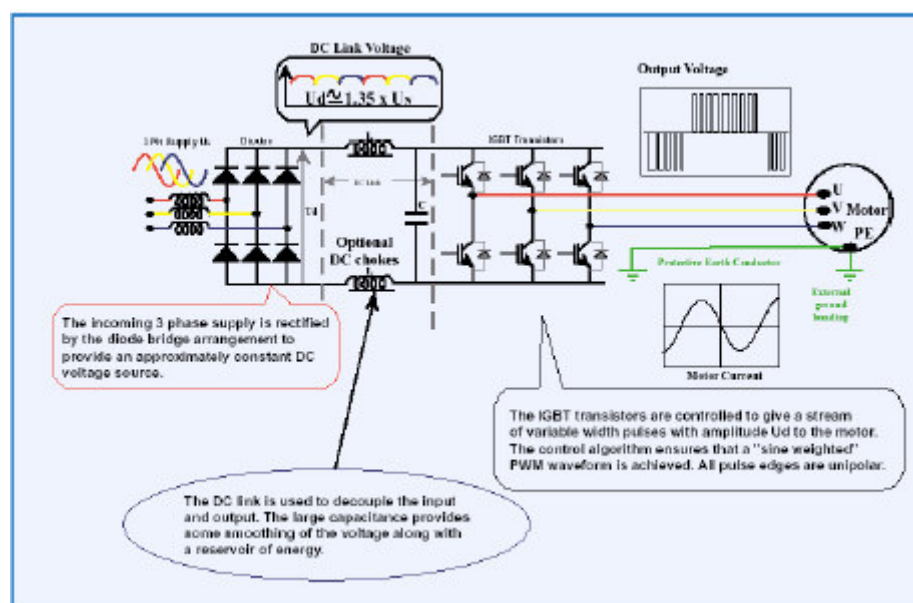


Figure 2.4: The basic elements of voltage source inverter [12]

The output voltage is generated as a pulse string, typically as shown in figure 2.5. The magnitude of the dc link voltage will normally lie between 135% and 140% of the incoming ac rms voltage, and this value is applied constantly, irrespective of the output voltage fundamental magnitude.

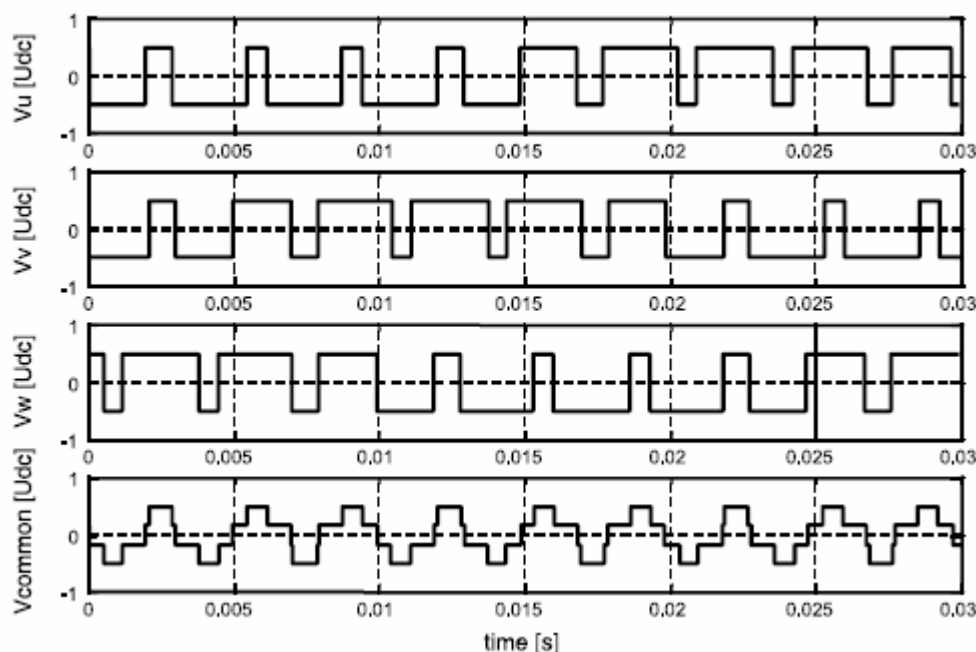


Figure 2.5: Three phase voltages of a PWM power supply & neutral point voltage in a modern AC drives system. The neutral point voltage is clearly not zero and its presence can be defined as common mode voltage [9].

With PWM inverter-driven motors, both internally and externally sourced bearing currents may exist. The internally sourced currents are the same as those discussed for sine wave motors above. The externally sourced currents are a result of the voltage wave shape that is applied to the motor by the inverter.

In a sinusoidal network supply, the vector sum of the three phases is usually zero. When an inverter synthesizes a voltage there are a limited number of potential switch positions and the switching pattern of the semiconductors is governed by a need to maintain acceptable switch positions. This leads to a non-zero neutral at the inverter output, which can be considered as a common-mode voltage source.

This voltage can be measured by creating an artificial Y connection at the motor terminals using three large resistors (Mega ohms). The voltage from the center of this Y to the motor ground is the common mode voltage.

Figure 2.5 shows the inputs at the windings of a three-phase motor relative to earth ( $V_u$ ,  $V_v$ ,  $V_w$ ). The common-mode voltage is equal to  $1/3(V_u+V_v+V_w)$ , assuming no

coupling capacitance. This voltage is proportional in magnitude to the dc link voltage and has a frequency equal to the inverter carrier frequency. When designing an inverter, the aim is generally to use the highest practical switching rate, which will have the benefits of lower additional losses of the motor and lower audible noise. The high dv/dt creates frequency content in the common mode voltage in the MHz range. The power switching devices have changed from thyristors to GTOs (gate-turn-off thyristors) and lately to bipolar transistors through to the latest high-performance IGBTs, which dominate the VSD market today. IGBTs are now using switching frequencies ranging from, say, 2 kHz in large drives and to around 20 kHz in smaller ratings. Ten years ago power transistor switching was measured in hundreds rather than thousands of hertz [15].

## 2.4 Main damage types of induction motor

The reason for motor damage can be an ambient factor (dust, temperature, vibration), defective manufacture or design, defective installation, defective use or normal deterioration due to abrasion, erosion and aging. In most cases there are several factors that lead to failure. The most usual direct reason for damage is failure of the bearing or windings but the primary reason is usually an ambient factor such as overheating caused by dust. Some results from the research by Albrecht (1986), where reasons for motor damage were studied, are presented in Table 2.1

Table 2.1 Types of damage

Cause of Damage	Percent (%)
Overheating	25
Ageing of windings	5
Earth fault	10
Defective bearing	12
Moisture	17
Oil, grease	20
Chemicals	1
Particles, dust	5
Other	5

## 2.5 Bearing faults

Electric machines are the key components of numerous industrial and transportation equipment. Bearing failure is one of the most common types of electric machine

failures. Early detection of these faults allows services to be performed during planned downtimes rather than costly emergencies. Bearing faults such as outer race, inner race, ball defect and train defect cause machine vibration. The vibration caused by the bearing defects results in air gap eccentricity. Oscillations in air gap length, in turn cause variation in flux density. The variations in flux density affect the machine inductances, which produce harmonics of the stator current.

Table-2.2 Fault statistics [12]

Bearings	41%
Stator	37%
Rotor	10%
Other	12%

The major source is sleeve bearings. Big motors are equipped with sleeve bearings due to the high load carrying capacity of these bearings. The sleeve bearings used in electric motors are lubricated with pressured oil. The primary faults of the sleeve bearing produce very low vibration levels because of the pressured oil between bearing surfaces.

## 2.6 Potential sources of Shaft Voltages

Shaft voltages arise from various sources in electrical machines, such as winding faults, unbalanced supplies, electrostatic effects, magnetized shaft or other machine members, and asymmetries of the magnetic field. With respect to [35], there are four distinct potential sources of shaft voltages. Each case will be reviewed separately and carefully in the section below.

### 2.6.1 Electromagnetic induction

Shaft voltages are generated by rotating a residual magnetic source in a magnetic housing or vice versa, an action similar to that of an electric generator [35]. According to Costello, the main difference is that an electric machine has armature windings in order to carry the induced current, whereas the mechanical machine's "secondary" winding is the bearings, shaft, seal, etc. The following factors have to be present for the mechanism to generate shaft voltages:

- (i) A source of high residual magnetism – possibly the rotor, bearings, casings, etc.
- (ii) High relative surface velocity (such as that found in turbo-machinery)
- (iii) A closed, low-reluctance magnetic circuit
- (iv) Very small clearances across which the voltage can discharge.

## 2.6.2 External voltages supplied to the rotor windings

This is largely related to the excitation system of electrical machine. The shaft voltage present is either a rectified or primarily dc signal. The pulses of the rectifier are often seen in the shaft voltages [35]. Other possible sources include voltage source or rotor winding insulation asymmetries, and active rotor windings. Consequently, external voltages raise the shaft to a potential according to the insulation capacitance and resistance of the source, the winding and the shaft versus ground. As a result, the voltage between the shaft and the bearing will stress the oil film. In the case of breakdown, electric discharge will occur and pitting will damage the surfaces of bearings and seals.

## 2.6.3 Magnetic Asymmetries in electrical windings

Even on pure sinusoidal supplies, asymmetries in the motor construction could cause various stray fluxes to be set up. These in turn manifest themselves in the form of shaft voltages and if these are above the natural insulation levels of the bearings, circulating current will exist.

### Ring flux linking shaft

The linkage of the alternating flux with the shaft is the most important cause of bearing currents. The flux flows perpendicular to the axis of the shaft and pulsates in the stator and rotor cores. It results from asymmetry in the magnetic circuit of the machine. The asymmetries arise from the design and construction of the machine and from inaccurate alignment.

Normally the flux from each pole crosses the air-gap and if the magnetic path is symmetrical, it divides equally, half clockwise and half anticlockwise. However, if there is a difference in the reluctance of the core in one direction compared with the other, there will be an unequal division of the flux and a net flux linking with the circuit consisting of shaft, bearings and frame will exist.

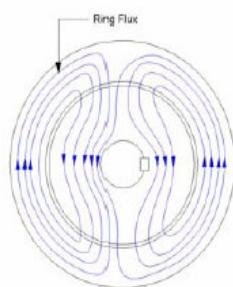


Figure 2.6a-End view depicting asymmetric field [12]

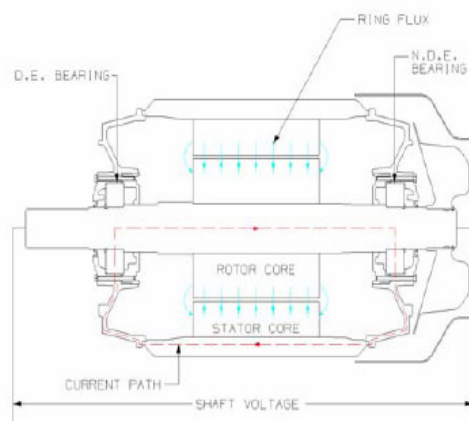


Figure 2.6b-Showing shaft current and voltages due to asymmetric magnetic field [12]

The ring flux is alternating and as such it establishes a potential difference between the ends of the shaft as shown in figure 2.6b. If this potential difference is large enough to create an electrical breakdown in the bearing grease lubricant film, the thickness of which usually ranges from 1  $\mu\text{m}$  to 20  $\mu\text{m}$ , arcing occurs between the races and the rolling element. The resulting bearing current will cause bearing failure. In addition, experience has shown that dirt, microscopic metallic particles and irregular film thickness permit lubricant film to be bridged. Under this condition, the impedance of the bearing circuit is so low that small shaft voltages may cause substantial bearing currents [12].

#### **2.6.4 Electrostatic voltages**

These are not due to the basic design of the machine but rather to do with special circumstances, for instance, low humidity environments, or the nature of application, e.g. belt and pulley driven loads.

The shaft voltage continuous to build up until a discharged occurs through the bearings. Sometimes all that is needed is a little friction of a belt or pulley to set up electrostatic charges. Voltages originating from such sources are not usually a major problem.

#### **2.6.5 Other Causes**

Accidental or irregular, contact of a part of the rotor winding to the rotor core can lead to stray currents through the shaft and bearings. This may result from damage to the insulation in an insulated rotor or intermittent contact of the bar in an un-insulated rotor, which is extremely rare in the die-cast rotor.

### **2.7 Effects of Shaft Voltages on Bearings**

During the past 20 years, industrial processes have experienced dramatic changes with advances in adjustable speed drive (ASD) technology. The introduction of fast switching semiconductor devices, such as the insulated gate bipolar transistors (IGBT), into pulse width modulation (PWM) inverter manufacturing has further improved the performance of PWM ASDs. However, problems related to shaft voltage and bearing currents have increased due to the inherently generated common-mode voltage, high-switching frequency, and high  $dv/dt$  created by fast switching [37].

As previously mentioned the best method for determining the presence and severity of shaft currents is probably through inspection of the affected damaged parts [35]. Often, however, bearings are replaced during normal maintenance procedures and the back laying cause of the problem is not always detected. As a result, elimination of the failure source is more difficult since the equipment is back in service. It is therefore essential that damaged parts can be inspected and possible voltage sources identified while the machine is shut down and disassembled.

### 2.7.1 Frosting/Fluting

This is, by far, the most common type of damage caused by shaft currents. Parts affected are bearings, seals, thrust collars, journals, and gears. Whether the damage takes the form of frosting or fluting depends on the nature of the motor. Deterioration will appear as frosting on the bearing race surface for motors operating over a wide speed range, and as fluting (grooves) in race for motors running at relatively constant speeds [37].

The appearance of frosting is that of a sandblasted surface, and if the entire available surface is affected, the damage is not noticeable to the naked eye due to its satin like appearance. When viewed under a microscope, however, the frosted surface is seen as very small individual “craters”. The bottom of the craters is round and shiny, a sign of the melting that has occurred. Frosting may sometimes look similar to chemical attacks but the damage is normally more severe [35].

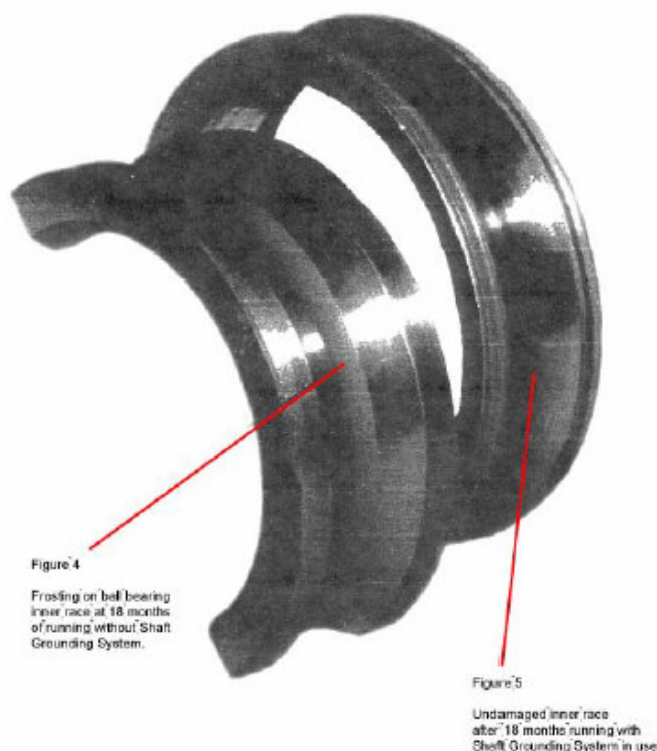


Figure 2.7: Illustration of Frosting [5].

Figure 2.7 gives an illustration of frosting. Fluting is often associated with continuous manufacturing processes that are operated at the same speed for several hours at a time. EDM currents cause permanent microscopic marks in the bearing race with marking interval evenly spaced according to the ball spacing. The initial marks cause slight vibration, which is too small to be picked up by vibration-analysis equipment. Continued deterioration usually occurs at the bottom of the original race markings. This is why fluting marks occur in the same place on the bearing-race load zone and why many bearing fluting failures appear the same [38]. An example of fluting damage is shown in figure 2.8.

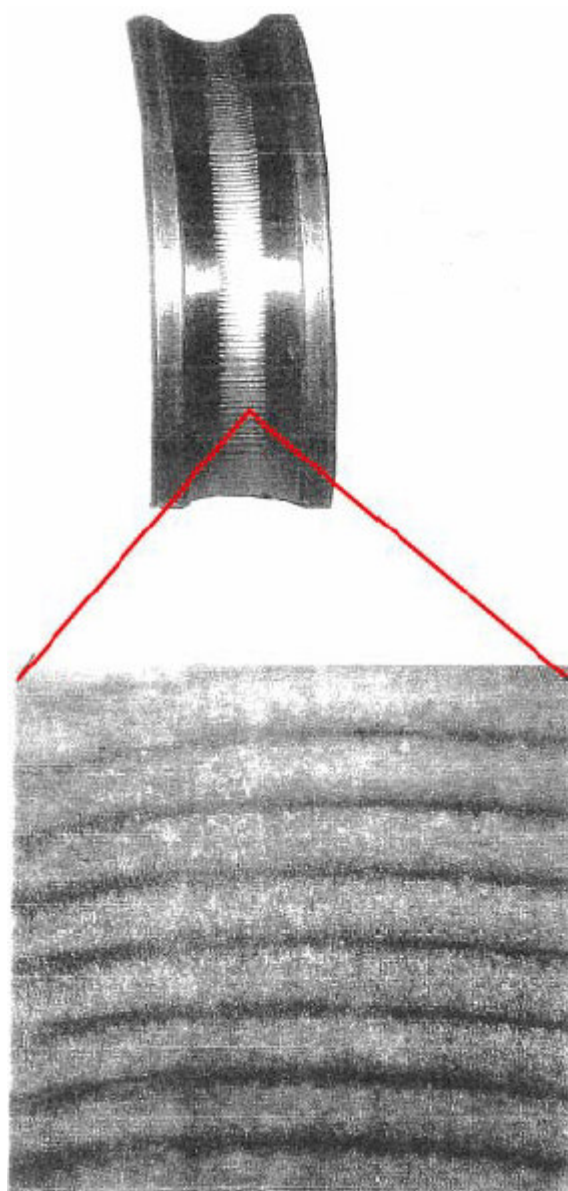


Figure 2.8: Micrograph showing in detail of bearing fluting [5].

### 2.7.2 Spark Tracks

Initially, these tracks can appear very similar to that of scratches in the surface from foreign particles in the lubrication or seal oil. However, a closer examination will often reveal that they are very irregular in nature and are often not in a level position to the direction of rotation. Under magnification, the bottom of the tracks is sometimes melted, and the corners are sharp. A dirt particle, on the other hand, would normally leave rounded corners. The dept of the spark track is generally the same over its entire surface [35].

### 2.7.3 Pitting

This type of damage is similar to frosting but it is generally much larger in size since its source is extremely powerful. It often occurs in gear teeth or on the backs of bearings or seals and sometimes between frame splits. As opposed to frosting, where the entire surface might be affected, pitting occurs more randomly, and it is sometimes possible to count the number of discharges [35].

### 2.7.4 Welding

Sometimes, welding of parts such as splits, bearing pads, and seals may occur due to a great amount of current passing through them. They are easily evident to the naked eye as spot-welded marks and, quite often, have to be separated by sledgehammers or other mechanical means [35].

## 2.8 Bearings and Bearing Lubricants

Induction motors typically have two bearings, which support and allow low-friction motion of the inner rotating shaft within the fixed outer stator housing. The normal bearing arrangement includes rolling elements, a bearing retainer to keep them in place, a bearing race that provides smooth inner and outer load surfaces over which the bearings roll, lubricant to reduce friction and aid cooling and an optional seal to keep out contaminants. The most common types of bearings used in low voltage standard ac induction motor are

- \* Ball
- \* Roller

The choice of bearings depends upon the application: whether torque transmission is through direct or indirect coupling, the external loading, mounting arrangement, and environmental and electrical conditions.

The bearings need suitable lubricants for their smooth operation. The main duties of the bearing lubricants are:

- \* to reduce friction between the various elements of the bearing
- \* to assist in dissipating heat generated within the bearings

\* to protect the highly polished working surface of the bearings from contaminants such as dust and moisture.

Bearing lubricants can also be used to block the path of damaging high frequency currents, or, if conductive grease is used, to provide a low impedance path to the common-mode currents. Conductive greases tend to be less effective lubricants, and must therefore be used with care.

Bearings may be lubricated by grease or oil, with the choice of lubricant usually being decided upon by operating conditions and bearing design.

Grease lubricants are widely used in low-voltage motors. It is usual to employ grease where temperatures are not excessive and the sealing arrangements do not allow successful lubrication by oil. Whatever type of grease that is used, it must not have a tendency to separate under the operating conditions.

Oil is generally considered to be a more effective lubricant and is preferred if the operating temperature or the surface speed is high. With the exception of motors for some special applications e.g. very high-speed operation, oil lubricants are very rarely used in low-voltage motors.

## **2.9 Bearings and the effect of bearing voltage and current**

Bearing operates with a thin film of lubricant (typically 1  $\mu\text{m}$ -20  $\mu\text{m}$ ) between the moving surfaces. The lubricant is generally an electrical insulator and the breakdown voltage is typically is the order of 3V-50V. If the current flows in the bearing either because the lubricant momentarily is bridged or because electrical breakdown occurs, its magnitude depends on the source impedance of the voltage source. It should be noted that one of the major causes of bearing currents results from voltage pulse overshoots created by the fast-switching IGBT (insulated gate bipolar transistor) in the ASD. Other sources of shaft voltage include non-symmetry of the motor's magnetic circuit, supply unbalances, transient conditions and etc. Any of these conditions can occur independently or simultaneously to create bearing currents. Shaft voltage accumulates on the rotor until it exceeds the dielectric capacity of the motor bearing lubricant, then the voltage discharges through the bearing. After the discharge, the voltage again accumulates on the shaft and the cycle repeats itself. This random and frequent discharging has an electric discharge machining (EDM) effect, causing pitting of the bearing's rolling elements and raceways. The principal effect of bearing current is the damage caused by arcing across the bearing surface. An electric current passes through the surfaces in contact, the flow is concentrated through the

contacting points and the local current density can be extremely high. Usually the first symptom of bearing current damage is the audible noise created by the rolling elements riding over these pits in the bearing race. Over time this deterioration causes a groove pattern in the bearing race called "fluting" which is a sign that the bearing has sustained severe damage.

## **3 Generating Bearing Currents**

### **3.1 How is high frequency bearing currents generated**

The source of bearing currents is the voltage that is induced over the bearing. In large motors, above 132kW, high frequency bearing currents are induced in the motor shaft due to asymmetrical flux distribution in the motor [9]. Voltage pulses fed by the inverter contain high frequencies and the leakage capacitances of the motor winding provide paths for currents to flow to the earth. This induces a voltage between the shaft ends. If the induced voltage is high enough to overcome the impedance of the oil film of the bearings, a circulating type of high frequency bearing current occurs.

#### **3.1.1 Small capacitive currents**

The high  $dv/dt$  causes along with the capacities between stator lamination, winding, rotor and the bearing capacity, a capacitive current flow of the range of 5-200 mA. These currents are so small that they are usually considered to be harmless [39].

In small motors, due to relative sizes of the internal stray capacitances, the internal division of the common mode voltage may be such that it causes shaft voltages high enough to create high frequency bearing current pulses [9].

#### **3.1.2 Electrical Discharge Machining (EDM)**

As the rotor voltage is developed, any bearing currents are limited by the effective bearing impedance. This is a complex value depending on a number of factors, including the type of lubricant, the speed of rotation and bearing size/design etc. Generally bearing impedance (resistive) is low at low speed and high (capacitive) at high speed. As the speed increases, the ball rides on the thickest film of lubricant, which forms a barrier between the race and the ball except for instantaneous roughness point contact. The grease or oil film acts as a dielectric that is charged by the rotor voltage. When the voltage exceeds the film breakdown voltage or the rolling element connects with the race, a destructive high frequency currents discharge occurs, thus pitting the bearing. This is often referred to as electrical discharge machining (EDM).

When high-resistance grease is used and the bearings are floating on the oil film, the equivalent circuit characteristic changes from a resistor to a capacitor. Imperfections on the bearing surfaces occasionally puncture the oil film and discharge the rotor. The better quality of the bearing, the less often these low level discharges occur, allowing the rotor to charge for longer periods of time and hence attain higher voltage levels. Typically, high quality bearings charge as much as 80% of the time due to a uniform oil film. Low quality bearings charge significantly less due to frequent metal-to-metal

contact. If the rotor voltage exceeds the threshold voltage ( $V_{th}$ ) of the oil film between the rollers and the races of the bearing, the oil film's dielectric strength is exceeded and destructive EDM currents and arching occur [13].

The following illustrations show step by step what is happen during an EDM cycle.

The electrical field is strongest at the point where the distance between the race and the roller is least, such as the high point shown. Normally, at this point the voltage still increases, but the current is zero.

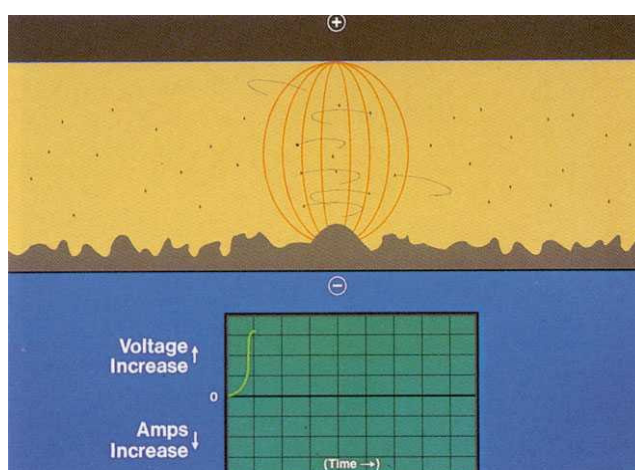


Fig.3.1 Electrical field distribution

As the number of charged particles increases, the insulating properties of the oil begin to decrease along a narrow channel centered in the strongest part of the field. Voltage has reached its peak, but the current is still zero.

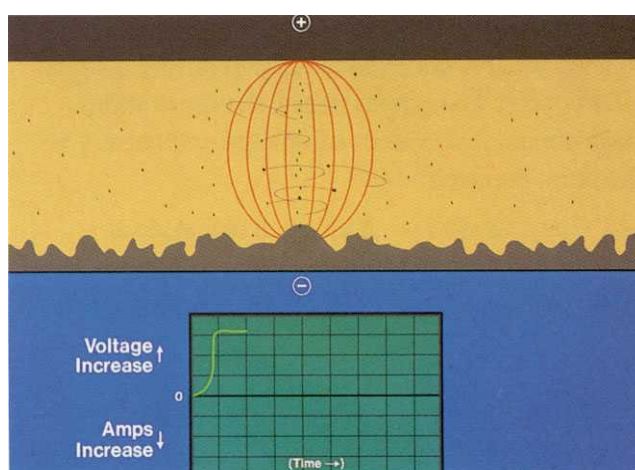


Fig.3.2 The charged particles concentration increases

A current is established, as the oil becomes less of an insulator. The voltage begins to decrease.

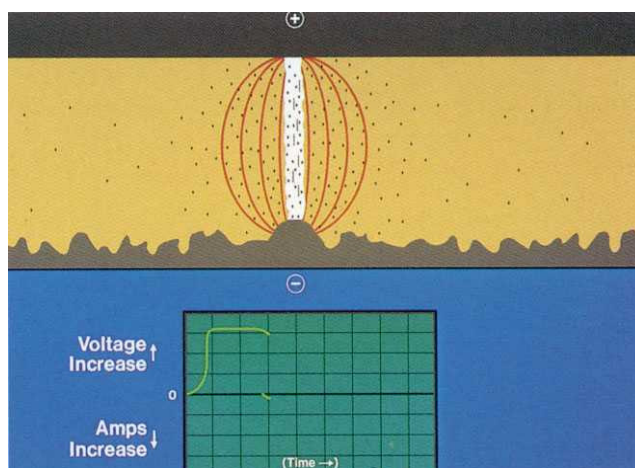


Fig.3.3 Voltage begins to decrease, as the oil becomes less of an insulator and current start flowing.

As the current increases, heat builds up very fast, and the voltage continues to drop. The heat vaporizes some of the fluid, and a discharge channel begins to form between the race and the roller.

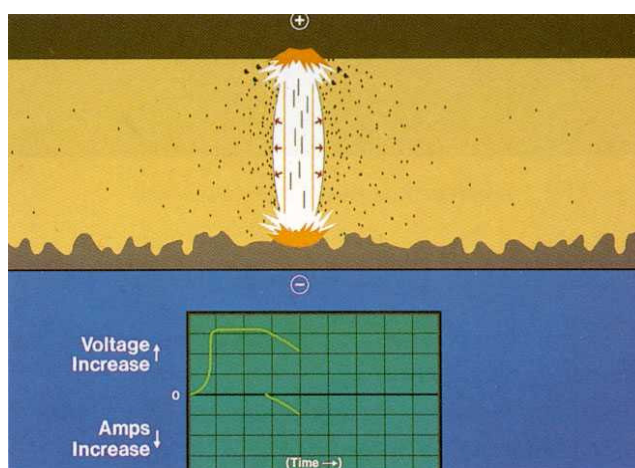


Fig.3.4 A discharge channel begins to form between the race and the roller

A vapour bubble tries to expand, but its expansion is limited by a presence of around towards the discharge channel. The extremely high electro-magnetic field that has built up attracts these ions. Current continues to rise, voltage drops.

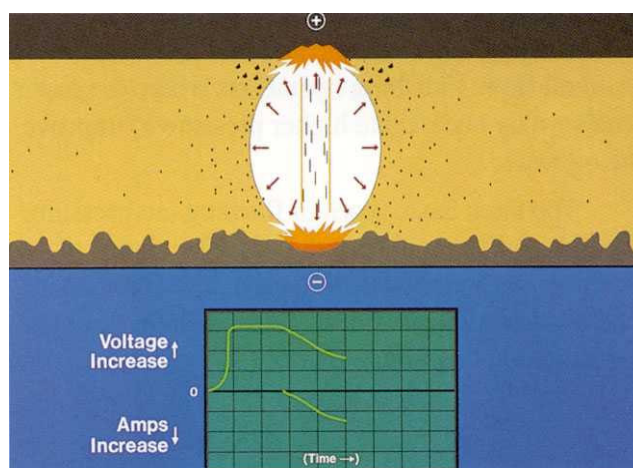


Fig.3.5 Current continue to rise and voltage drops

After certain amount of time, current and voltage have stabilized, heat and pressure within the vapour bubble have reached their maximum, and some metal is being melted. The layer of metal directly under the discharge column is in molten state, but is held in place by the pressure of the vapour bubble. The discharge channel consists now of a superheated plasma made up of vaporized metal, dielectric oil, and carbon with at high current passing through it.

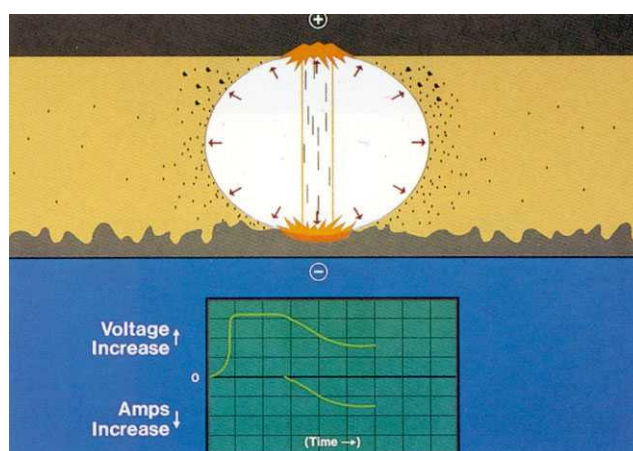


Fig.3.6 The discharge channel with high current passing through it

After a while, the current and voltage drop to zero. The temperature decreases rapidly, collapsing the vapor bubble and causing the molten metal to be expelled from the race and roller surface.

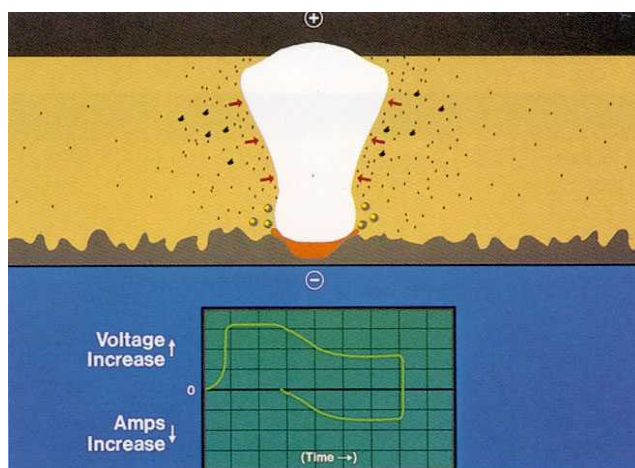


Fig.3.7 The voltage & current drops

Fresh dielectric fluid changes the polluted one due to the difference in the races and rollers speed, flushing the conductive particles away and quenching the surface of the race. The remained molten metal solidifies and form new layer.

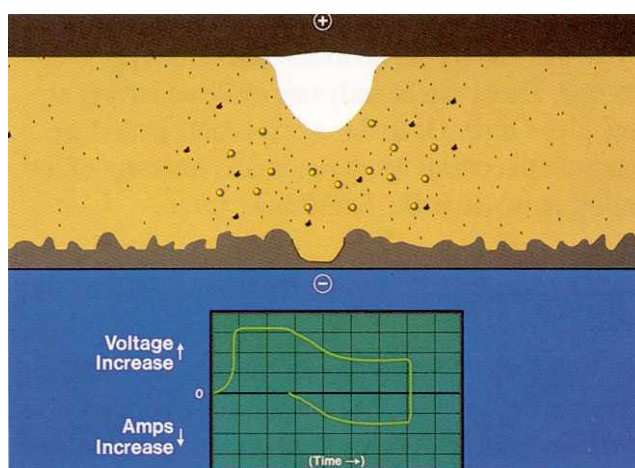


Fig.3.8 Molten metal solidifies

The extracted metal form tiny spheres dispersed in the dielectric oil. The remaining vapor rises to the surface. Without a sufficient off time, conductive particles would collect making the spark unstable.

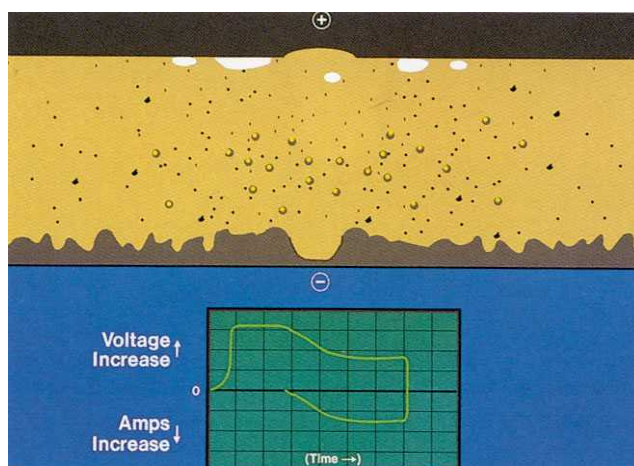


Fig.3.9 The extracted metal dispersed in the dielectric oil.

This sequence is believed to happen 500 times per second in most of the bearings installed in frequency converter driven motors.

[Courtesy EDM Tech. Manual, Poco graphite Inc.][14]

### 3.1.3 High Frequency Circulating Current

A typical three-phase sinusoidal power source, under normal operating circumstances, is balanced and symmetrical. That is, the vector sum of the three phase voltages always equals zero. Thus it is normal that the “neutral” is at zero volts with respect to the system safety ground of the particular installation. In fact, if the power supply is WYE connected, the neutral voltage can be easily measured. This is not the case with any PWM solid state “switched” three-phase power supply. While the voltages may be balanced in peak amplitude, it is impossible to achieve perfect balance between phases instantaneously, when pulses of different widths are produced. The neutral voltage is clearly not zero and its presence can be defined as a common mode voltage (CMV) source. Sometimes called a zero-sequence voltage, it has a frequency equal to the inverter switching frequency. This results in a circulating high frequency flux in the stator core around the rotor shaft. The flux caused by these common-mode currents induces current to flow axially along the rotor, through the motor bearing and back through the other bearing. This is the dominant bearing current.

---

## 4 Measurement of Bearing Currents

### 4.1 Introduction

It is impossible to measure bearing currents directly from a standard motor. If high frequency bearing currents are suspected, field measurements can be taken to verify the existence of suspected current loops. Measuring equipment need to have a wide bandwidth. The current may flow in unusual places, such as rotating shafts. Thus, special equipments are needed to measure. There are three principle methods of current measurement in widespread use: Rogowski Coil, Co-axial shunt and current transformer. Of these, the Rogowski coil is probably the most common for measurement of bearing current, that's why it has been described more in detail in this thesis.

### 4.2 Rogowski Coil Technique

#### 4.2.1 Introduction

Rogowski transducers are useful for measuring currents in excess of several hundred amps and currents, which have significant high frequency components.

A Rogowski current transducer is used for measuring and detecting electric current. It provides an output voltage, which is proportional to current (e.g. 1mV/A). It tracks the current as it changes with time and therefore it can reproduce the current waveform on any type of data recorder such as a digital multimeter, oscilloscope, transient recorder etc.

The coil is wound on a thin plastic tube of circular cross section and surrounded by insulation. It is looped around the conductor or device carrying the current to be measured. One end of the coil is permanently attached to the connecting cable. The other end is free and is normally inserted into a socket adjacent to the cable connection.

The coil is flexible and therefore it can be inserted between closely mounted conductors or devices where access is restricted. The loop does not need to be circular and the current does not need to be centrally situated or evenly distributed within the loop.



Figure: 4.1 Rogowski Transducer and integrator unit [44]

## 4.2.2 Background

In 1887, Professor Chattock of Bristol University used a long, flexible coil of wire as a magnetic potentiometer and made magnetic reluctance measurements in iron circuits to investigate ‘the more satisfactory designing of dynamos’. In 1912, Rogowski and Steinhaus also described the technique. They were also interested in measuring magnetic potentials. They described a large number of ingenious experiments to test that their coil was providing reliable measurements. Since then, many other authors have subsequently described applications of Rogowski coils for current measurement.

## 4.2.3 Principle of Rogowski Coil

An air-cored coil is placed round the conductor in a toroidal fashion so that the alternating magnetic field produced by the current induces a voltage in the coil. The coil is effectively a mutual inductance coupled to the conductor being measured and the voltage output is proportional to the rate of change of current. To complete the transducer this voltage is integrated electronically to provide an output that reproduces the current waveform. This combination of coil and integrator provides a system where the output is independent of frequency, which has an accurate phase response and which can measure complex current waveforms. The output from the integrator can be used with any form of electronic indicating device such as a voltmeter, oscilloscope, protection system or metering equipment.

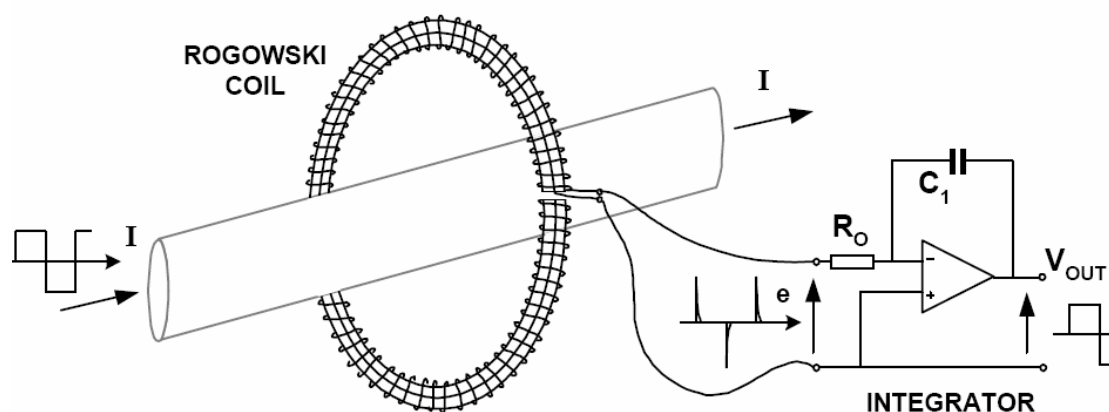


Fig. 4.2 Arrangement of coil and integrator [16]

The coil is uniformly wound with  $N$  turns/m on a non-magnetic former of constant cross section area  $A$  m<sup>2</sup>. If formed into a closed loop then the voltage  $e$  induced in the coil is given by the equation

$$e = \mu_0 NA \frac{dI}{dt} = H \frac{dI}{dt} \quad (4.1)$$

Where  $H$  (Vs/A) is the coil sensitivity and  $I$  is the current to be measured passing through the loop. The loop does not need to be circular and  $e$  is independent of the current position in the loop. To reproduce the current waveform as a measurement signal which can be displayed on an oscilloscope or quantified using a DVM, all that is required is means for accurately integrating the coil voltage, such that

$$V_{out} = \frac{1}{T_i} \int e \cdot dt = R_d I \quad (4.2)$$

Where  $T_i = R_0 C_1$  and  $R_d = \frac{H}{T_i}$  is the transducer sensitivity in  $\frac{mV}{A}$

#### 4.2.4 Rogowski coil basic equations

- The bandwidth  $f_b$  of the coil can be expressed as:

$$f_b = \frac{1}{4\sqrt{LC}} \quad [24] \quad (4.3)$$

- Self resonance

$$f_{res} = \frac{1}{2\pi\sqrt{LC}} \quad (4.4)$$

- Coil inductance

According to ARRL 
$$L = \frac{D^2 T^2}{457,2D + 1016l} \quad (4.5)$$

According to Surry University 
$$L = \frac{D^2 T^2}{228r + 254l} \quad (4.6)$$

These formulas are useful for estimation, but do not apply well to extreme cases.

- Shunt capacitance of the coil [3]

$$C_s = \frac{r.a.N^2}{l} 4\pi\epsilon_0\epsilon_r \quad (4.7)$$

- Characteristic coil impedance

$$Z_0 = \sqrt{\frac{L}{C}} \quad (4.8)$$

- Damping resistance

$$Rd = \frac{\pi}{2} \sqrt{\frac{L}{C}} \quad (4.9)$$

#### 4.2.5 Advantages of Rogowski transducers

- ⇒ Can measure current transients with exceedingly fast rise times.
- ⇒ The Rogowski coils have a wide range in that the same coil can be used to measure currents ranging from a few milliamperes to several millions of amperes.
- ⇒ Calibration is easier because the coil may be calibrated at any convenient current level and the calibration will be accurate for all currents including very large ones.
- ⇒ The coils respond accurately to transient currents which makes them an excellent choice for use in protection systems and for measuring current pulses.
- ⇒ They are useful in situations where the approximate value of the current to be measured is not known beforehand.

#### 4.2.6 Applications

- ⇒ Monitoring current waveforms for semiconductor switches.
- ⇒ Development and servicing of power electronic equipment
- ⇒ Monitoring high frequency sinusoidal currents
- ⇒ Measuring fault current or circuit breaker interruption currents
- ⇒ Measuring pulses of current

- ⇒ Measuring ac currents superimposed on large dc currents
- ⇒ Measuring harmonic current components
- ⇒ Measuring signal or earth leakage currents in 3-phase supply systems.

### 4.3 Co-axial Shunt

The high frequency coaxial shunt in figure 6.7 is designed for the measurement of current pulse. A co-axial shunt has the advantage that the current flowing in the shunt does not produce any electromagnetic fields outside the gap between the tubes. Accurate measurement requires a thorough protection against capacitive and inductive coupling as well as high common mode rejection.

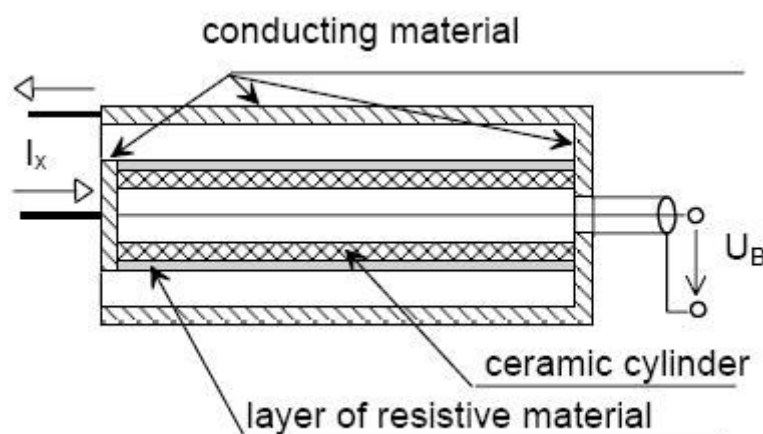


Figure: 6.7 High frequency coaxial shunt [43]

Current flow may be determined by measuring the voltage drop across a resistor connected in series with a circuit. Resistors have a parasitic inductance and capacitance associated with them. The ratio of parasitic inductance to pure resistance determines the high frequency limit of the measurement. Increasing the value of resistance to reduce this ratio can cause dissipation and insertion loss problems. It is not easy to produce a low-resistance shunt capable of matching the high-frequency performance of a broadband transformer, even with the aid of coaxial techniques.

The resistor suffers from the disadvantage of not providing isolation from the circuit under test. If this is not important, then resistive shunts can prove useful for the measurement of low current for frequencies stretching from dc into the MHz region or, for higher currents, to a few hundred kHz. Coaxial shunts with very low values of parasitic inductance may be used at moderately high currents to frequencies up to about 20MHz

## 4.4 Current Transformer

The current transformer /monitor is usually used for measuring pulse currents which are more complicated transients and periodic signals from a few hertz up to the megahertz region.

### Operation

To use a current monitor one needs an oscilloscope and an appropriate length of coaxial cable, which would usually have a  $50\Omega$  impedance. For RF work an RF voltmeter may be used. The output holder of the current monitor is connected via the coaxial cable to the high-impedance oscilloscope or voltmeter input. The conductor carrying the current to be measured is passed through the hole in the current monitor. The voltage waveshape as displayed on the oscilloscope will then be a faithful reproduction of the actual current waveshape within the limitations of rise time and droop specified. The voltage amplitude will be related, on a linear basis, to the current amplitude by the sensitivity in volts-per-ampere.

### Typical Applications

Current monitors can be used for measuring and monitoring:

- Current waveshape and amplitude in high and low voltage circuits, from microamperes to mega amperes.
- Circuits where the use of viewing resistors is unsuitable because of ground-loop noise, insertion resistance, or a lack of high voltage isolation.
- Pulse currents at high voltage, as associated with microwave or x-ray tube modulators, particle accelerators and lasers.
- Current transients and harmonics in power systems.
- Lightning-strike currents.
- Pulsed charged-particle beam current.
- Current in electrolytes and plasmas.
- EMI currents.
- Video and RF currents.
- Currents in spot and induction welders.
- Antenna phasing.
- Flash-tube current.

## 4.5 Oscilloscope

A Tektronix TDS544A digitizing oscilloscope was used in our project, which has, a superb tool for acquiring, displaying and measuring waveforms from the antenna, motor shaft etc. Its major specification can be found below:

- 1) 500 MHz maximum analog bandwidth.
- 2) 1 Gigasample / second maximum digitizing rate.
- 3) 4 channel

## 5 ANTENNAS

### 5.1 Introduction

An antenna belongs to a class of devices called transducers. This term is derived from two Latin words, meaning literally “to lead across” or “to transfer.” Thus, a transducer is a device that transfers, or converts, energy from one form to another. The purpose of an antenna is to convert electromagnetic waves to radio-frequency electric current.

We cannot directly see or hear, taste or touch electromagnetic waves. In everyday life we come across many types of transducers, although we don’t always recognize them as such. A comparison with a type of transducer that we can actually see and touch can differ.

The loudspeaker/microphone can exhibit the principle of reciprocity, derived from the Latin word meaning to move back and forth. Now, let’s look more closely at that special transducer we call an antenna. When fed by a transmitter with RF current the antenna launches electromagnetic waves, which are propagated through space. This is similar to the way sound waves are propagated through the air by a loudspeaker. In the next town, or perhaps on a distant continent, a similar transducer (that is, a receiving antenna) intercepts some of these electromagnetic waves and converts them into electrical current for a receiver to amplify and detect.

In the same fashion that a loudspeaker can act as a microphone, a radio antenna also follows the principle of reciprocity. In other words, an antenna can transmit as well as receive signals. However, unlike the loudspeaker, an antenna does not require a medium, such as air, through which it radiates electromagnetic waves. Electromagnetic waves can be propagated through air, the vacuum of outer space or the near vacuum of the upper ionosphere. [19]

### 5.2 Characteristics of Antennas

What other things make an antenna different from an ordinary electronic circuit? In ordinary circuits, the dimensions of coils, capacitors and connections usually are small compared with the wavelength of the frequency in use. Here, we can define wavelength as the distance in free space traveled during one complete cycle of a wave. The velocity of a wave in free space is the speed of light, and the wavelength is thus:

$$\lambda_{METERS} = \frac{299,7925}{f_{MHZ}} \quad (5.1)$$

Antennas come in an enormous assortment of shapes and sizes. Ground has a big influence on how an antenna performs in the real world. No matter what form an antenna takes, simple or complex, its electrical performance can be characterized according to the following important properties:

1. Feed-Point Impedance
2. Directivity, Gain and Efficiency
3. Polarization

### 5.3 Induced voltage in an antenna coil

Faraday's law states that a time-varying magnetic field through a surface bounded by a closed path induces a voltage around the loop. When the source and antenna are in close proximity, the time-varying magnetic field  $B$  that is produced by a antenna coil induces a voltage (called electromotive force or simply EMF) in the closed antenna coil. The induced voltage in the coil causes a flow of current on the coil. This is called Faraday's law. The induced voltage on the printed antenna coil is equal to the time rate of change of the magnetic flux  $\Psi$ .

$$V = -N \frac{d\psi}{dt} \quad (5.2)$$

Where:

$N$  = number of turns in the antenna coil

$\Psi$  = magnetic flux through each turn

The negative sign shows that the induced voltage acts in such a way as to oppose the magnetic flux producing it. This is known as Lenz's law and it emphasizes the fact that the direction of current flow in the circuit is such that the induced magnetic field produced by the induced current will oppose the original magnetic field. The magnetic flux  $\Psi$  in Equation 5.3 is the total magnetic field  $B$  that is passing through the entire surface of the antenna coil, and found by:

$$\psi = \int B * dS \quad (5.3)$$

$B$  = magnetic field

$S$  = surface area of the coil

$*$  = Inner product (cosine angle between two vectors) of vectors  $B$  and surface area  $S$ .

The presentation of inner product of two vectors in (5.3) suggests that the total magnetic flux  $\psi$  that is passing through the antenna coil is affected by an orientation of the antenna coils. The inner product of two the vectors becomes minimized when the cosine angle between the two are 90 degrees, or the two ( $B$  field and the surface of coil) are perpendicular to each other and maximized when the cosine angle is 0 degrees [23].

## 5.4 Applications

### Loop Antennas

A loop antenna is a closed-circuit antenna—that is, one in which a conductor is formed into one or more turns so its two ends are close together. Loops can be divided into two general classes, those in which both the total conductor length and the maximum linear dimension of a turn are very small compared with the wavelength and those in which both the conductor length and the loop dimensions begin to be comparable with the wavelength. A “small” loop can be considered to be simply a large coil, and the current distribution in such a loop is the same as in a coil. That is, the current has the same phase and the same amplitude in every part of the loop. To meet this condition, the total length of conductor in the loop must not exceed about  $0.1 \lambda$ .

### Small Loop Antennas

The electrically small loop antenna has existed in different forms. Probably the most familiar form of this antenna is the ferrite loopstick found in portable AM radio receivers. Applications of the small loop include direction finding, low-noise directional receiving antennas for LF and HF band

### Tuned Loops

We can easily tune the loop by placing a capacitor across the antenna terminals. This causes a larger voltage to appear across the loop terminals because of the Q of the parallel resonant circuit that is formed. The voltage across the loop terminals is now given by

$$V = \frac{2\pi ANEQ \cos \theta}{\lambda} \quad (5.4)$$

where Q is the loaded Q of the tuned circuit. The tuned-loop antenna has some particular advantages. For example, it puts high selectivity up at the first stage of a receiving system (when Q is relatively high). Loaded Q values of 50-100 or greater are easy to obtain with careful loop construction. Lower Q values can also be obtained for special purpose applications.

Let us now look a little bit more in detail on its design. First, the loop forms an inductor having a very small ratio of winding length to diameter. The square loop antenna inductance can be calculated by using:

$$L = 0,006N^2s \left[ \ln \left( \frac{1,4142sN}{(N+1)l} \right) \right] + 0,37942 + \frac{0,3333(N+1)l}{sN} \quad (5.5)$$

Where:

L= inductance in  $\mu\text{H}$

N = number of turns

s = side length in cm

l = coil length in cm

The value of a tuning capacitor for a loop is easy to calculate from the standard resonance equations. The only aspect to consider before calculating this is the value of distributed capacitance of the loop winding and connection cable. This capacitance shows up between adjacent turns of the coil because of their slight difference in potential. This causes each turn to appear as a charge plate. As with all other capacitance's, the value of the distributed capacitance is based on the physical dimensions of the coil.

This distributed capacitance appears as if it were a capacitor across the loop terminals. Therefore, when determining the value of the tuning capacitor, the distributed capacitance must be subtracted from the total capacitance required to resonate the loop. The distributed capacitance also determines the highest frequency at which a particular loop can be used, because it is the minimum capacitance obtainable [23].

### **Electrostatically Shielded Loops**

In order to minimize the antenna noise and reduce the E field received by the antenna an electrostatic shield can be used. This shield generally takes the form of a tube around the winding, made of a conductive but nonmagnetic material (copper or aluminum). Also it will maintain loop balance with respect to ground, by forcing the capacitance between all portions of the loop and ground to be identical. This is illustrated in Fig 5.2. When the antenna becomes unbalanced it appears to act partially as a small vertical antenna. Adding the shield will reduce the pickup of the loop. Proper balance of the loop antenna requires that the load on the loop also be balanced. This is usually accomplished by the use of a balun transformer or a balanced input preamplifier. Two important points regarding the shield are that it cannot form a continuous electrical path around the loop perimeter, or it will appear as a shorted coil turn. Usually the insulated break is located opposite the feed point to maintain symmetry. Another point to be considered is that the shield should be of a much larger diameter than the loop winding, or it will lower the Q of the loop. Various construction techniques have been used in making shielded loops. The antenna can be shielded using the outer conductor as a shield.

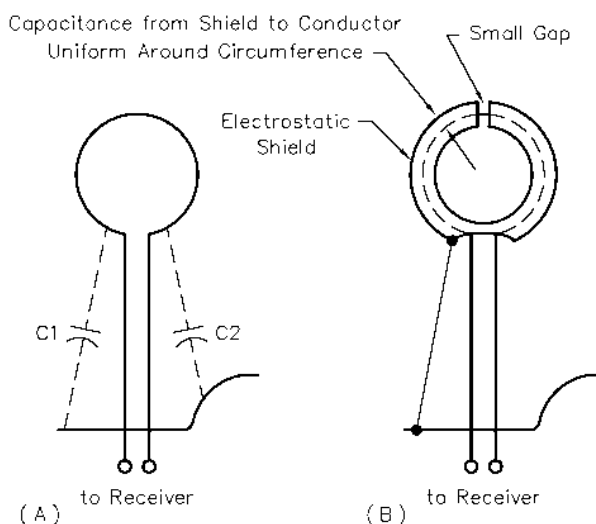


Figure: 5.2 [19]

## Loop Q

As previously mentioned,  $Q$  is an important consideration in loop performance because it determines both the loop bandwidth and its terminal voltage for a given field strength. The loaded  $Q$  of a loop is based on four major factors. These are (1) the intrinsic  $Q$  of the loop winding, (2) the effect of the load, (3) the effect of the electrostatic shield, and (4) the  $Q$  of the tuning capacitor.

The major factor is the  $Q$  of the winding of the loop itself. The ac resistance of the conductor caused by skin effect is the major consideration. For the bearing current measurements the bandwidth of the antenna should be wide which means less  $Q$ .

## Direction Finding Antenna

The ability of certain RDF antennas to reject signals from selected directions has been used as advantage in reducing noise and interference. One of the typical applications is tracking down noise sources.

Required for any RDF system are a directive antenna and a device for detecting the radio signal. One example of a simple RDF antenna is a Loren Norberg's design.[19]

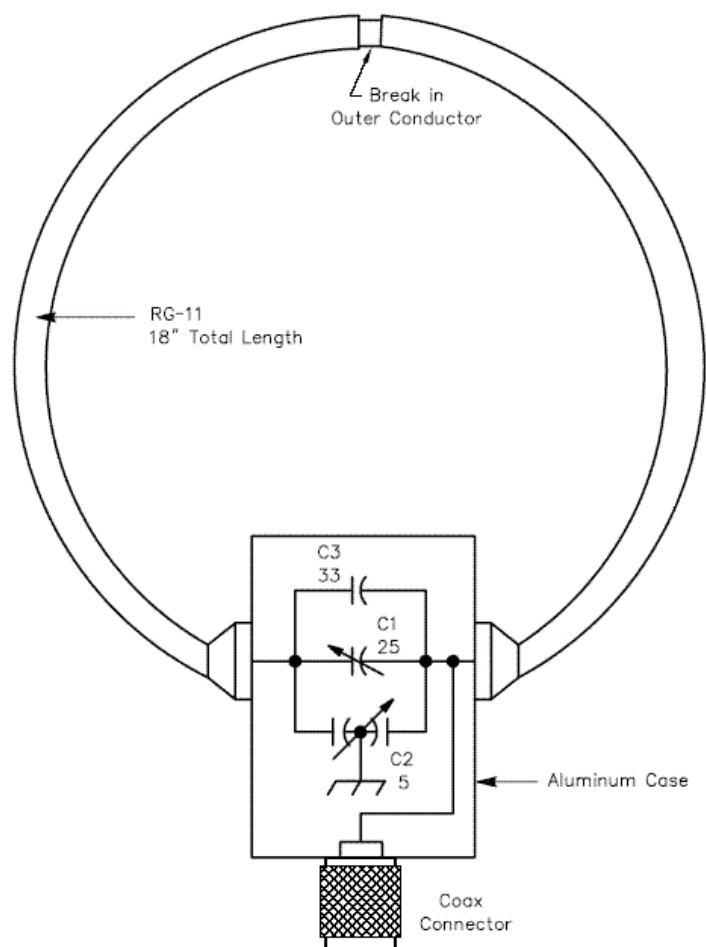


Figure: 5.3 Direction finding antenna [19]

### Frequency Scaling

Any antenna design can be scaled in size for use on another frequency or on another amateur band [19]. The dimensions of the antenna may be scaled with Eq 5.6 below,

$$D = \frac{f_1}{f_2} d \quad (5.6)$$

Where:

D = scaled dimension

d = original design dimension

f1 = original design frequency

f2 = scaled frequency (frequency of intended operation)

### 5.10 Advantages and disadvantages

The main advantage of the antenna detection system can be formulated in some points:

- Mobility
- Direct contact is not required
- Selectivity (with appropriate device)
- Good sensitivity

## 6 Description of the Experimental Model and Measurement setup

### 6.1 Experimental setup in general

The tests and measurements, which were performed, can be divided into two types. The first configuration consists of three SNL bearing housings mounted on massive cast iron table using 10mm isolating plates. These housings are used to support the bearings, which are mounted on the same shaft. A 7.5 kW motor is mounted on the same cast iron table. In order to insulate the motor from the table, plastic spacers were used. The shaft is connected to the motor using a flat belt. To control the motor speed, different frequency converters were used.

As a second type test arrangement, different induction motors sizes were used. They can be considered as real installations. Their configurations will be keep as is with no changes in the connection circuit. Different frequency converters were used when it is applicable.

DA, OLA, Rogowski coil, coaxial shunt and slip rings were used in order to the monitor the currents and voltages in the investigated arrangements. As measurement devices, a Fluke 123 and a Tektronix TDS544A was used.

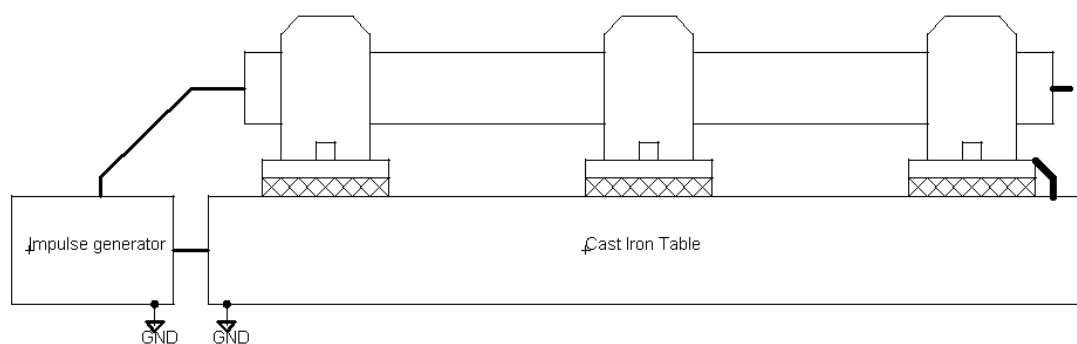


Fig.6.1 Synthetic test configuration

### 6.2 Investigation of few elements

To minimize the measurement error it was decided to investigate the DC and transient behavior of the components used in the test bench. Based on the estimated rotor to ground capacitance, rotor voltage and bearing impedance bearing currents in the range of 1-10A approximately were expected. Special attentions should be paid to the connections and current carrying components.

In the circuit, the current flows from the impulse circuit through the cables, slip ring, bearing shaft, one bearing into ground. In this sequence, the slip ring, slipping caps and cable connections can affect the current path to a great extent. To understand the behavior of these components several tests have been performed. Slip ring and slip ring caps were tested with DC and impulse currents, cables and soldering were tested only with impulse currents due to the negligible resistance that they have.

### 6.3 Design of the impulse circuit for the test/synthetic motor

The main purpose of the impulse circuit is to charge the rotor shaft to a certain voltage for a specified time. The circuit capacitor in combination with the shaft capacitance will determine the discharge current.

To obtain conditions, close enough to the real motor we search for the typical values of rotor to ground capacitance, bearing breakdown voltage and bearing impedance during discharge.

Table 6.1 Typical values for 5-kVA range motor can be summarized as:

Parameter	Value	Dimension
Csf	7-	nF
Csr	68-	nF
Crf	0,8-10	nF
Cb	0,1-	nF
Zb	0,5-12	Ohm
Ubd	1-40	V
Current pulse interval	100-500	usec

To obtain different time characteristics six different capacitors have been used. The output voltage versus time can be calculated using:

$$U_{out} = U_{in} \left( 1 - e^{-\frac{t}{RC}} \right) \quad (6.1)$$

By rewriting (6.1) R can be found for different values of C and times

$$R = \frac{t}{C * \ln \left( 1 - \frac{U_{out}}{U_{in}} \right)} \quad (6.2)$$

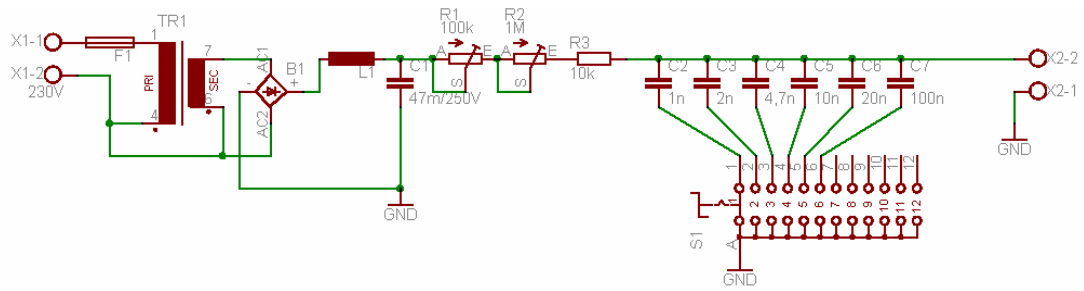


Figure 6.1 Power supply and impulse circuit

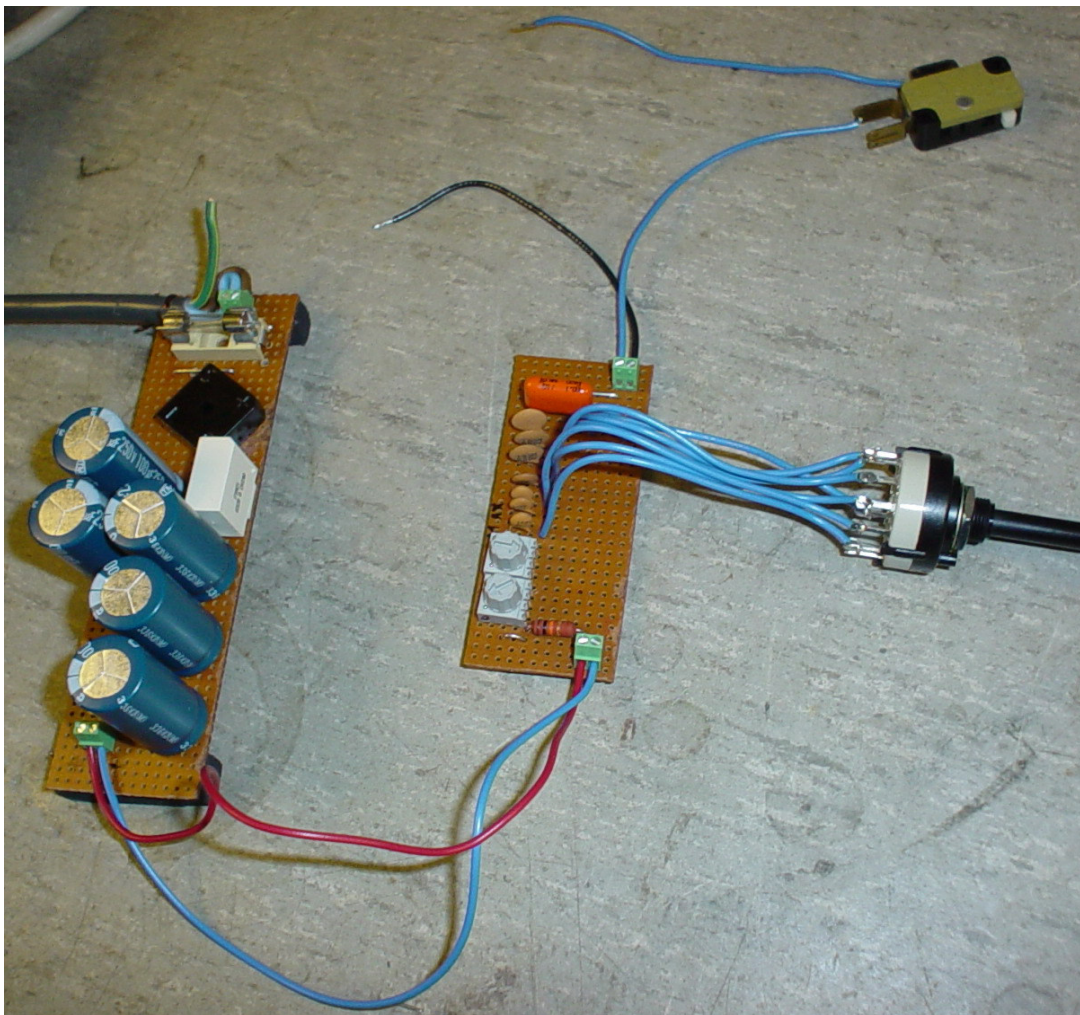


Figure 6.2 Power supply and impulse circuit.

## 6.4 Rogowski coil design

Rogowski coils produce an output voltage proportional to the rate of change of the current.

$$V_{out} = M \cdot \frac{dv}{dt} \cdot I \quad (6.3)$$

Where  $M$  is the mutual inductance.  $I$  is the measured current. By using the right techniques, it is possible to make flexible coils capable to measure currents with demanding precision. The sensitivity of a complete coil and integrator is the ratio between the voltage output and the current being measured. Generally, the sensitivity can be expressed as:

$$\frac{V_{out}}{I} = \frac{M}{CR} \quad (6.4)$$

Where  $I$  is the measured current,  $M$  is the mutual inductance between the coil and the conductor,  $C$  and  $R$  are the integrator values. The coil sensitivity can be varied by using different number of turns or changing the  $C$  and  $R$ -values.

All the literature sources claim that the coil upper frequency limit is determined by the self-resonance frequency of the coil and depends of the coil design. Typically, an upper frequency limit of several megahertz can be obtained. Very high frequency measurements can be made using a Rogowski coil, which is terminated with a low value resistor. In this case, the coil self-inductance is used to perform the integration. Coils operating on this principle can be used to measure currents up to frequencies of several hundreds megahertz.

Our first coil design mainly was focused on helping us to better understand the principle of operation of the Rogowski coil and the problems connected with the integration of the measured signal. This first prototype should help us to design such a coil that will be suitable for the measurements of bearing currents.

The main pre-design consideration can be summarized as:

- As short as possible - less windings
- Less winding - low self-inductance
- Smallest diameter - low coil capacitance
- Small wire diameter - low coil capacitance
- Small coil diameter - high frequency coil
- Flexible core, which is in the same time mechanically enough rigid to keep coil windings equally distributed along the core.

For the core a 5mm PET compressed air pipe was used. The mechanical length was chosen to be 500mm, which is quite enough to be put around the bearing shaft of our test rig and 90 turns were wound with 0,6mm solid copper wire. For the return path, the thinnest isolated wire was used which we put inside the PET pipe. Over the whole structure we put thermo shrink pipe to hold the winding in place. Also, over the two

coil ends we put small pieces of PET pipes, which are used to connect the coil ends and keep it as a circle.



Fig.6.3 The Rogowski coil, which we made in SKF

#### 6.4.1 Measuring Rogowski coil inductance

The different capacitors and the coil form a parallel LC circuit. The signal generator frequency varied until a maximum signal was observed on the oscilloscope and the present frequency was noted. L was then calculated using the formula given below with the measured frequencies and different capacitors.

The capacitor value was chosen to be more than ten times the coil capacitance. This was done in order to minimize the error, which can be introduced of the coil-distributed capacitance. For more precise measurements, capacitors with +/-1% should be used.

$$L = \frac{1}{(2.\pi.f)^2.C} \quad (6.5)$$

Table 6.2 Measurement of coil inductance

Number	f [Mhz]	C [pF]	L [uH]
1	1,8	4700	1,66
2	3,5	1400	1,48
3	7	220	2,35
4	1,76	4270	1,92
5	0,96	13870	1,98
6	0,51	52370	1,86
7	0,54	48100	1,81
<b>Average</b>	NA	NA	<b>1,89</b>

#### 6.4.2 Measuring coil self resonance

The signal generator frequency was varied until the signal observed on the oscilloscope has a maximum. The coil self-capacitance is calculated using the measured frequency and the averaged coil inductance (from table above) and the formula below. The self-resonant frequency of the yellow coil were measured to be 10,43 MHz. The calculated self-capacitance is 124 pF.

$$C = \frac{1}{(2\pi \cdot f)^2 L} \quad (6.6)$$

Table: 6.3 Coil parameters

Coil	Turns	Wire diameter	Core diameter	Self resonance	Coil capacitance	Coil inductance	Coil impedance
Yellow	90	0,5	5	10,43	124 pF	1,89 uH	124 / 87

#### 6.4.3 Measuring coil frequency response

To measure the frequency response of the coil a sinusoidal signal from a function generator has been used. The signal was injected into the other end of 50  $\Omega$  resistor by using a 50  $\Omega$  coaxial cable. This resistor is placed inside the Rogowski coil in a direction, perpendicular to the coil plain. The alternating magnetic field produced by the current, induces voltage in the coil. A two-channel oscilloscope used to monitor the function generator voltage and the voltage induced in the coil.

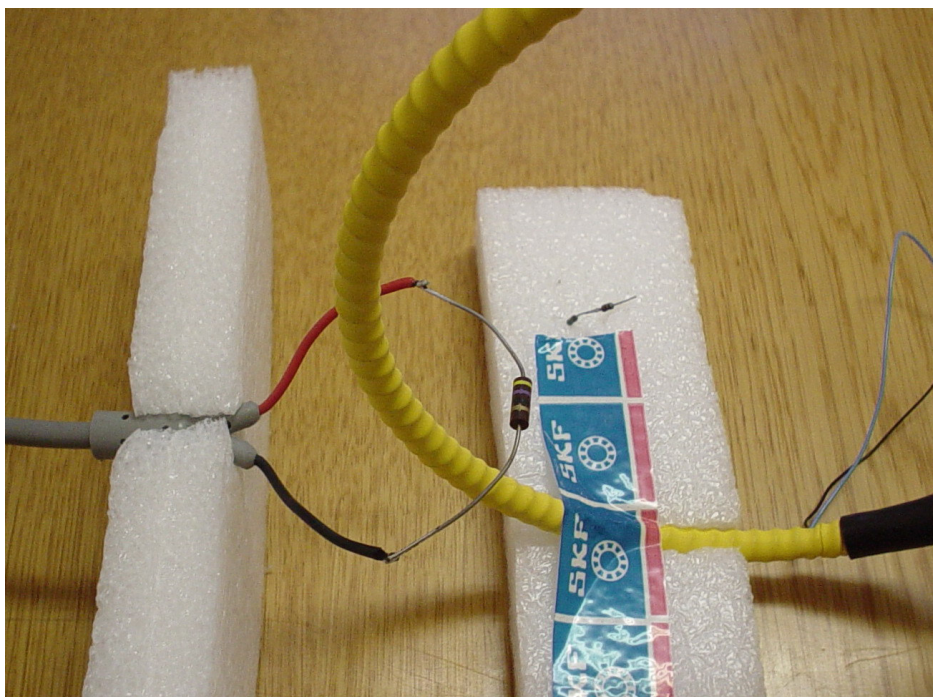


Fig. 6.4 Frequency response test configuration

The coil response in dB was calculated using:

$$dB = 20 \log_{10} \left( \frac{U_{out}}{U_{in}} \right) \quad (6.7)$$

The signal frequency was changed from 1MHz to 20MHz in 1MHz steps. Several tests by varying the integrator parameters were performed. The coil response with no other components attached, looks like a slope going down with the frequency increase.

According to [24] the coil upper frequency limit is determined by the self-resonance and can be calculated using:

$$f_B = \frac{1}{4\sqrt{LC}} \quad (6.8)$$

In our case it appears to be 16,33Mhz

According to [25]

$$\omega_B < \frac{1}{\sqrt{LC}} \quad (6.9)$$

Which give us upper frequency of 10,4Mhz

In order to provide the coil with appropriate damping, a damping resistance should be used. Its value can be determined by:

$$Rd = \frac{\pi}{2} \sqrt{\frac{L}{C}} \quad (6.10)$$

The value obtained using this equation is 194  $\Omega$ .

The other limitation of the passive integration is that the low frequency band is limited by the integrator time constant [25]

$$\omega_A > \frac{1}{(C_0 R_0)} \quad (6.11)$$

It was decided that an integration circuit based on low pass filter layout was to be built.

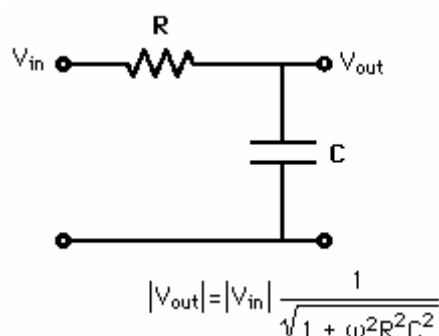


Fig.6.5 Low pass filter

To have good transient response, the coil has to be terminated. Since at the high frequency the impedance of C is quite low, R can be used as a damping resistor equal to  $\sqrt{L/C}$ . The author of [24] claims that better transient response can be obtained if the damping resistor value is calculated using:

$$R_d = \frac{\pi}{2} \sqrt{\frac{L}{C}} \quad (6.12)$$

Since we were not sure which way of determining the damping resistor is the best, we decided to experiment with different values of R in the range between 47 and 200  $\Omega$

Using the equation  $C = \frac{1}{2\pi f_B R}$  for given  $f_B$  and R we calculated the needed capacitance

Table 6.4

$f_B$ [MHz]	R [Ohm]	C [nF]
6,78	50	0,47
6,78	75	0,313
10	56	0,284
10	82	0,194
20	56	0,142
20	82	0,097
20	200	0,040

With both integrators we obtained the response curve, which haven't a flat area. As can be noted from figure 6.6, the best frequency response was obtained using an integrator with parameter  $76\Omega/470$  pF. Although it is the best one from the CR integrators it is not good enough to be used in real measurement system.

Based on our early experience, it was decided to try with L/r integration. To do this, the coil should be terminated with a relatively low value resistor  $R_d$ . The upper frequency limit approximately can be obtained by:

$$\omega_B < \frac{1}{CR} \quad (6.13)$$

Where C is the equivalent coil capacitance and R is the damping resistor.

The main disadvantage of this method is that, R needs to be much lower than the coil characteristic impedance  $Z_0$ . This will reduce the transducer sensitivity, which will have a negative effect on small current measurements. In this case the output voltage can be approximated by:

$$V_{OUT} = I \frac{R}{N} \quad (6.14)$$

Where I is the measured current and N is the total numbers of coil turns.

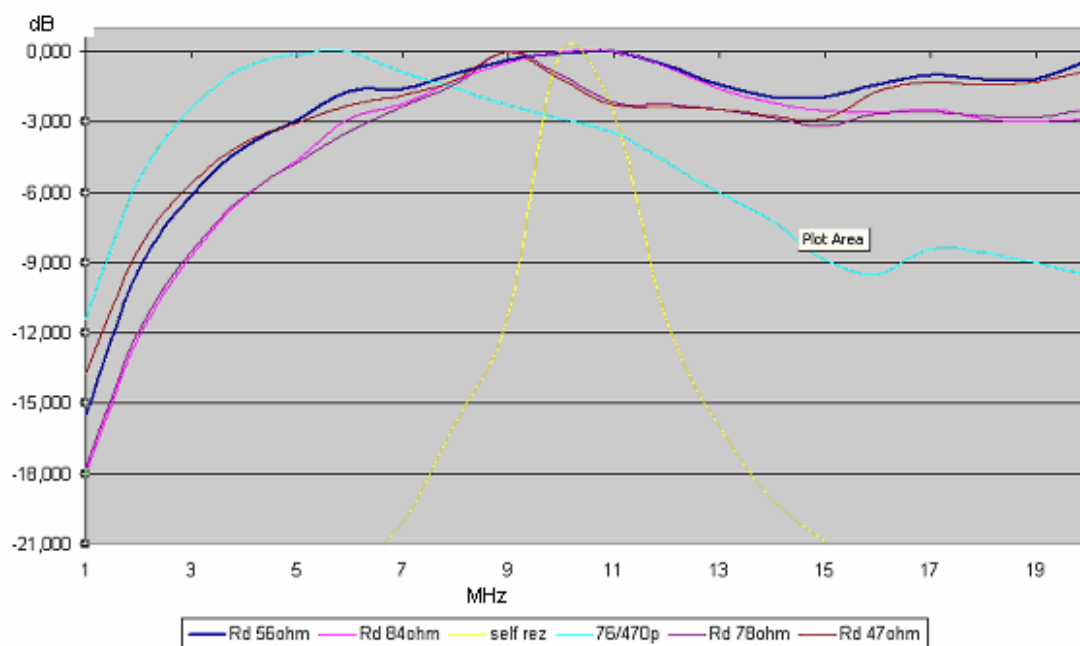


Fig.6.6 Different coil response characteristics

Surprisingly we obtained better results with L/r, compared to the CR integration. With a  $56 \Omega$  damping resistor the 3dB-bandwidth start from 5Mhz and continue up 20Mhz with no visible tendency to go down. This is the highest frequency that we can

generate and measure with our present equipment. The frequency response below 5Mhz can be compensated by combining a passive and an active integrator.

Every coil has a self-resonant frequency caused by its self-inductance and turn-to-turn capacitance. The resonance also depends of other factors such as cable capacitance. The resonance can be controlled by suitable damping circuitry, but generally all authors say that it is not practicable to use a coil above its resonant frequency. The coil frequency response surprisingly goes up more than twice the self-resonance frequency. It was decided to test the coil with impulse voltages and more high frequency equipment.

## 6.5 Slip ring

### 6.5.1 Slip ring investigation

The voltage measured over the slip ring and  $2.8 \Omega$  resistance connected in series in fig 6.8

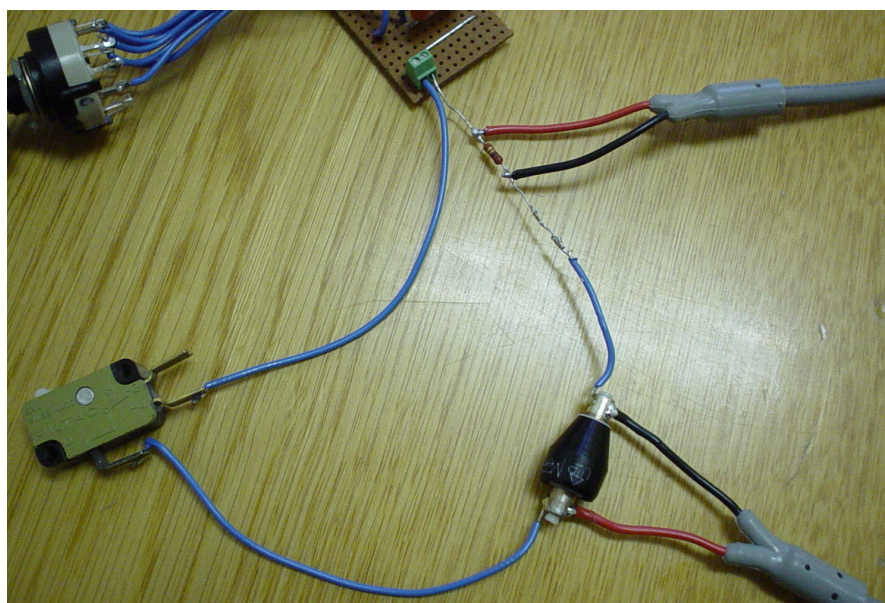
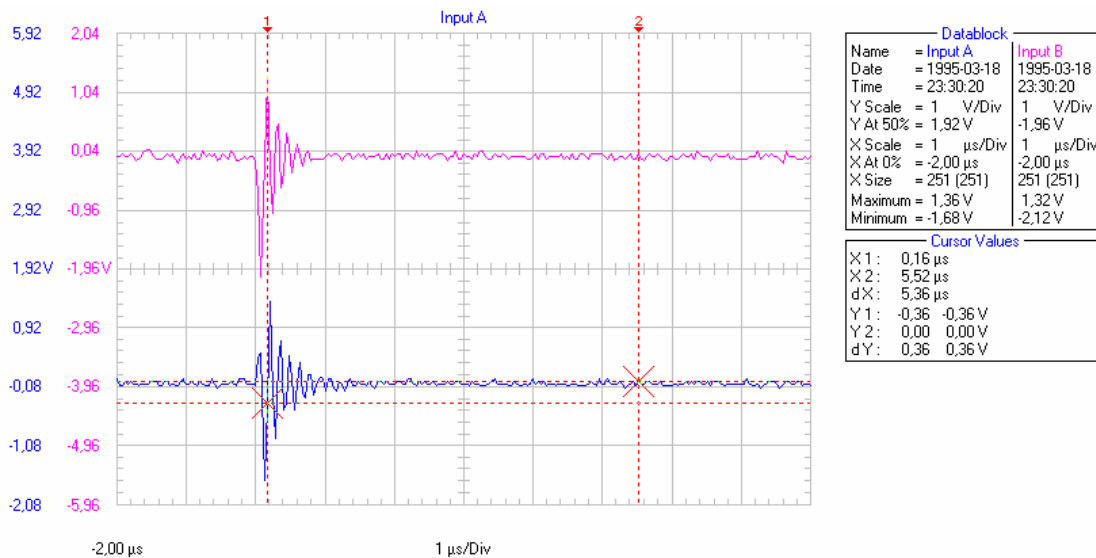


Figure 6.8 Slip ring investigations

The magnitudes are almost the same, which made us very suspicious. We tried with different slip ring caps to locate the problem. Aluminum caps have very high resistance due to the aluminum oxide.



A slip ring , B resistor 2.8 ohm position 1

Fig.6.9 Waveforms measured over the slip ring and the coil. 1 square is equal to 1  $\mu$ s.

To minimize the contact resistance between the slip ring and corresponding cap we decided to solder the connection wires directly to the slip ring. The measurement probes were soldered on the opposite side of the first two soldering. This is done to minimize the soldering impedance and to make it possible to measure the true voltage drop over the slip ring.



Figure 6.10 Soldered slip ring

After these corrections another test was performed.

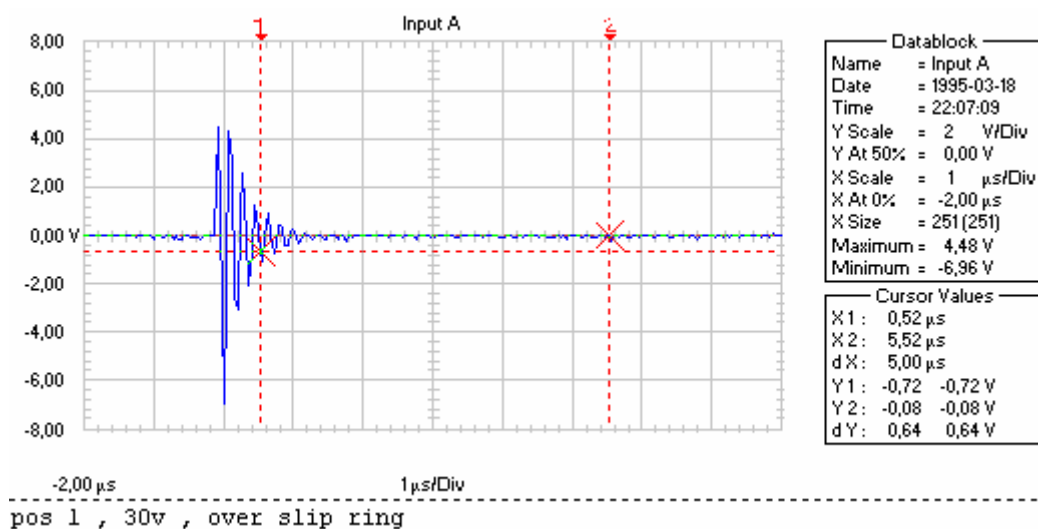


Fig. 6.11 presents the Voltage waveform measured over the slip ring with caps. 1 square is equal to 1  $\mu$ s.

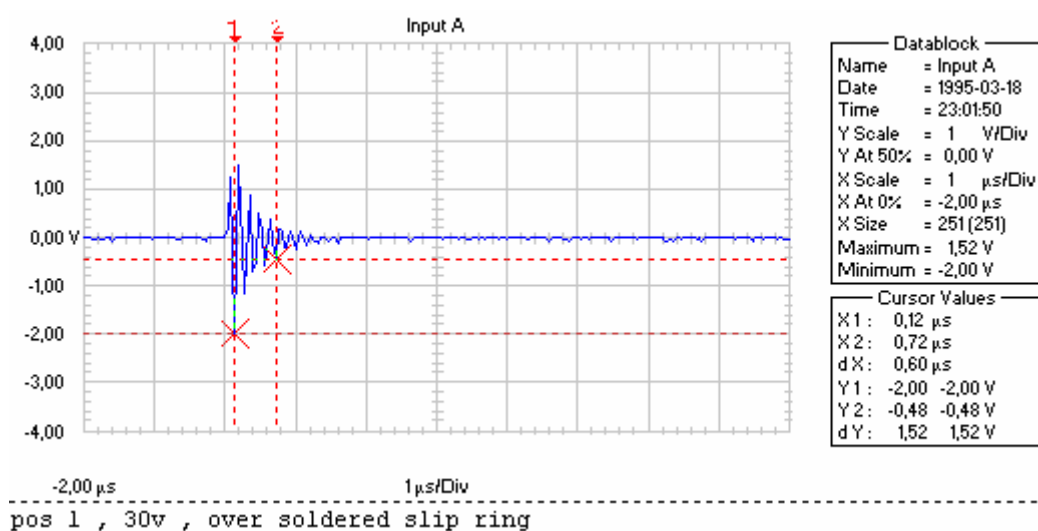


Fig.6.12 Voltage waveform measured over soldered slip ring. 1 square is equal to 1  $\mu$ s.

With soldered connection wires directly to the slip ring contacts, the voltage magnitude measured over the slip ring decreases from 11,28 to 3,52 Vpp. This solution is not recommended from the manufacturer due to the fact that insulation material used between inner and outer contacts in the slip ring are not capable to withstand the 350 degree Celsius, that can be the result during the soldering.

After these tests it can be said that the major cause for this big voltage drop is located. We found and test another slip ring caps, in which conducting media silver-coated steel is used. The test results are comparable with the soldered slip ring.

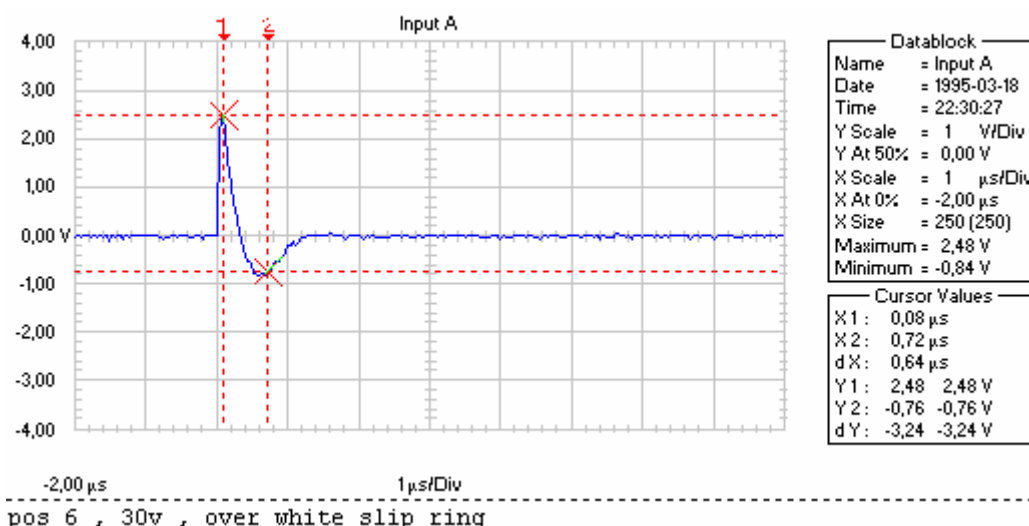


Fig.6.13 Voltage waveform measured over white slip ring. 1 square is equal to 1  $\mu$ s

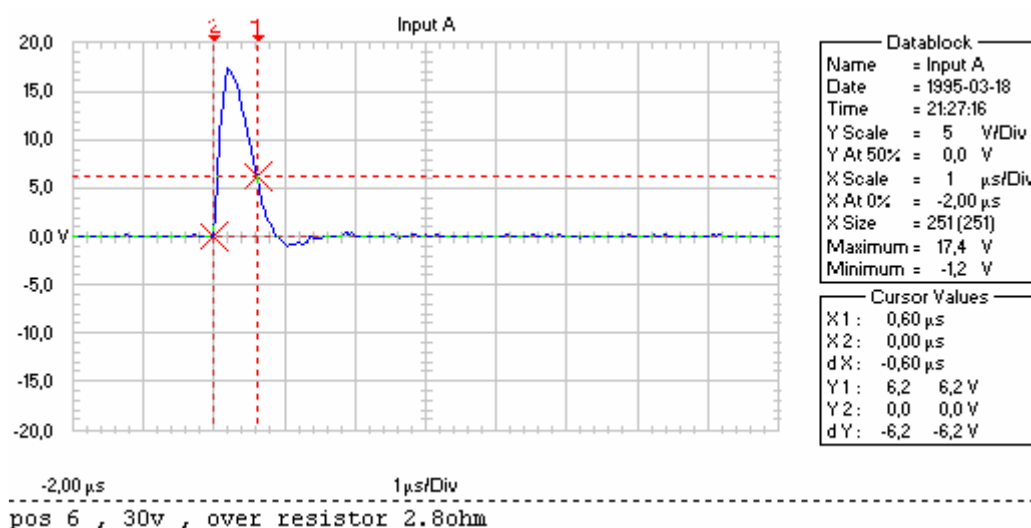


Fig.6.14 Voltage waveform measured over the 2.8  $\Omega$  resistor. 1 square is equal to 1  $\mu$ s

From figure 6.14, it can be seen that the voltage magnitude over the 2,8  $\Omega$  resistor is 18,6V. Figure 6.13, shows the voltage magnitude over the slip ring with white cap, which is 3,32V. It gives as total slip ring resistance of 0,5  $\Omega$ , the current magnitude was 6,6A. This impedance is connected in series with the test bearing and can have a substantial influence on the measurement results, keeping in mind that bearing impedance during conducting stage can vary between 0,5 and 12  $\Omega$ .

The results obtained using the same test configuration and discharge current from a 1nF capacitor shows us that the slip ring impedance increases when the impulse oscillation frequency increases.

As can be seen in figure 6.15 the voltage magnitude over the  $2,8 \Omega$  resistor is  $4,44 \text{ V}$ . The voltage over the slip ring with white caps is  $2,16 \text{ V}$ . From here we get the slip ring impedance to be  $1,36 \Omega$ .

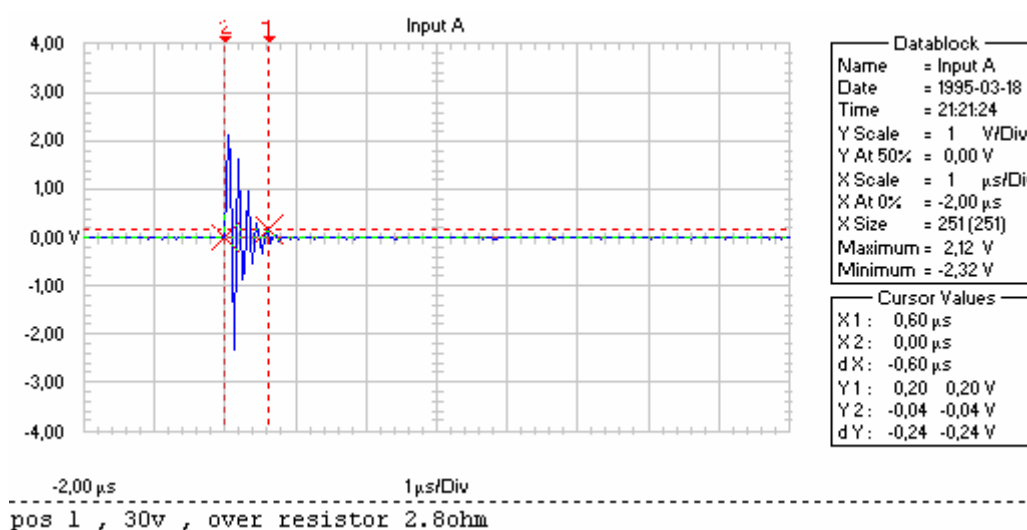


Fig.6.15 Voltage waveform measured over the  $2.8 \Omega$  resistor. 1 square is equal to  $1 \mu\text{s}$

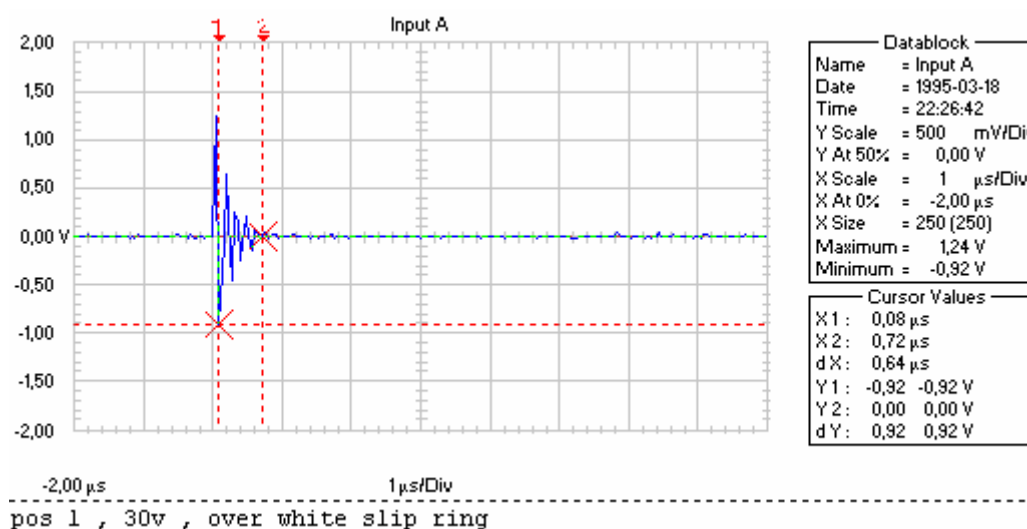


Fig.6.16 Voltage waveform measured over white slip ring. 1 square is equal to  $1 \mu\text{s}$

We also performed several tests with different impulse voltages and a  $1 \Omega$  resistor connected in series and used as a voltage reference.

The next two graphs show the voltage over a  $1 \Omega$  resistor and the measured voltage over the slip ring with white caps. Using a  $30 \text{ V}$  impulse voltage, we measure  $13,2 \text{ V}$  magnitude over the resistor and a voltage magnitude over the slip ring with white cap:

4,8V. It gives us a total slip ring impedance of  $0,36 \Omega$ , the current magnitude was 13,2A

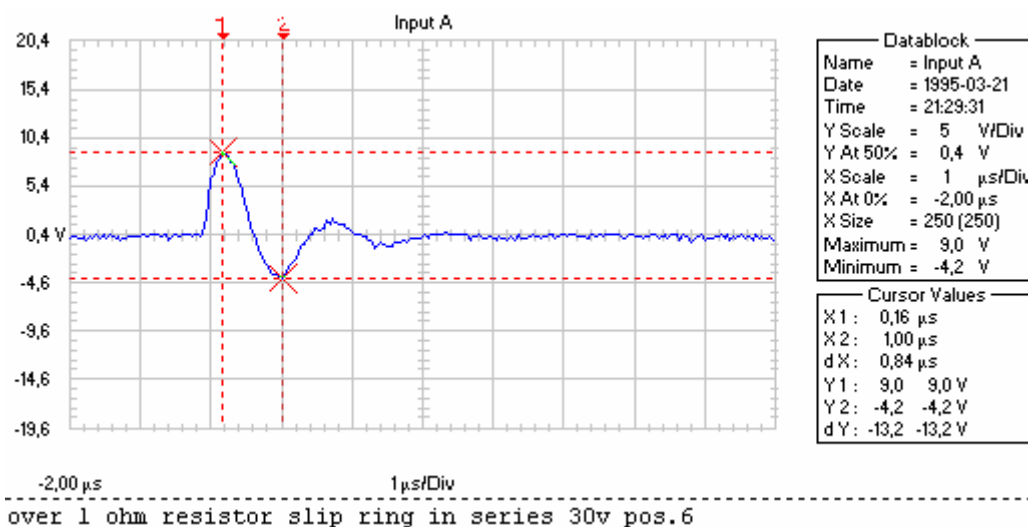


Fig.6.17 Voltage waveform measured over a  $1\Omega$  resistor. 1 square is equal to  $1 \mu$ s

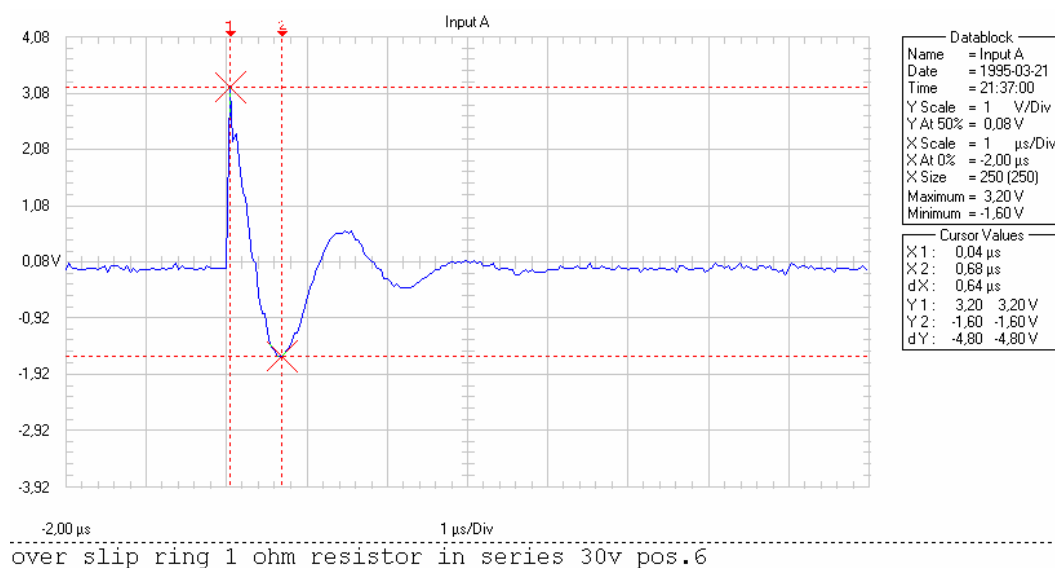


Fig.6.18 Voltage waveform measured over the slip ring connected in series with  $1\Omega$  resistor. 1 square is equal to  $1 \mu$ s

The same test as before is conducted, only the pulse voltage is reduced to 15V to reduce the slip ring current. Here the voltage magnitude over the resistor is 6,8V, the voltage magnitude over slip the ring with white caps is 2,16V and it gives us a total slip ring impedance of  $0,32 \Omega$  and the current magnitude 6,8A.



### 6.5.2 Slip ring DC test

To determine the slip ring resistance, we simply measure the voltage drop over the slip ring when currents having different magnitudes are leading through it.

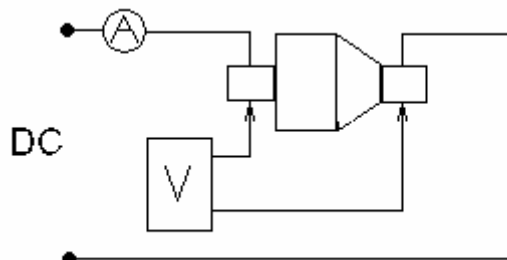


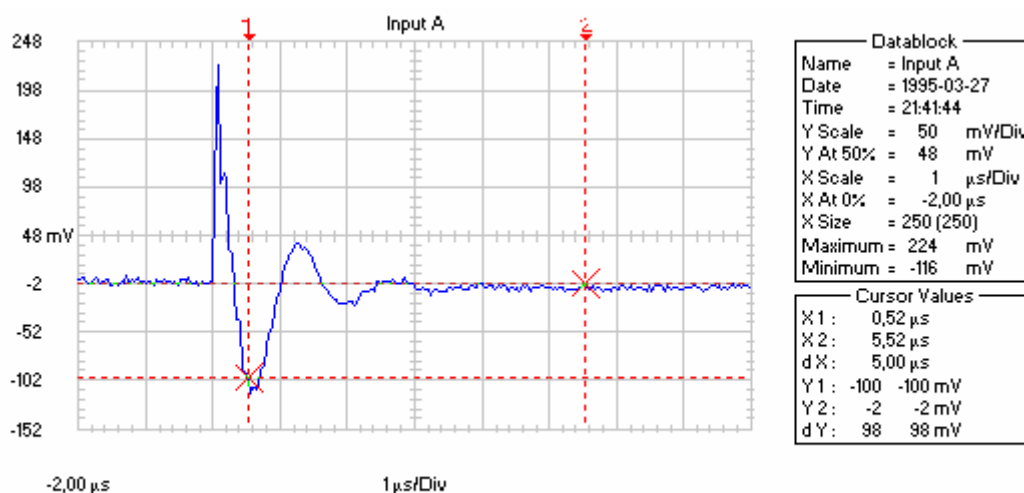
Fig.6.21 DC test configuration

The slip ring resistance is calculated from Ohms law.

Table 6.5 measurements from different meters

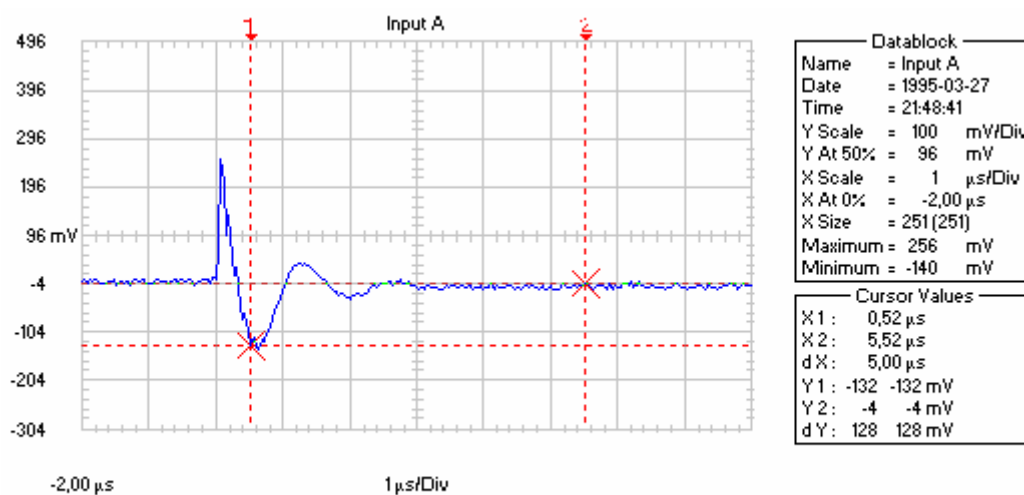
Meter	V/A	0,5	1	1,5	2
F87	mV	0,3	0,6	0,9	1,2
F123	mV	0,5	1	1,3	1,7
F87	m $\Omega$	0,6	0,6	0,6	0,6
F123	m $\Omega$	1	1	0,9	0,85

The calculated slip ring resistance is close to the one given by the manufacturer, which is  $<1\text{m}\Omega$ . During the above-mentioned tests, a doubt about soldering impedance rises up. To clear it and to be sure that it gives as little error as possible, we have tried to measure it. For this purpose, we soldered to each other two of our commonly used wires. By connecting (soldering) the scope probes at a distance of app. 8mm on both sides of the soldering and measure the voltage drop across the soldering. To compare the result we also connected both probes to one resistor leg with 8mm distance between them. The voltage drop over the 16mm resistor leg is more than the voltage drop over a regular thick soldering.



P.6 , 15V , coax probe derectly soldered in both sides of the soldering  
b/n r and sr 8mm distance between probes

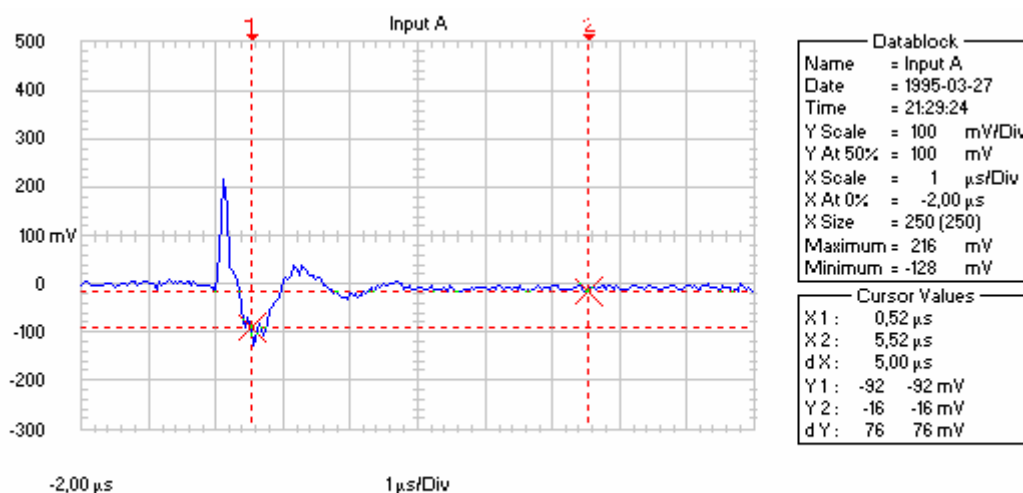
Fig.6.22 Coaxial probe legs are soldered at both sides of the soldering at a 8mm distance between the probes. 1 square is equal to 1 μs



P.6 , 15V , coax probe derectly soldered over second R leg  
with 8mm distance between probes

Fig.6.23 Coaxial probe legs are soldered over one resistor leg with a 16mm distance between probes. 1 square is equal to 1 μs

We also soldered the probe wires to the resistor leg at the same point. The whole measured voltage in this case is induced in the 40mm probe wires and the coaxial cable.

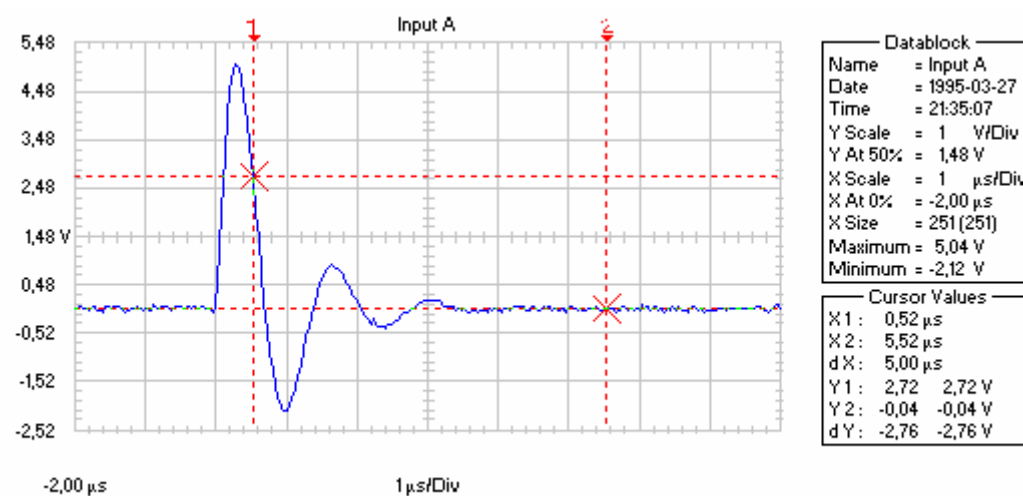


P.6 , 15V , two probes are short circuited and connected to the second resistor leg

Fig.6.24 Coaxial probe legs are soldered in the same place over the resistor leg. 1 square is equal to 1 μs

The magnitude of the induced voltage and the magnitude of the voltage measured over the soldering are virtually the same. By comparing these values with the voltage drop measured over the 1Ω resistor gave us, as idea how large the difference is.

0,30V - 0,34V and 7,6V



P.6 , 15V , coax probe derectly soldered over lohms resistor

Fig 6.25 Waveform measured over 1Ω resistor. 1 square is equal to 1 μs

DC tests are not performed due to the fact that the soldering resistance is very low and special equipment has to be used. In reality, this resistance will generate negligible error in our measurements.

## 6.6 Machine Specifications

Table 6.6 Different machine specifications

Motor	Voltage rating (V)	Current rating (A)	Frequency Hz	rpm rated
7.5 kW	400/690 $\Delta/Y$	15.5/8.6	50	2855
5.5 kW	380/660 $\Delta/Y$	12.5/7.1	50	1440
132 kW	400/690 $\Delta/Y$	235/136	50	986
3 kW	220/380 $\Delta/Y$	11/6.2	50	2890

## 6.7 Antenna Design

Our first antenna design is based on the information provided by Texas Instruments. As a base, considering our needs for mobility and miniaturization we use the well-studied RFID small loop antenna. The antenna uses a printed circuit and the artwork for the board is given in the figure below.

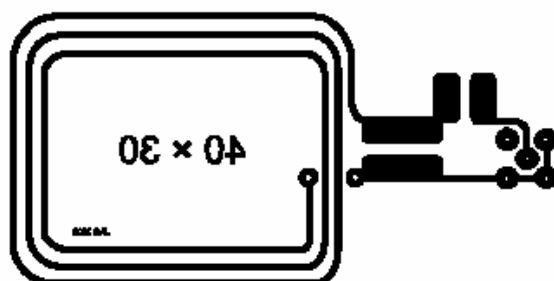


Figure: 6.26 PCB design for the antenna [21,22]

The antenna resonance frequency is 13,5 MHz, as RFID standard requires. From our previous measurements on a 7,5kW motor using current transformer we obtain current pulses with a dominant ringing frequency of 4.5 MHz. This frequency is 3 times lower than the antenna resonance frequency. With a Q factor of 20 this antenna cannot be used directly for our purposes. It is well known that the antennas can be scaled with great successes. In our particular case the scaling factor should be 3. We will apply slightly different approach. The original antenna resonance is obtained by using 150-177pF capacitors. Knowing the resonance frequency and the capacitance we calculate the coil inductance to be 0,85 $\mu$ H. To obtain as much as possible inductance from the existing antenna layout we add three more windings.

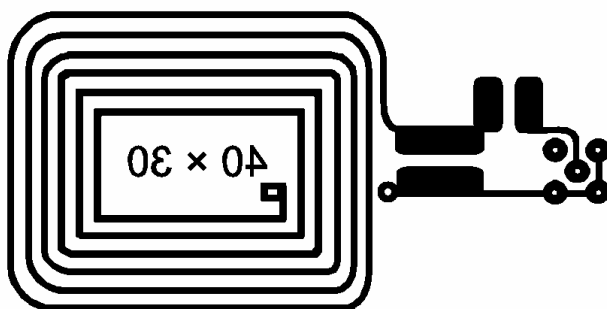


Figure: 6.27 PCB design for the new antenna

### 6.7.1 Antenna Matching

For optimum performance, the antenna and coaxial cable must have impedance of 50 Ohms. Matching changes the impedance of a resonant loop to 50 Ohms and the accuracy of the matching can be checked by the Voltage Standing Wave Ratio (< 1:1.2) on the VSWR meter. At the moment we did not have a SWR meter and due to this fact no matching tests were performed. If the damping resistor value is very different from the cable impedance, a capacitive matching should be considered.

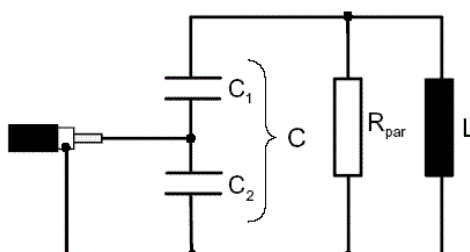


Figure: 6.28 Antenna Matching [22]

Knowing  $R_{par}$  from:

$$R_{par} = 2\pi f L Q \quad (6.15)$$

and total resonance capacitance  $C$  we can calculate the  $C_2$  and  $C_1$  using:

$$C_2 = C \sqrt{\frac{R_{par}}{Z_{cable}}} \quad (6.16)$$

$$C_1 = \frac{1}{\frac{1}{C} - \frac{1}{C_2}} \quad (6.17)$$

These values are only the starting point for tuning, as the equations are not very accurate.

### 6.7.2 Building up

We build the first antenna prototype using single layer fiberglass plate. To minimize the active resistance we put a thick layer of PbSn over the copper. Having the antenna in hand, we still don't know any of its parameters. Using different capacitors and the equation below:

$$L = \frac{1}{(2\pi f)^2 C} \quad (6.18)$$

a coil inductance of approximately 1,35 $\mu$ H has been obtained. The coil Q factor was between 6 and 13 depending of the resonance frequency for which the coil is tuned. To be able to cover a wide frequency range we need an antenna with a small Q. The realistic value that was chosen was 1.1 to 2 which will make the antenna less sensitive but in the same time more broadband. In order to obtain this low Q factor it was needed to add a damping resistor in parallel to the coil. The resistor value is calculated using:

$$R_{par} = \frac{Q_{Present} \cdot Q_{required} \cdot 2\pi f L}{Q_{Present} - Q_{required}} \quad (6.19)$$

It is a good idea to keep the resistor value close to the cable impedance.

### 6.7.3 Measuring the Quality Factor (Q)

The Quality factor of an antenna can be readily measured if we have an instrument capable of generating frequencies up to 20 MHz and a spectrum analyzer or oscilloscope.

We use the oscilloscope method, which is slightly more time consuming. In this case the maximum voltage is recorded as the frequency is adjusted and this value is multiplied by 0.707 in order to obtain the equivalent -3dB value. The frequency is then raised and lowered to get the  $f_1$  and  $f_2$  values. Response curves were also made by changing the generator frequency with a step of 0,5MHz and by measuring the generator and antenna voltage.

Table 6.7 Different configurations of response curve

Case	Capacitance [nF]	$R_{par}$	Q	$f_l$ [MHz]	$f_{res}$ [MHz]	$f_h$ [MHz]
1	1,01	No	6	4	4,4	4,73
2	1,03	68	1,75	3	4,2	5,4
3	2,07	68	2,06	2,5	3,1	4
4	2,07	47	1,46	2,05	3	4,1
5	4,6	No	13,5	2,025	2,1	2,18
7	4,6	22	1,1	1,3	2	3,1
6	0,78	No	10,7	4,68	4,8	5,13
9	0,78	56	1,23	3,32	5	7,38
10	0,132	?	?	?	12	?

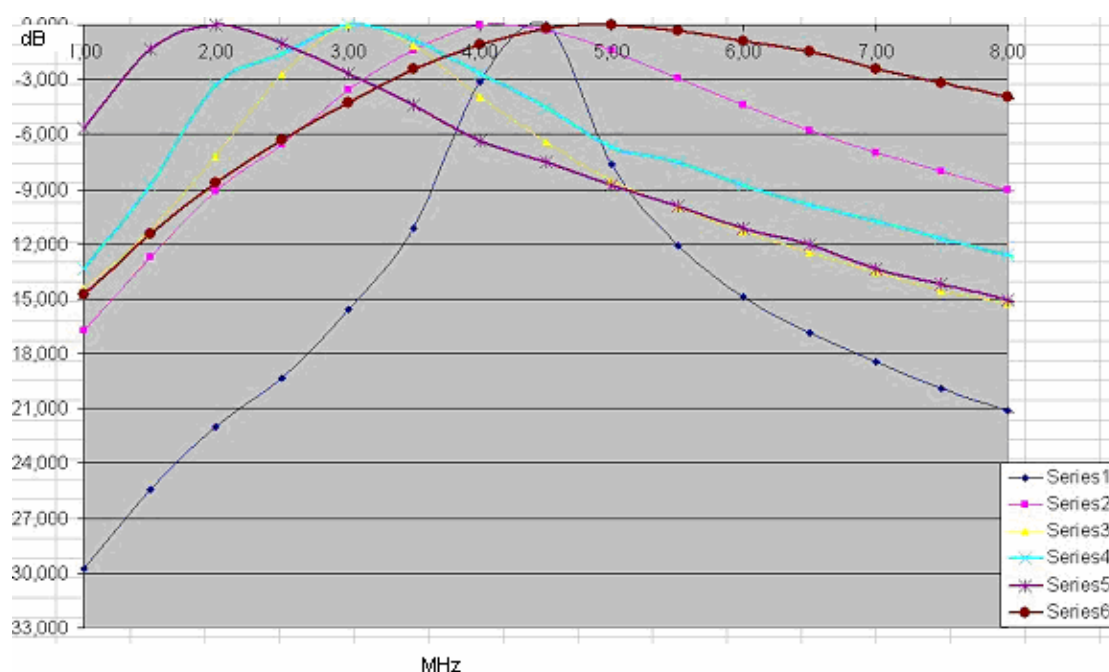
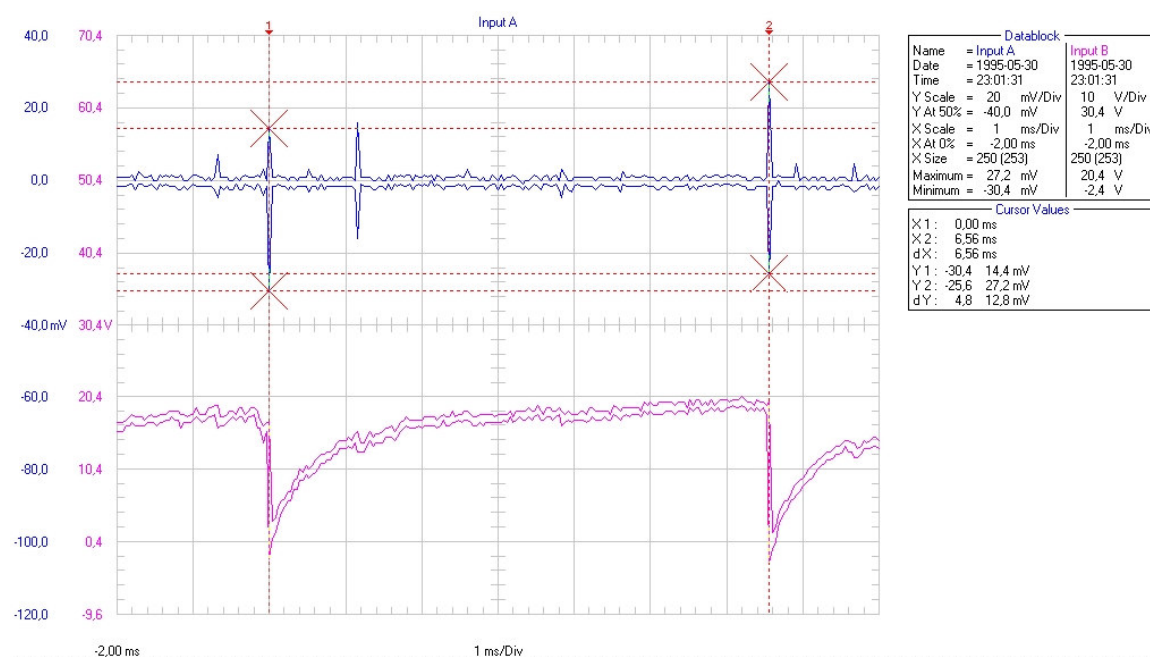


Figure: 6.29 Antenna frequency response

The coaxial cable, which we use to connect the antenna to the oscilloscope, has capacitance of 150pF. This capacitance affects the coil resonance frequency and should be kept in mind. In order to minimize the errors in all tests we use the same cable and device configuration.

### 6.7.4 Test on a synthetic and a real motor



Ch.A antenna close to the bearing, Ch.B shaft voltage. Housing is grounded by 12mm bolt 960RPM

Fig.6.30 Antenna output compared with shaft voltage. Upper one is antenna o/p and bottom one is for shaft voltage. 1 square is equal to 1 ms

Figure 6.30 presents the captured events from the synthetic test bench. It is clear, that for every voltage drop the corresponding impulse is detected by the antenna, and even more.



Fig.6.31 Synthetic test bench configuration

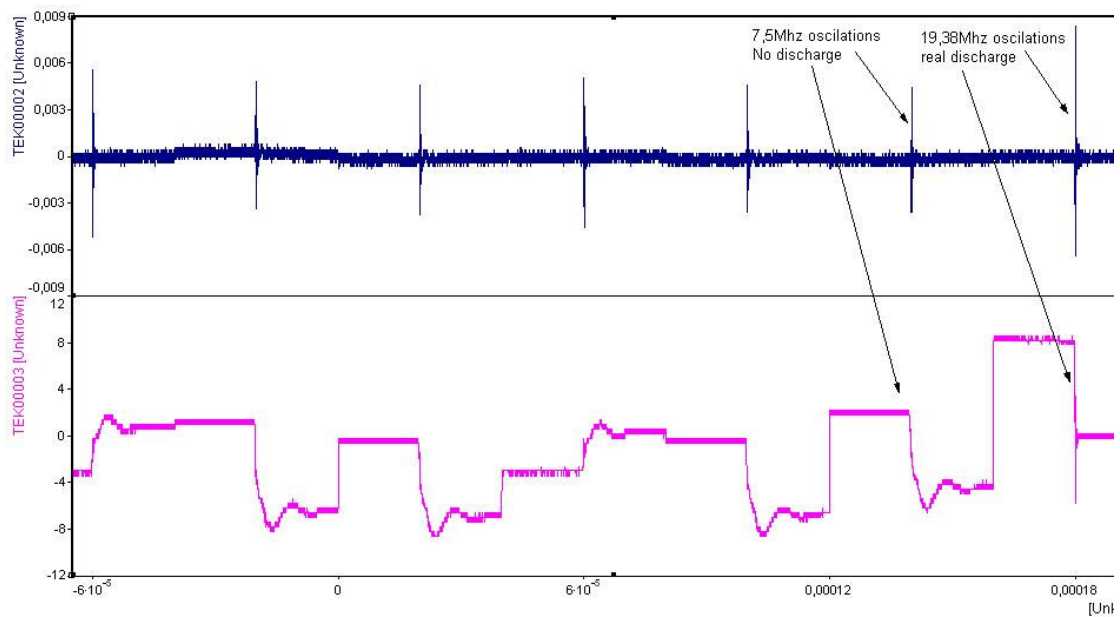


Fig.6.32 Upper one is close loop antenna output signal and bottom one is motor shaft voltage. The time subscription is  $10^{-5}$

Fig. 6.32 shows the impulses received with the closed loop antenna and the motor shaft voltage. There are two types of impulses, one with a ringing frequency of 7,5 MHz and others are, with a frequency of 19,38 MHz. Only the second one, correspond to a very steep voltage drop. At this point it can be concluded that the antenna works on both synthetic and real test configurations.

## 7 Bearing Current Measurements

### 7.1 Bearing current measurement equipment

Table 7.1 Bearing current measurement equipment, which we used

Equipment	Quantity measured	Equipment Specification	Equipment Example
High speed oscilloscope	Shaft voltage/current/frequency	500 MHz	Tektronix TDS 544A
High frequency current probe	Shaft current	200 MHz	Pearson current monitor -2877
Co-axial shunt	Motor drive shaft current	20 MHz	HM
High frequency current probe	Motor drive shaft current	10 MHz bandwidth	PEM high frequency Rogowski coil CWT-1
Oscilloscope	Shaft voltage/current/frequency	1 MHz	Fluke 123

### 7.2 Synthetic test configuration

To perform bearing current measurements, a small test bench was constructed. It consists of three SNL bearing housings mounted on massive cast iron table using 10mm isolating plates. These housings are used to support the bearings, which are mounted on the same shaft. On the same table, one 7.5 kW motor is mounted. In order to insulate the motor from the table, plastic spacers were used. The shaft is connected to the motor using flat belt. To control the motor speed, one very old Danfoss thyristor based frequency converter was used.

To provoke discharge-bearing currents, we connected our impulse circuit to one end of the shaft using slip ring. On the other end another slip ring is used for shaft voltage measurement. The impulse circuit can provide impulses with six different time constants. To provide a low impedance path for the bearing currents, one of the SNL housing should be grounded. A coaxial shunt, a Rogowski coil or a current transformer can be used in this connection for current measurement.

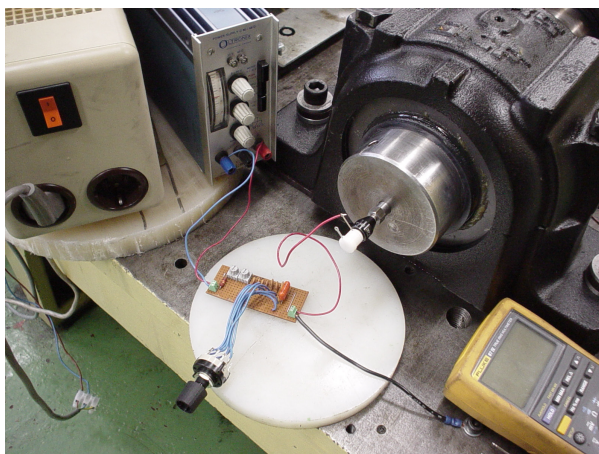


Fig. 7.1 Impulse circuit

### 7.2.1 Measuring system

As a measuring device, a handheld oscilloscope Fluke 123 and Compaq Contura as storage device was used. The Fluke View computer software was used for visualization of the recorded events. As current probes we experimented with DIY coaxial shunt, Pearson current monitor and DIY antenna. In our first measurements, the antenna was simply two pieces of wire.

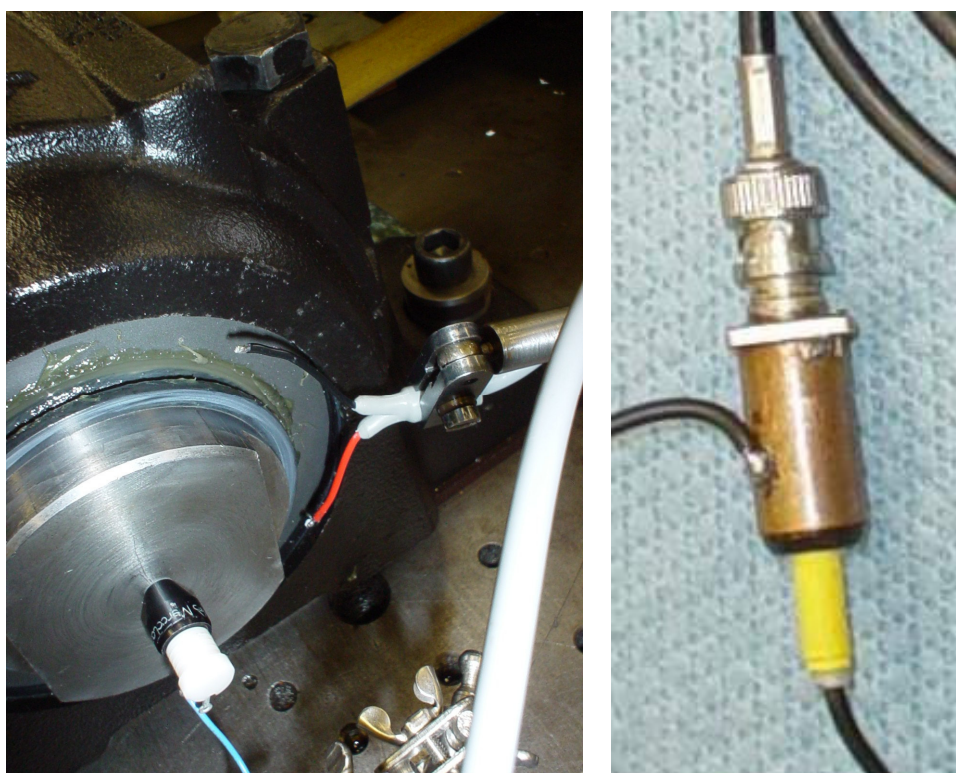


Fig. 7.2 Antenna and DIY coaxial shunt

## 7.2.2 Measuring Procedure

From the very beginning we started using the Fluke 123 oscilloscope. The shaft voltage was displayed on channel B, and the bearing currents on channel A. The trigger input was in most of the cases set to channel A. In some cases the shaft voltage falling front was used as a triggering point.

The coaxial shunt and Pearson current monitor was always connected between the bearing housing number three and the metal table. The antennas were placed in many different positions and distances around the motor in order to obtain a stronger signal. The measurements were performed with different fixed shaft speeds and different impulse time constants.

The events were recorded in real-time and storage mode.

## 7.2.3 Obtained Results

The quality of the displayed signals is not so high, but it is enough to see the relation between the shaft voltage and the signal obtained from the dipole antenna.

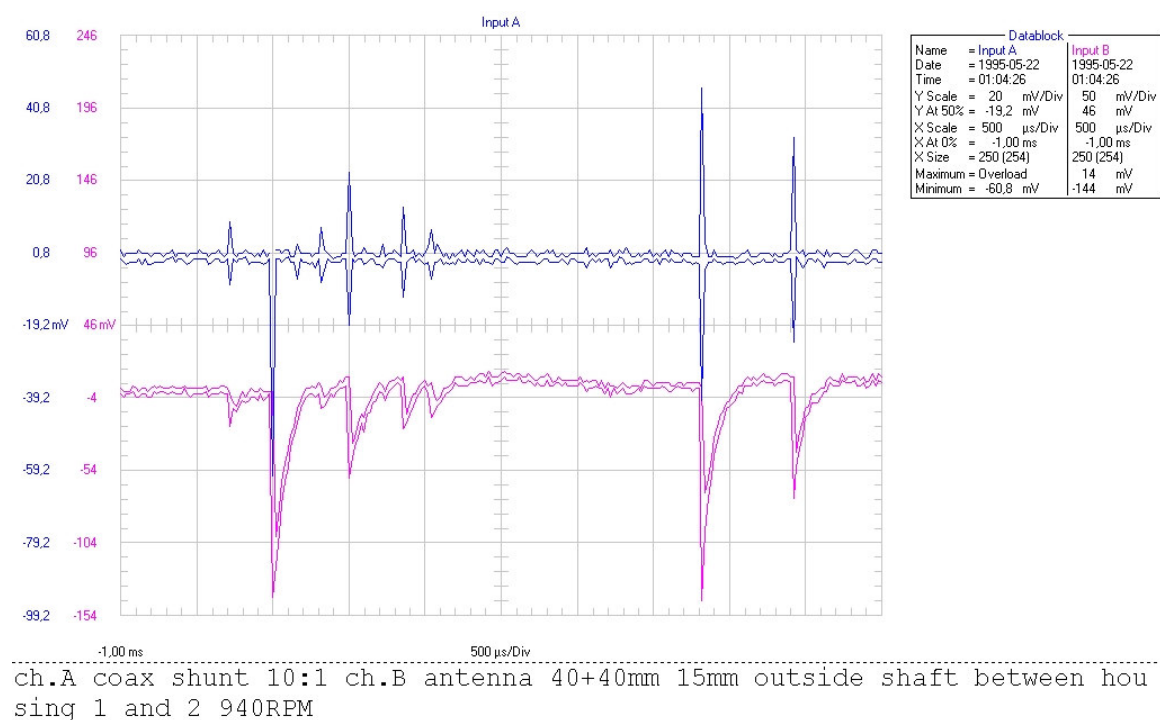
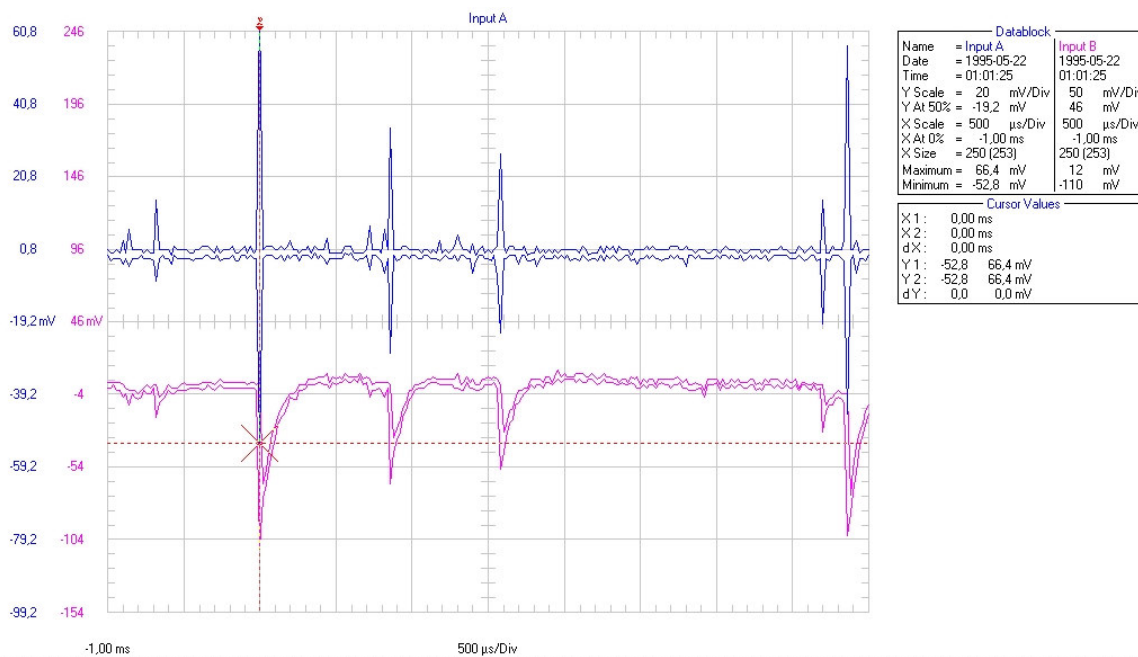


Fig. 7.3 Upper one is OLA output and the bottom is shaft voltage output. 1 square is equal to 500  $\mu$ s.

As it can be seen from Fig.7.3, the captured events using the antenna exactly match the current pulses captured from the coaxial shunt. It can be observed that the antenna voltage pulses are proportional to the current pulses. Not exactly, but this tendency is clearly visible with naked eye.

We performed a large number of measurements with different antenna positions.

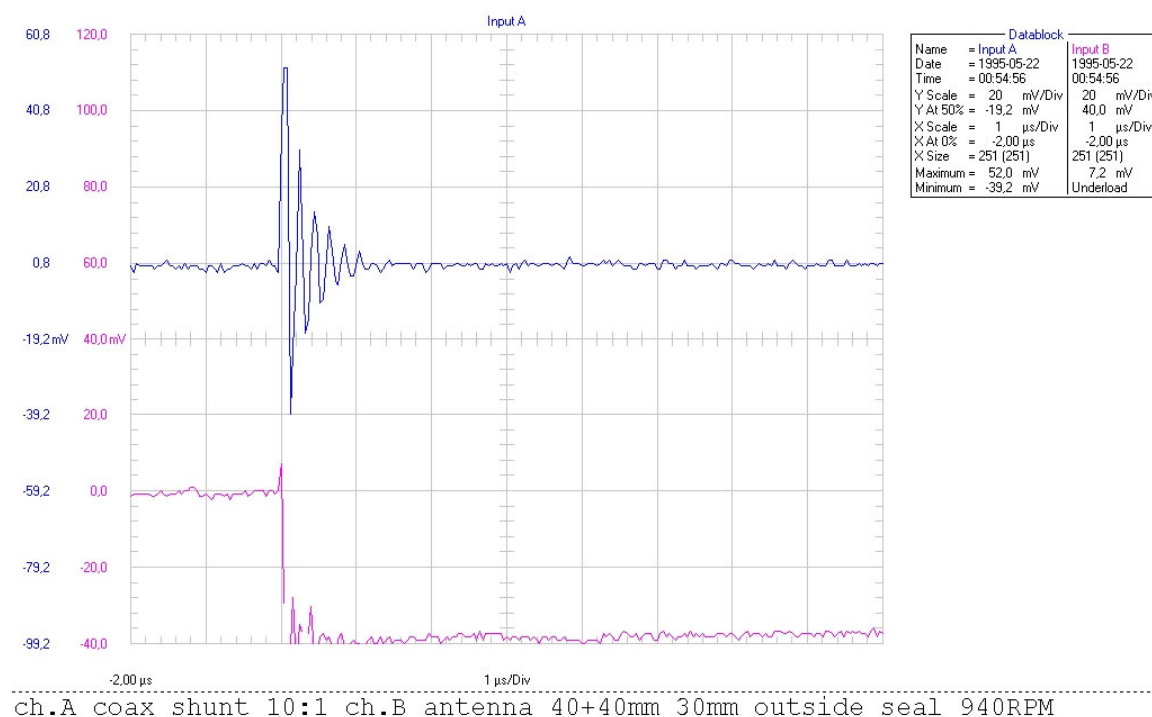


ch.A coax shunt 10:1 ch.B antenna 40+40mm 15mm outside shaft centre 940R PM

Fig.7.4 Upper one is OLA output and the bottom is shaft voltage output. 1 square is equal to 500  $\mu$ s.

Fig.7.4 presents the signal captured, when the antenna is placed in front of the right shaft end. The antenna voltage again precisely follows the current pulses captured with the shunt.

Let's take a look on one event, when the oscilloscope time resolution is set to 1  $\mu$ s/Div. From fig.7.5 it can be observed that the starting time of the current impulse match the time when antenna voltage drops down.



ch.A coax shunt 10:1 ch.B antenna 40+40mm 30mm outside seal 940RPM

Fig.7.5 Upper one is OLA output and the bottom is shaft voltage output. 1 square is equal to 1 μs.

The current pulse has a 5 MHz oscillation. There are almost no oscillations in the antenna output signal. At this point of our measurements we had a suspicion, that the bearing current, that flows from the housing to the table can be captured with some kind antenna. This was a promising result and we decide to test it on a real motor.

### 7.3 7.5kW motor test configuration

In these tests the same test bench was used. The difference is that instead of using our impulse-generating circuit to provoke discharges, we used a real motor, connected to Danfoss frequency converter.

The coaxial shunt was connected between the motor housing and the table. We made several tests with different antenna placements. The most interesting results were obtained when the antenna is placed in front of the motor shaft end and close to the cooling fan cover. In order to monitor the motor shaft voltage, one slip ring was used.

#### 7.3.1 Measuring Procedure

The same equipment as in the previous set up was used. For the each antenna position several events were captured and clear ones was saved.

The events were recorded in real-time and storage mode.

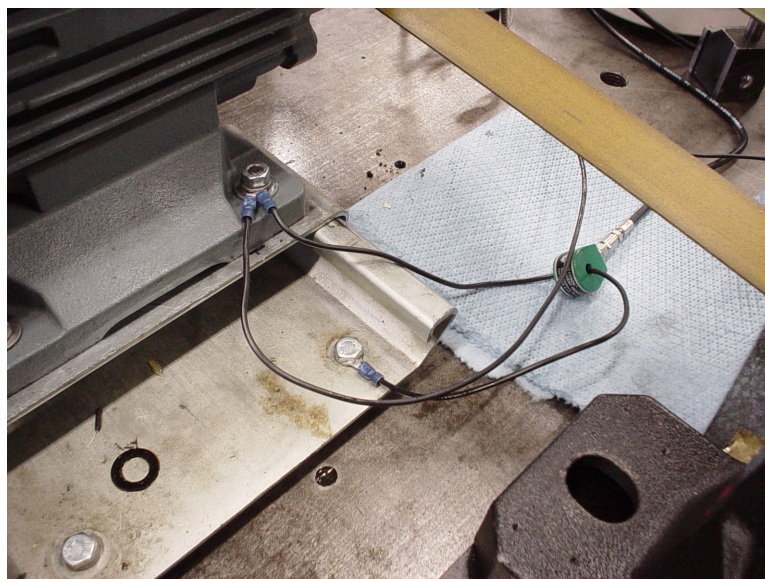


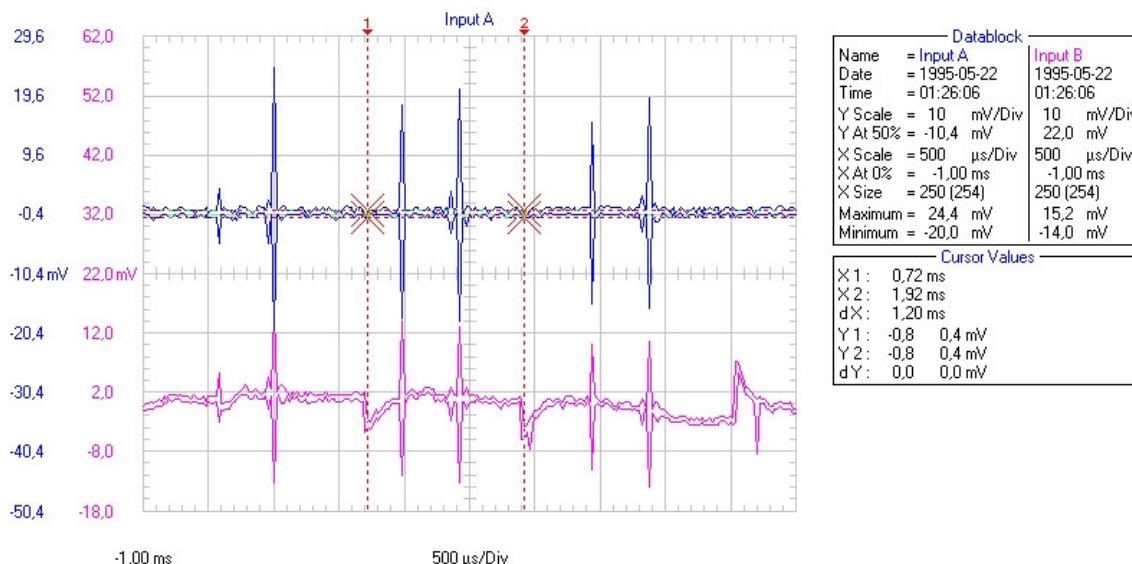
Fig.7.6 Frame to ground connection and the current monitor

Fig.7.6 shows the current probe connection. Instead of the coaxial shunt the Pearson current monitor can be seen.

### 7.3.2 Obtained Results

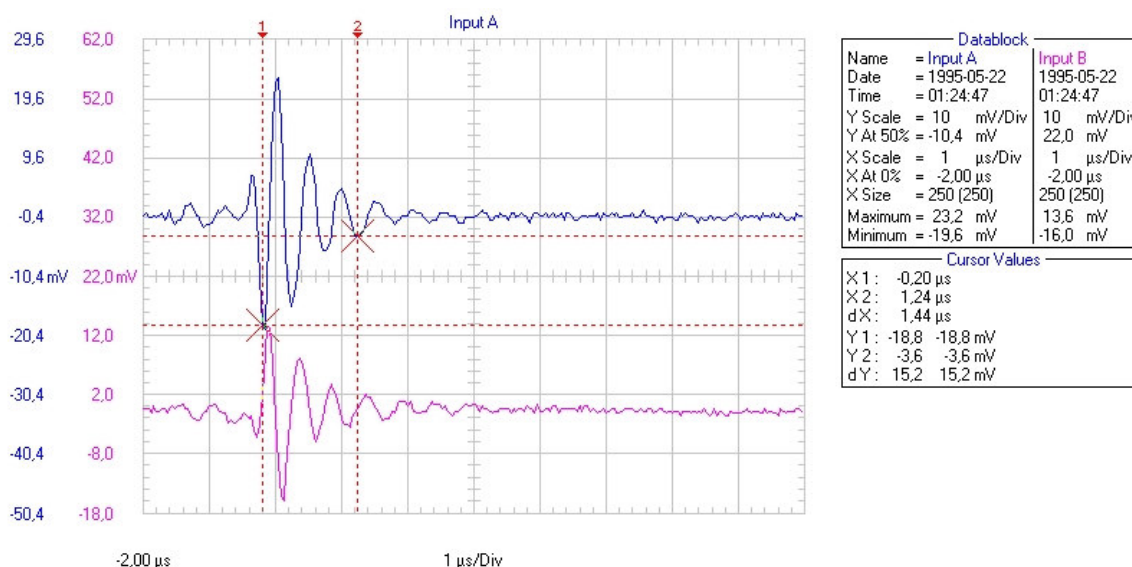
For the first measurement we placed the antenna 30mm in front of the motor shaft end. The coaxial shunt was connected as it is described above. From the upper trace in fig.7.7, an impulse repetition with a frequency of approximately 8kHz can be observed. This seems to be linked to the converter switching frequency. Also from the bottom trace, two types of impulses can clearly be seen, one with a higher magnitude and tendency for repetition and another, which looks like a "capacitor charging" slope. All peculiarities give a sign that the antenna output signal is more related to the electric, instead to magnetic field.

The current impulse shown in Fig.7.8 has ringing frequency of about 2.08MHz, which is more than two times smaller than the impulse oscillations obtained from the Synthetic test configuration.



ch.A coax shunt 10:1 ch.B antenna 40+40mm 30mm in front of the shaft 831 RPM 8kHz inverter freq?

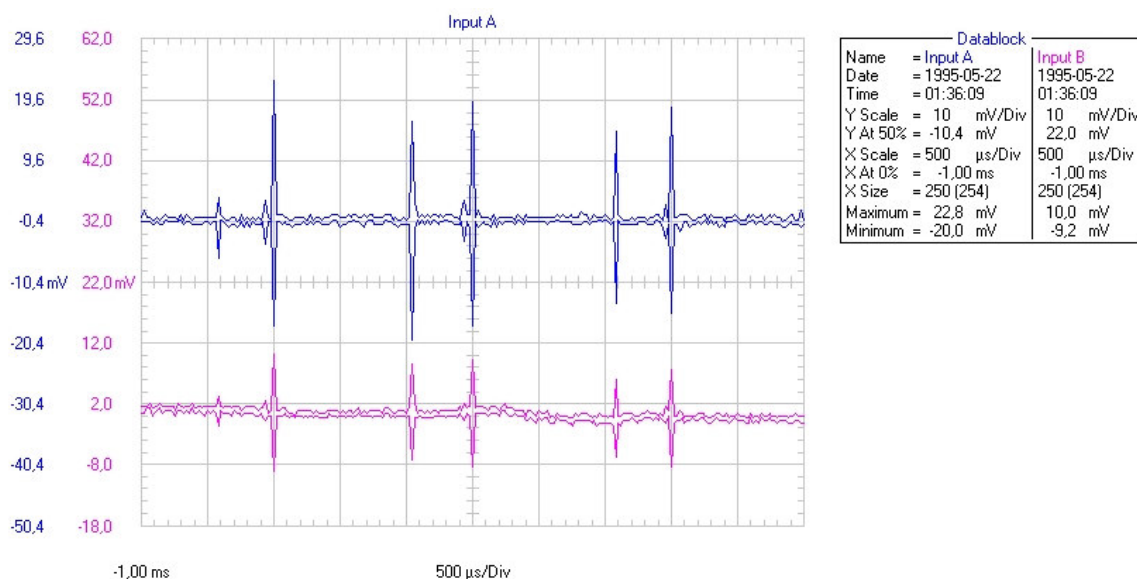
Fig.7.7 Frame to ground current (bottom) and antenna voltage (upper) measured 300mm in front of the motor shaft. 1 square is equal to 500  $\mu$ s.



ch.A coax shunt 10:1 ch.B antenna 40+40mm 30mm in front of the shaft 831 RPM 2,08Mhz oscillations

Fig.7.8 The same conditions as for previous figure. Oscilloscope time is set to 1 $\mu$ s/Div

Fig.7.9 presents the shunt current, flowing from the motor frame to the table and antenna voltage. The signal, obtained by the antenna, follows closely the shunt current. At this time, it can be considered as a good result, the only confusing thing is the repetition of the signal. Normally the discharge phenomena should have a random distribution.

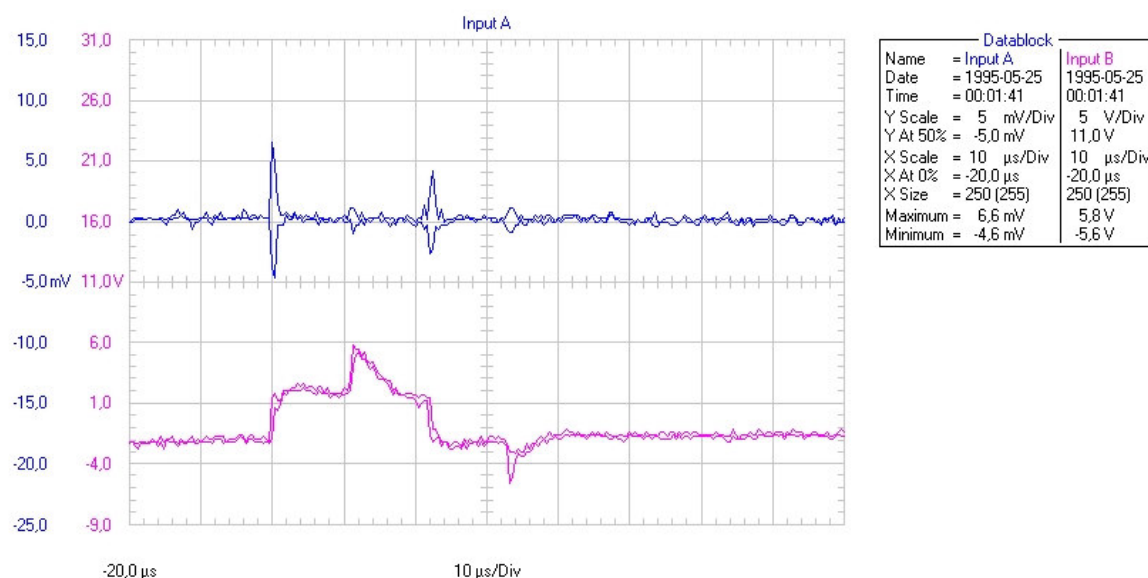


ch.A coax shunt 10:1 ch.B antenna 40+40mm outside the cooling fan cover  
831RPM

Fig.7.9 Frame to ground current (bottom) and antenna voltage (upper) measured close to the cooling fan cover. 1 square is equal to 500 μs.

In all captured events a good relation between the antenna voltages and the captured current pulses can be seen. The question is: are these pulses discharge current or not? To make the picture clearer, instead of comparing the antenna output with the shunt output, we try to compare it with the shaft voltage. We also put the antenna close to the motor feeding cable.

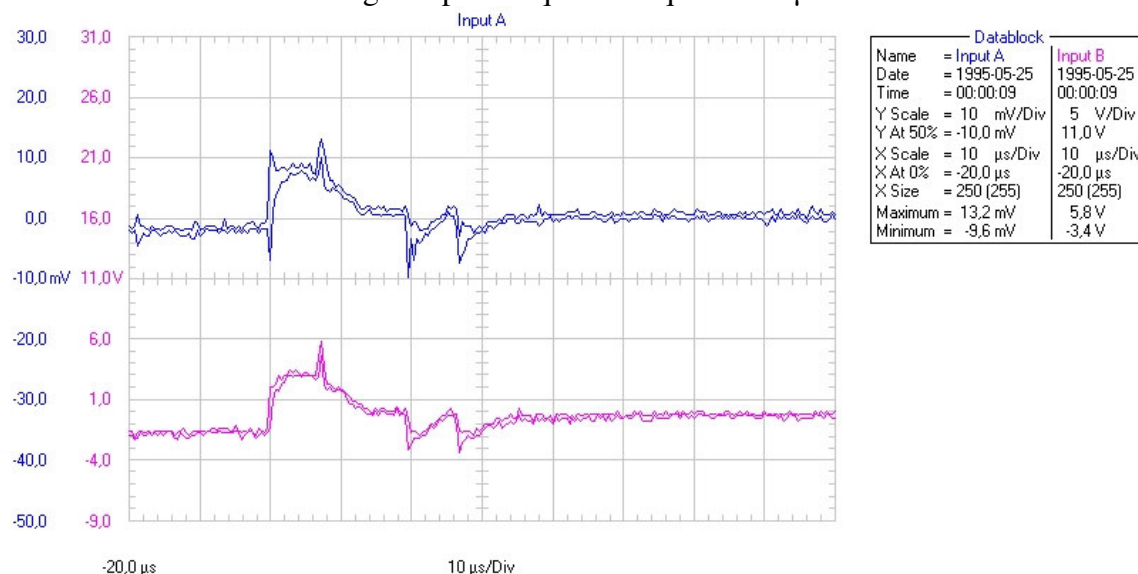
Fig.7.10 and fig.7.11 presents the signals obtained from two different locations



Antenna outside fan cover, ch.B shaft voltage, slip ring 160  
0RPM

Fig.7.10 The antenna is placed close to the motor fan cover. Upper one is OLA output

and the bottom is shaft voltage output. 1 square is equal to 10  $\mu$ s.



Antenna between pulley and motor, ch.B shaft voltage, slip ring 160 ORPM

Fig.7.11 The antenna is placed between belt pulley and motor housing. Upper one is OLA output and the bottom is shaft voltage output. 1 square is equal to 10  $\mu$ s.

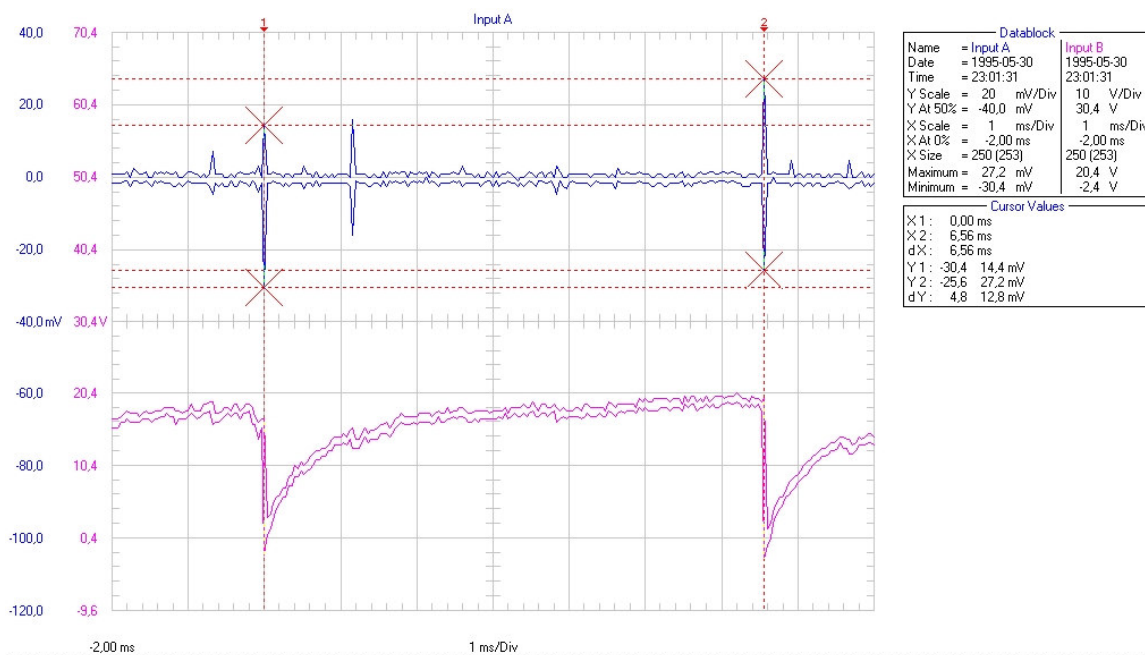
From fig.7.11 it can be seen that, the antenna voltage follows the shaft voltage very closely, which is not the case in fig.7.10. When the antenna is placed outside the fan cover, the antenna voltage does not follow the shaft voltage. At this position there is only a match between the rising and falling edges and the antenna output. Two more voltage shaft pulses can be seen, which are missing in the antenna output. This is a sign that this type of antenna is not suitable for discharges detection. Its output is more related to the disturbances emitted from the cables, converter and the surrounding equipment.

## 7.4 Closed loop antenna

### 7.4.1 Synthetic test configuration

The first antenna shows good results on a synthetic test configuration but fails in a noisy environment. Now we have a completely new antenna with a different design, which now will be investigated. To do this, we will follow almost the same measurement procedure as before. A synthetic test configuration will be used first.

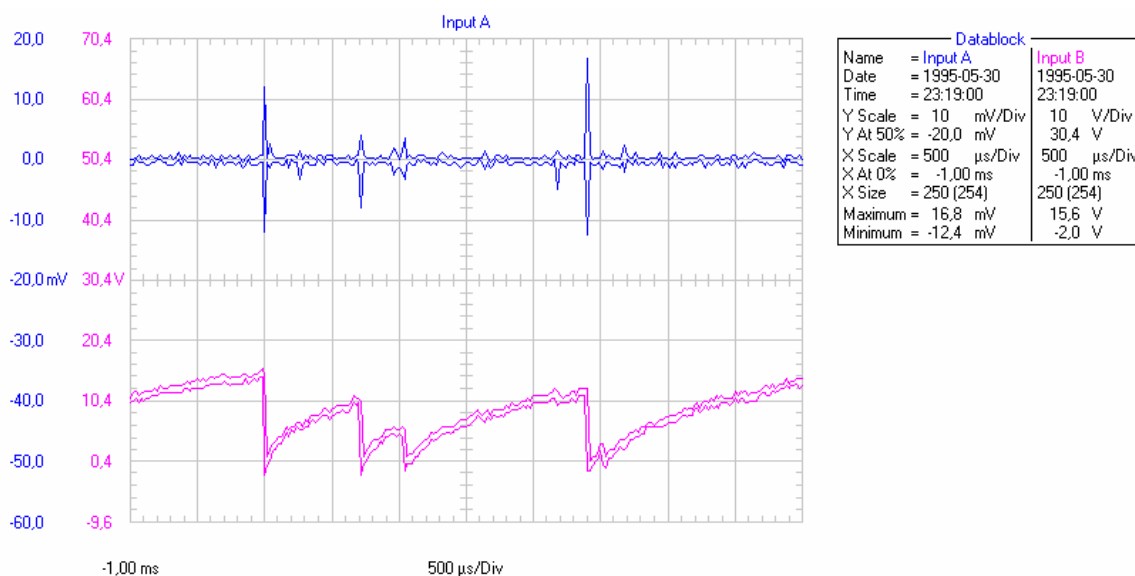
For the very first test, the antenna was placed close to housing number three. A 12mm bolt was used to ground it. This type of grounding removes the possibility of having radio emissions from the grounding cable. It also provides a very low impedance path compared to the bearing impedance in the conducting stage. The antenna output voltage and the shaft voltage can be seen in fig.7.12.



Ch.A antenna close to the bearing, Ch.B shaft voltage. Housing is grounded by 12mm bolt 960RPM

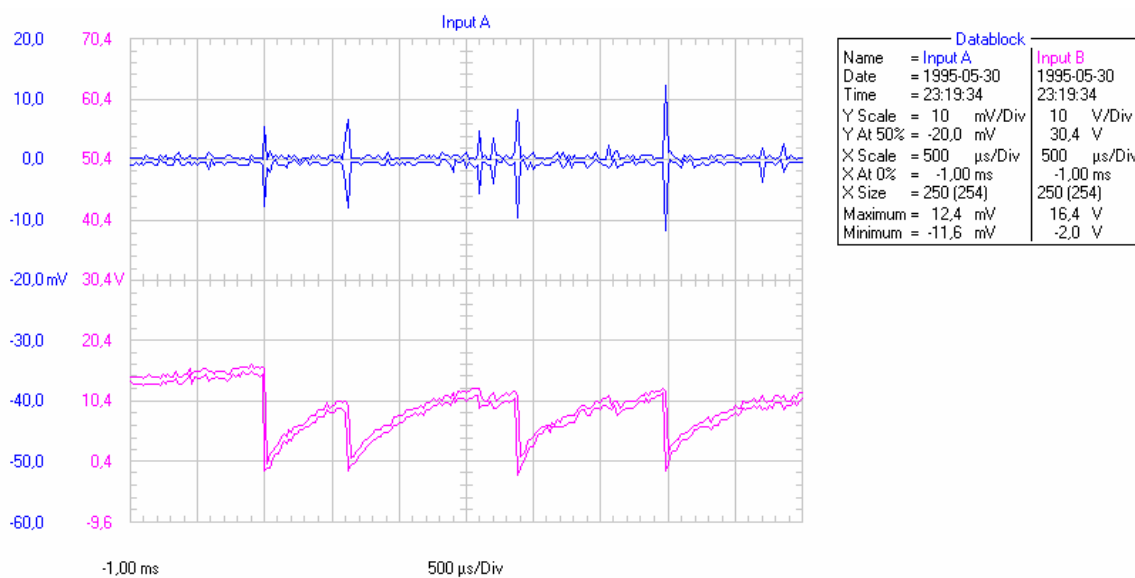
Fig.7.12 DA output (upper) and shaft voltage (bottom). 1 square is equal to 1 ms.

In this case the discharge repetition time is 6.5ms, which corresponds to a frequency of 154Hz. Initially the shaft voltage increases with the preprogrammed time constant until it reach the bearing threshold value. For a speed of 960RPM and bearing temperature of approximately 24 degrees, the threshold voltage was 20V. The observed shaft voltage drop is a secure indication for discharge inside the bearing. For every voltage drop we can see the corresponding impulse detected with the antenna, and even more. There is one more pulse, which should not be here. Its origin is not known.



Ch.A antenna 150mm over the housing, Ch.B shaft voltage. Housing is grounded by 12mm bolt 960RPM

Fig.7.13 The antenna is located 150mm over the third housing. DA output (upper) and shaft voltage (bottom). 1 square is equal to 500 μs.



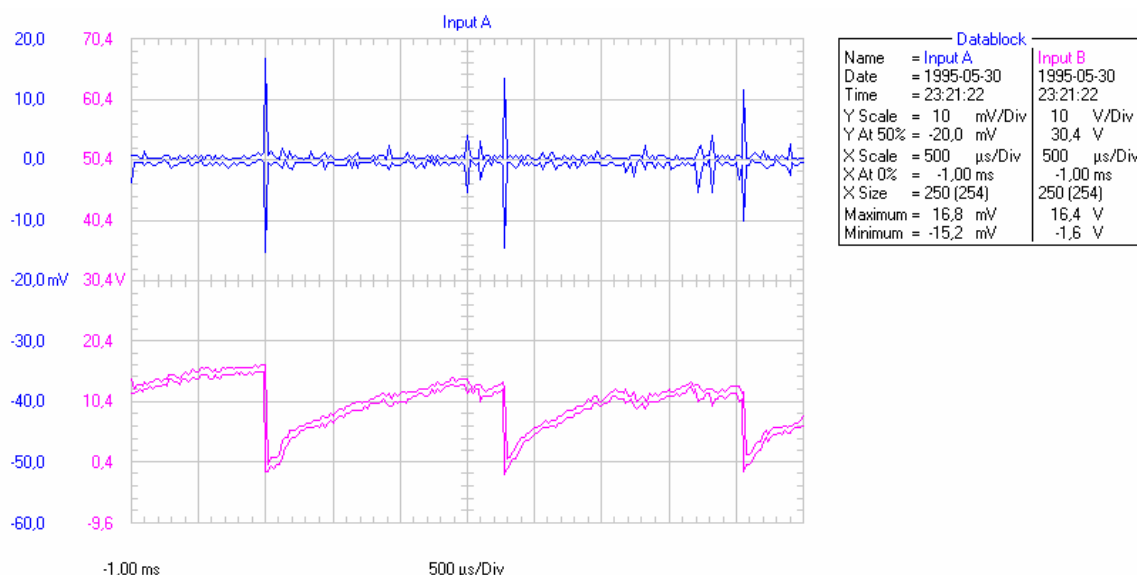
Ch.A antenna 150 mm in front of the shaft, Ch.B shaft voltage. Housing is grounded by 12mm bolt 960RPM

Fig.7.14 The antenna is located 150mm in front of the right shaft end. DA output (upper) and shaft voltage (bottom). 1 square is equal to 500 μs.

In order to find the best place for the antenna, different locations and distances were tried. In Fig.7.13 and Fig.7.14 the obtained signals from 150mm distance where the antenna is placed over the SNL housing and in front of the shaft end are shown. In both cases for every change in the shaft voltage we have an indication from the antenna. At this case the threshold voltage goes down due to the increase of lubrication oil temperature.

Based on the obtained results upto now, it can be concluded that the discharges can be counted easily. The question is how far away from the shaft that the antenna can be placed.

In order to investigate this, the antenna was placed 600mm away from the housing. The result was impressive. We still receive a strong signal.

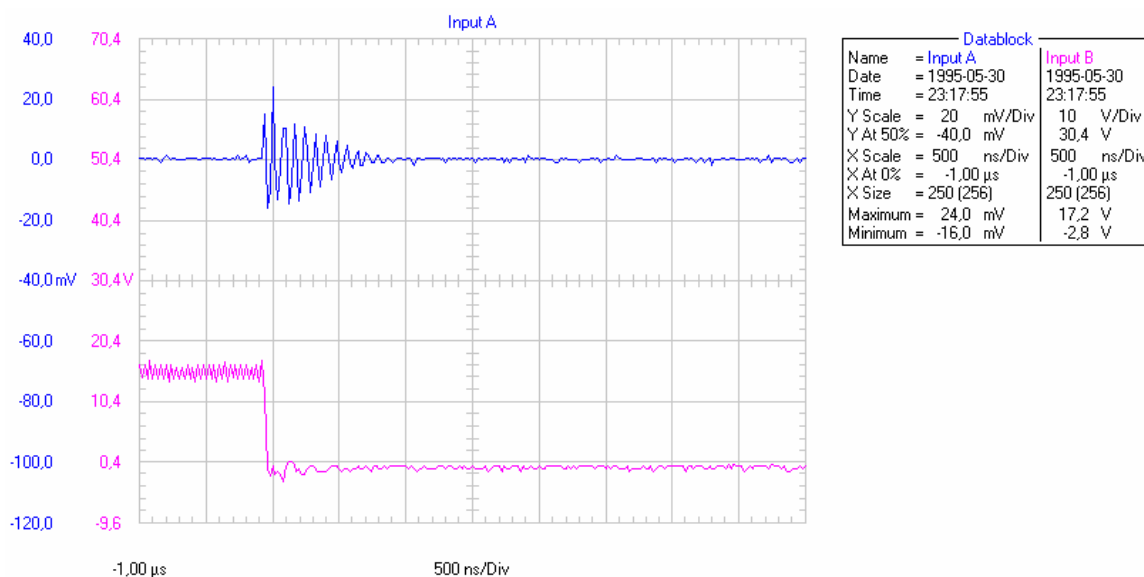


Ch.A antenna 600 mm in front of the shaft, Ch.B shaft voltage. Housing is grounded by 12mm bolt 960RPM

Fig.7.15 Received signal from antenna, placed 600mm away if the housing. DA output (upper) and shaft voltage (bottom). 1 square is equal to 500 μs.

After a half an hour the temperature of the bearing housing increased and the received signal is not that strong any more. The threshold voltage goes down and the signals received by the antenna decreases.

In order to study the impulses more in detail the time resolution was decreased. The result can be observed in Fig.7.16



Ch.A antenna 150mm over the housing, Ch.B shaft voltage. Housing is grounded by 12mm bolt 960RPM

Fig.7.16 DA output (upper) and shaft voltage (bottom). 1 square is equal to 500 ns.

When the shaft voltage goes down, a corresponding impulse is received with the antenna. This impulse has a ringing frequency of 8MHz. The shaft voltage has a very stiff slope that is clear indication for bearing current. At this point we decided to tune the antenna to 8Mhz center frequency and to try to obtain the lowest possible Q factor.

#### 7.4.2 7.5kW motor test configuration

Using the test described earlier it will be shown that the closed loop antenna will give as a secure reading of bearing discharge, taking place in the synthetic test configuration. The remaining question now is, whatever it is capable to detect "bearing discharges" in the real motor or not.

To be able to compare the closed loop antenna and open loop one, we chose the same 7,5kW motor as a test object. The same test configuration was used. The shaft voltage is displayed on oscilloscope channel B. The connection was made using slip a ring. The antenna was placed on different locations around the motor in order to find the best reading. It was connected to channel A.

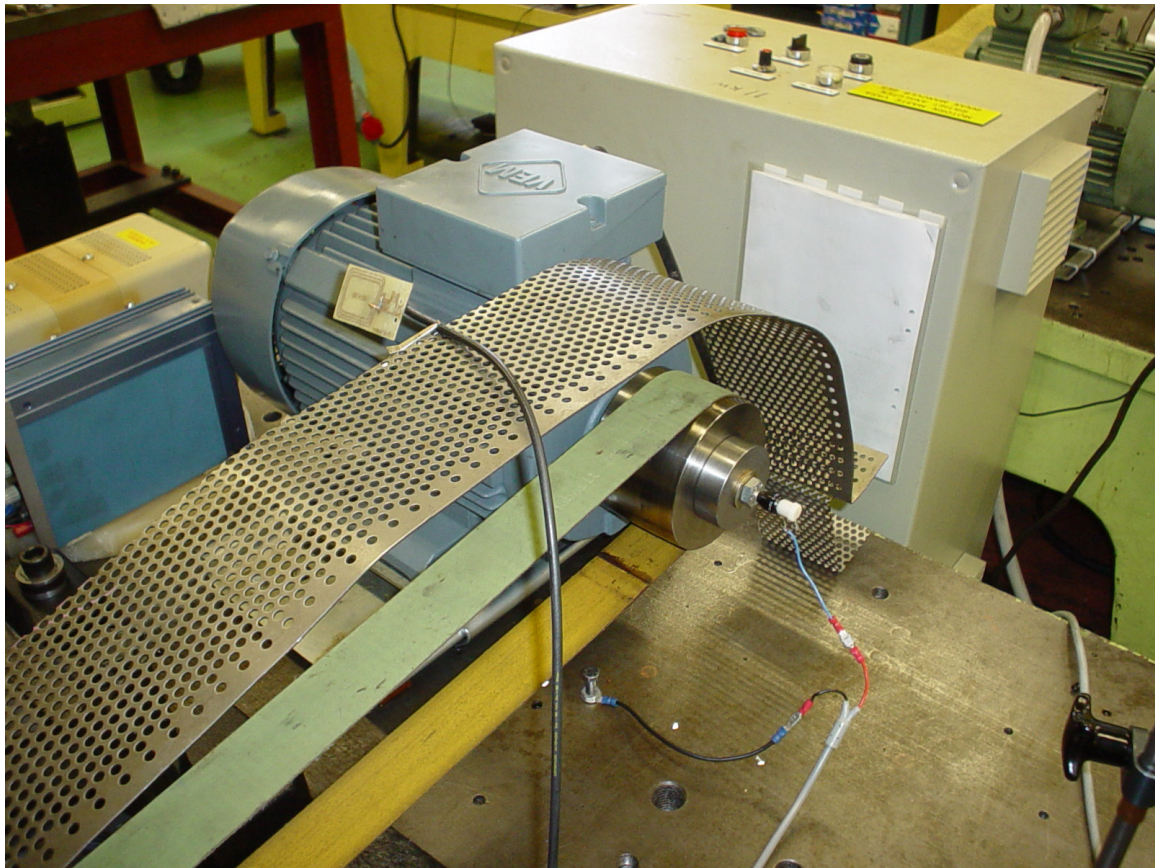
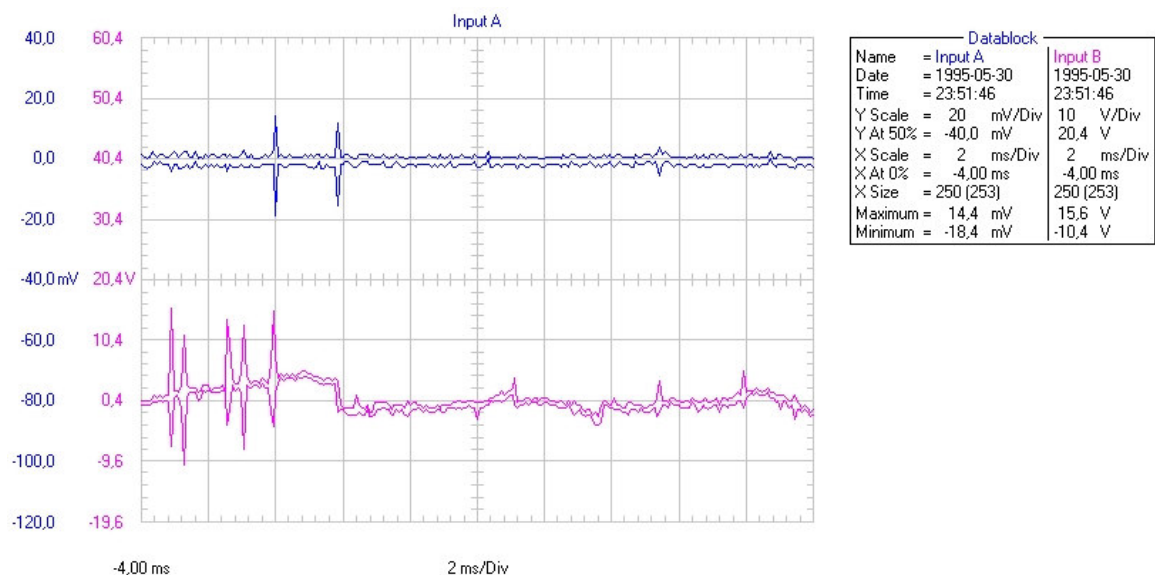


Fig.7.17 Shaft connection and antenna placement

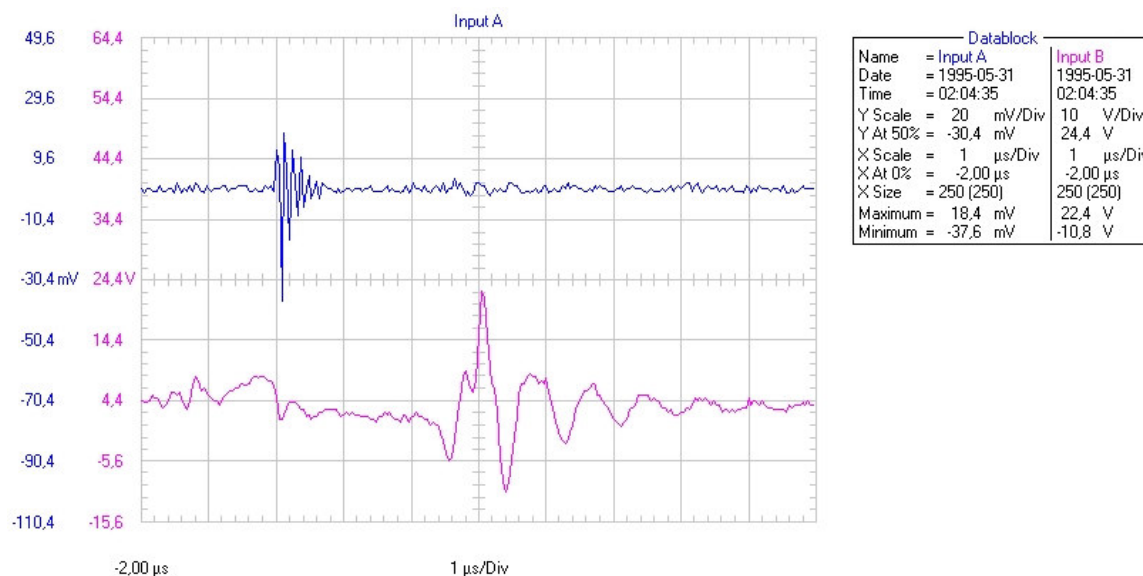
On Fig.7.17, the shaft connection and the antenna, placed close to the motor frame are presented. The signals obtained from this location can be seen on Fig.7.18



Ch.A antenna 100mm beside of the motor. Ch.B shaft voltage 850RPM

Fig.7.18 Antenna output (upper) and motor shaft voltage (bottom).1 square is equal to 2 ms.

The difference between the two signals can clearly be seen. Using the DA, we capture only two impulses, in contrast to the motor shaft voltage (MSV). It seems that the antenna output is not pure dependent of the MSV. It seems like the output signal is related to something else. In Fig.7.19 the DA output voltage is presented.

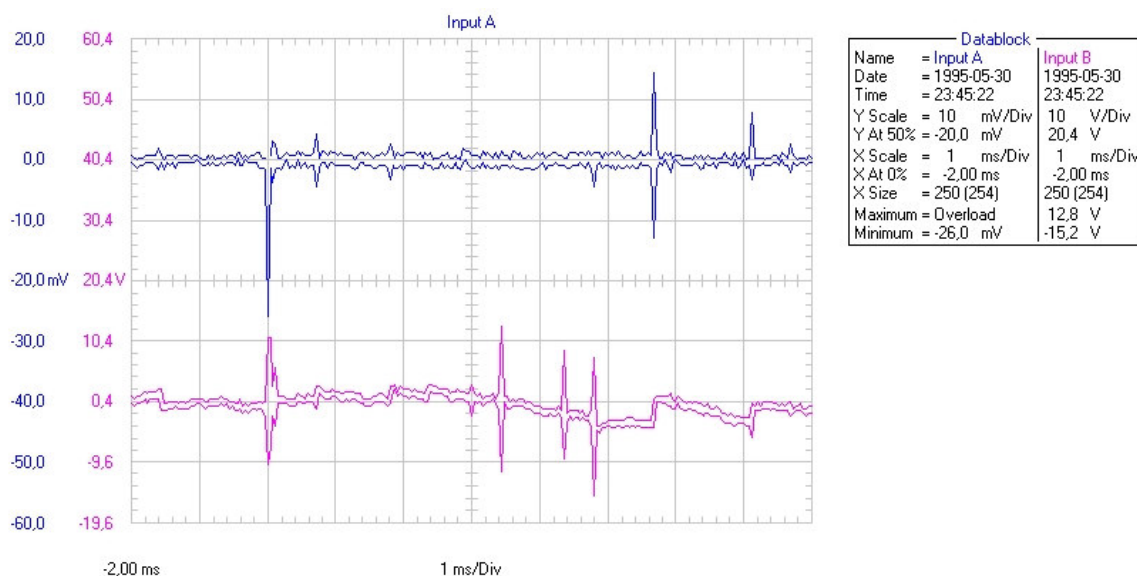


Ch.A antenna 100mm beside the motor, Ch.B shaft voltage 1000R PM

Fig.7.19 Total "mismatch" between DA output and the motor shaft voltage.

The impulse received from DA has a corresponding voltage drop in the motor shaft of about 9V. After 3μs, high voltage oscillations are observed in the motor shaft, but nothing came from the antenna.

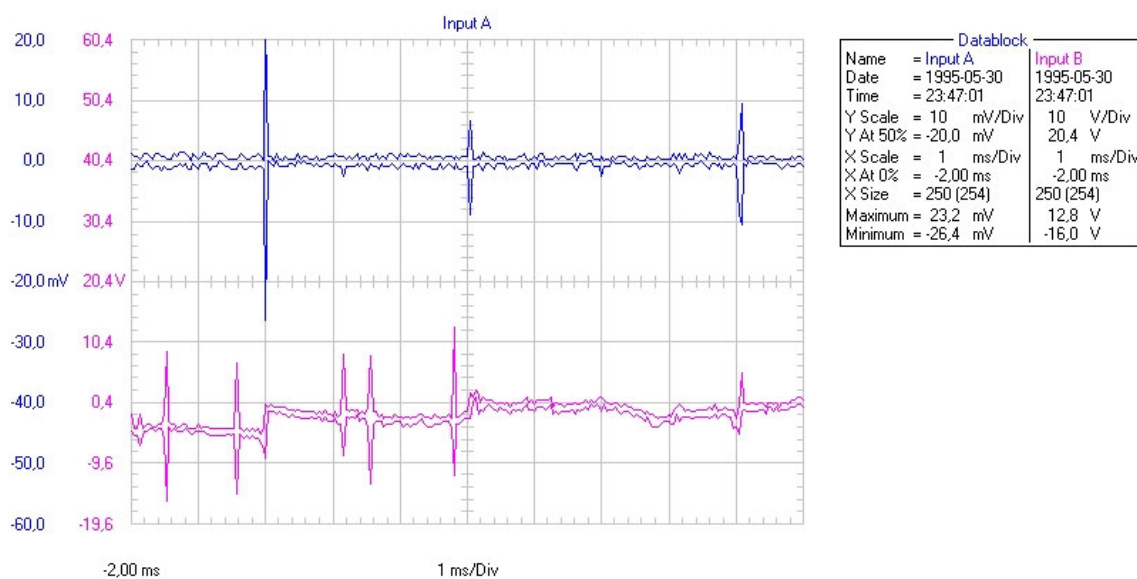
As was mentioned before, the antenna was placed in front of the motor at different distances. It was unexpected that the DA output didn't follow the MSV. Placing it 150mm away, for the last two voltage drops, corresponding DA pulses are obtained; there is also one for the first big MSV impulse. According to the technical papers, the last two voltage changes are good indication of bearing currents. For three of the MSV pulses there is no output from the antenna. At this point it can be observed that there is some kind of pulse separation, which gave as an opportunity to detect bearing discharge currents.



Ch.A antenna 150mm in front of the motor shaft. Ch.B shaft voltage 850RP M

Fig.7.20 DA (upper) and motor shaft voltages (bottom). 1 square is equal to 1 ms.

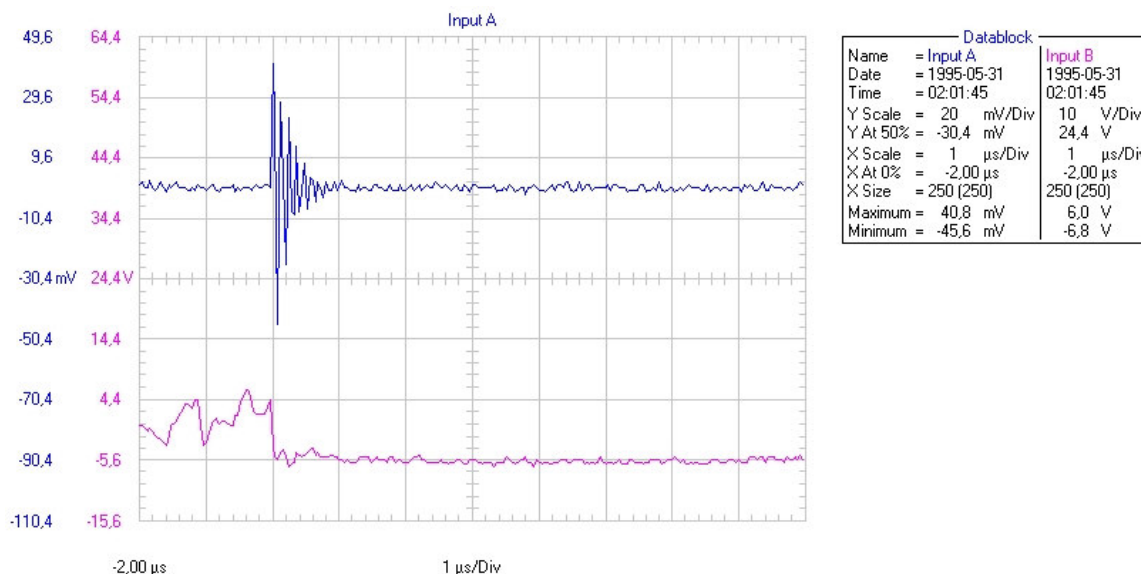
The situation is almost the same when the antenna is placed 600mm away of the motor. The signals presented in Fig.7.20 will only confirm our expectations. We can detect the discharges.



Ch.A antenna 600mm in front of the motor shaft. Ch.B shaft voltage 850RP M

Fig.7.21 DA output (upper) compared with motor shaft voltage (bottom). 1 square is equal to 1 ms.

Fig.7.21 is an only one example, how the antenna output and the MSV looks like when they match.

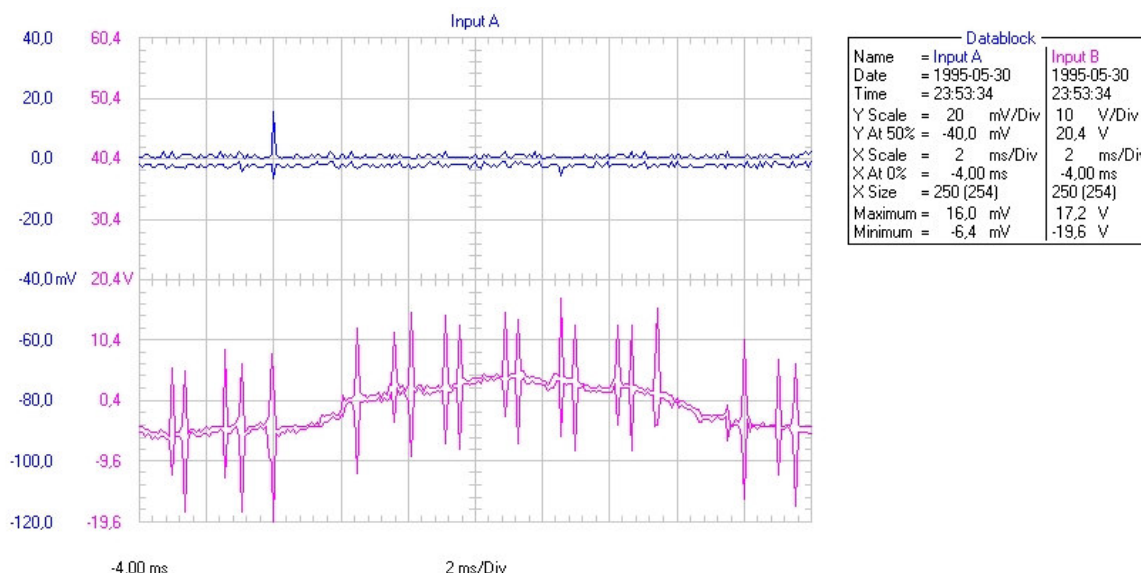


Ch.A antenna 150mm in front of the motor shaft, Ch.B shaft voltage 1000R PM 8MHz ringing

Fig.7.22 Almost 10V voltage drop (bottom) and the corresponding impulse, received from DA (upper). 1 square is equal to 1 μs.

Probably someone will ask why the MSV goes to -5,6V? One of the reasons is that the oscilloscope input was set to AC coupling. Another one is that the MSV is never zero; it changes positive and negative and vice versa during the time.

A good example of "impulse separation" is presented on Fig.7.23



Ch.A antenna 50mm in front of the fan cover. Ch.B shaft voltage 850RPM.hot bearing

Fig.7.23 The upper one is DA output and the bottom one is for shaft voltage. 1 square is equal to 2 ms.

There is only one impulse coming from DA, compared to the big series in the MSV. With the information given earlier we calculated that the Fluke 123 was useless. Its great advantage is that it is handheld but it does not provide enough samplings frequency. In reality, it is just a 1Mhz oscilloscope.

We will conclude in one sentence. Great beginning. Lets now improve the antenna and use a better oscilloscope.

## 7.5 Measurements using Tektronix TDS 544A

### 7.5.1 Dipole antenna

In the first measurement setup using the Tektronix oscilloscope we used the three bearing synthetic test configuration driven by the 7.5kW motor. The oscilloscope was connected to our first dipole antenna, the Pearson current probe and the slip ring cable. The shaft speed was set to 966 RPM.

All three signals can be seen from Fig.7.24. The upper one is the shaft voltage, the middle is the housing to ground current and the bottom one is the dipole antenna. The antenna voltage follows closely the shaft voltage. The outputs from the Pearson probe also match to the shaft voltage except for the first discharge. There is no indication that at this point we have current flow between the SNL housing and ground. At the same time the shaft voltage goes to zero, which is clear indication for bearing discharge. It is also possible that a discharge has taken place in one of the other two bearings.

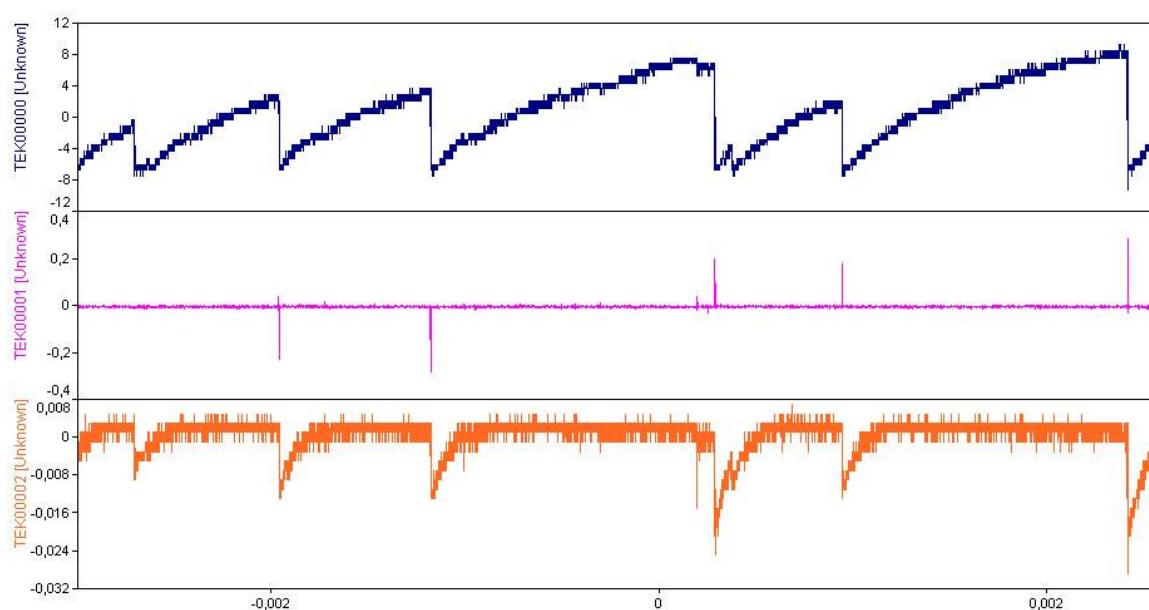


Fig.7.24 Shaft voltage (upper), Pearson probe (middle) and dipole antenna (bottom).

### 7.5.2 7.5kW motor with Pearson current probe

The 7,5kW motor was connected to the old VLT20 Danfoss converter. The motor shaft voltage and the frame to ground current was monitored. Pearson current monitor model 2877 was used in the frame to ground current detection.

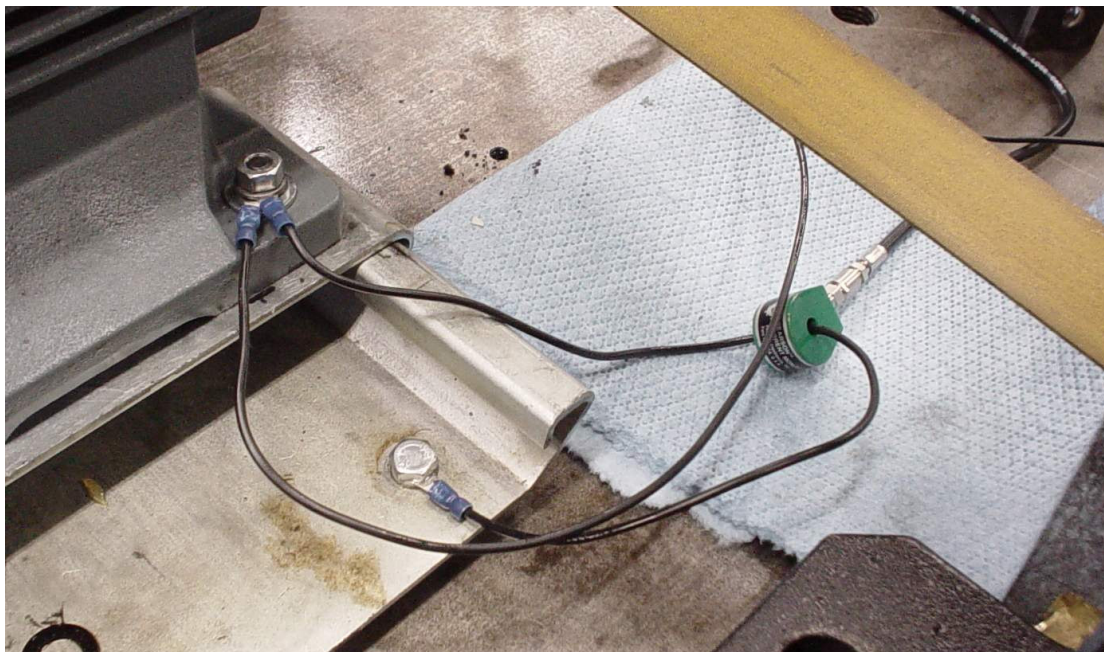


Fig.7.25 Pearson current monitor connected between motor frame and ground

On Fig.7.26 the shaft voltage and frame to ground current waveforms are present.

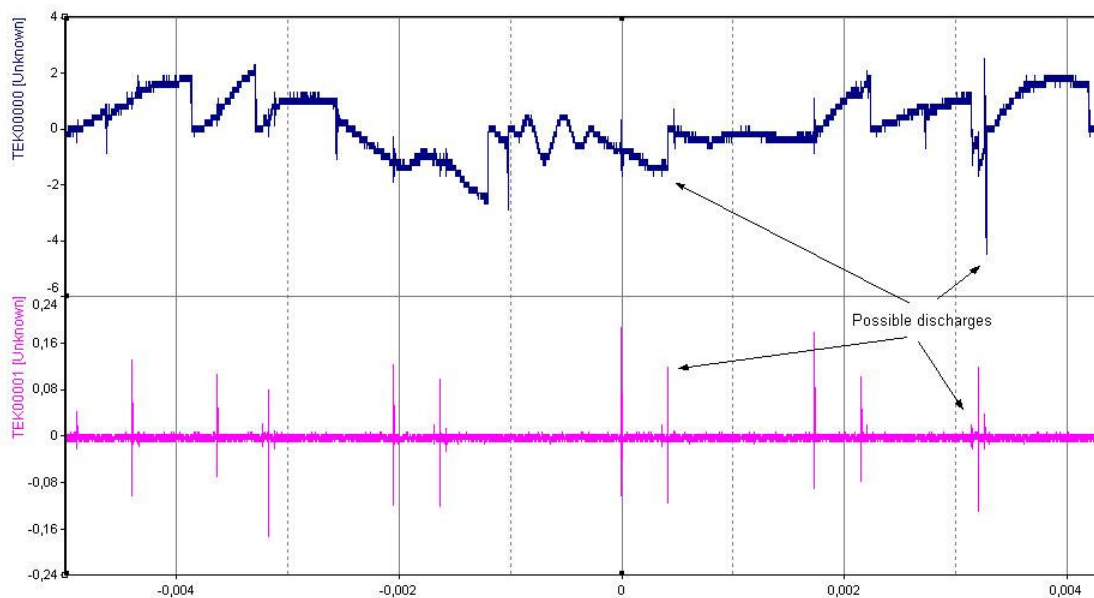


Fig.7.26 Shaft voltage (upper) and frame to ground current (bottom).

If we look only on the bottom trace, it is impossible to say where are the discharges.

It is clear that most of the pulses are grouped in pairs. These pulses are associated to the switching of the converter rather than to the discharge phenomena.

On the other hand, the voltage waveform is rich of steep falling fronts, which can be connected to bearing discharge currents.

For example, in the first 2ms, there are two voltage drops from two to zero volts. It can be a discharge, but there is no indication for that from the current probe. Only two of the voltage and current pulses can be connected together. At this point this is secure indication that the shaft discharges trough the bearings.

In Fig.7.27 another set off captured events is presented. There is only one voltage and current pulses that are 8 $\mu$ s close each other. At the same time, if only the shaft voltage is studied, see six indications for probable discharges can be seen.

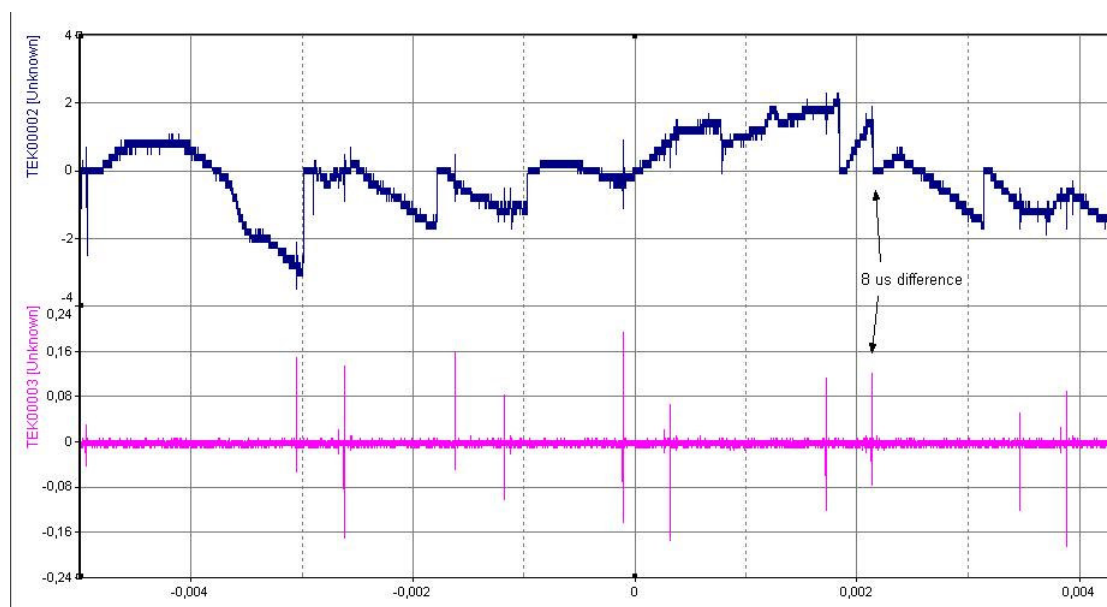


Fig.7.27 Motor shaft voltage (upper) and motor frame to ground current (bottom)

It is now clear, that the measurement of the motor frame to ground current cannot provide a clear information for bearing discharges. It can only be used with combination with other signals.

### 7.5.3 Closed loop antenna

Now it is time to compare the closed loop antenna output with the open loop one and the motor shaft voltage. Two antennas were connected to channel 1 and 2 using coaxial cables with the same length. The ordinary oscilloscope probe is used to connect the slip ring to the oscilloscope. FastFrame mode was set to ON [40]. The

recorded signals can be seen from Fig.7.28 and the second event, more in detail, from Fig.7.29

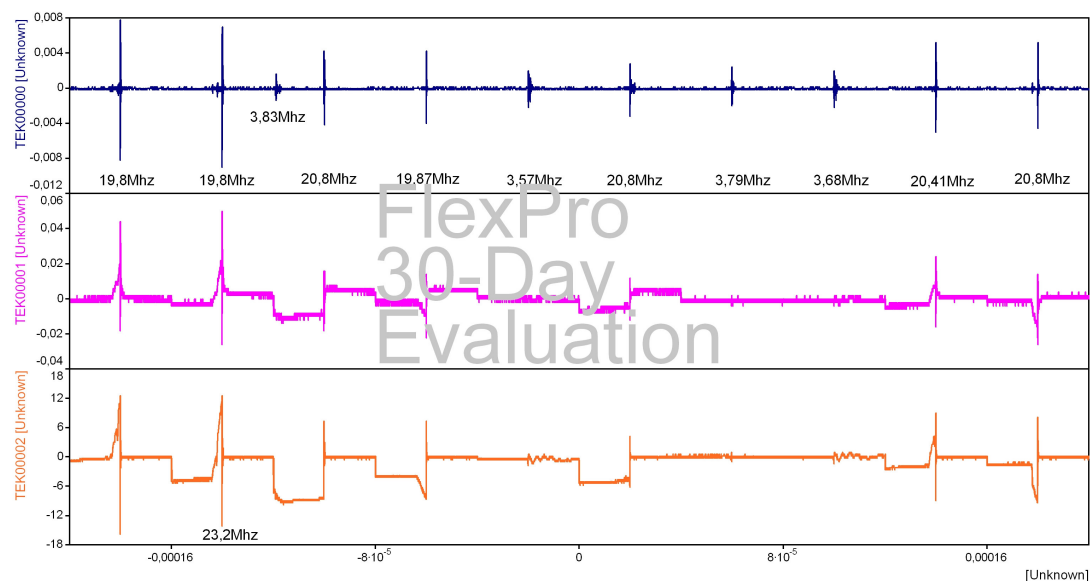


Fig.7.28 Closed loop antenna, dipole antenna and shaft voltage. Ten Fast Frame events.

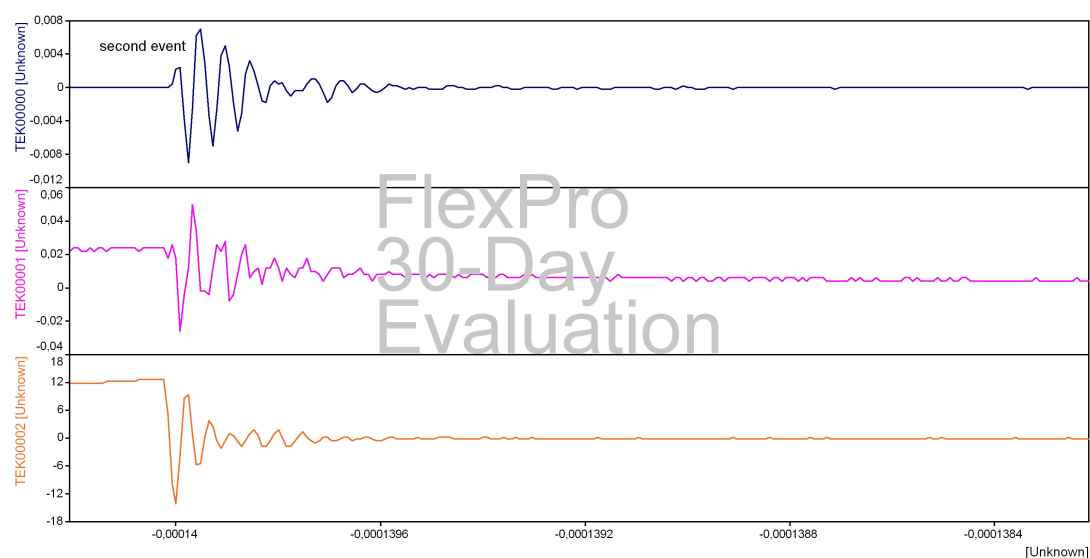


Fig.7.29 Second event zoomed.

Almost all pulses from the three traces match each other. For every voltage step slope, there is an impulse, coming from the dipole antenna (DA). But not only for every voltage impulse, there is much more. From the DA trace, four impulses can be seen, which haven't corresponding ones from in the shaft voltage plot. At this point we decided to take a closer look on every DA impulse. The big surprise was the fact that the pulses are two types. One part of them has a dominant ringing frequency of 20 MHz, and other - 3.8 MHz.

As can be seen from Fig.7.30, the 20 MHz impulses correspond to motor shaft voltage drops, for the 3.8 MHz ones, there is no shaft voltage changes observed. It seems that a simple frequency separation can be made. Simply it can be formulated as: If you have 20 MHz impulses - you have bearing discharges (currents). There are also several steps in the voltage trace due to the FastFrame mode, which has no affect of our investigation.

The same relation can be seen in the next couple of figures.

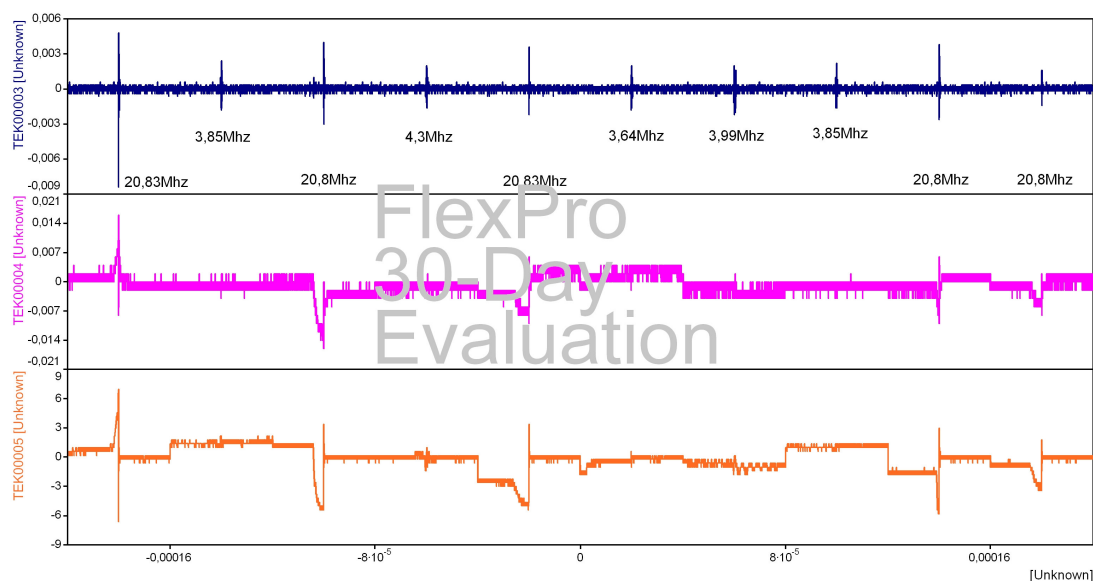


Fig.7.30 Closed loop antenna, dipole antenna and shaft voltage. Ten FF events

#### 7.5.4 Fan motor ASEA MT100L28-2 3kW investigation

To confirm the discovered connection between bearing discharge currents and received signal frequency, a different motor was tested. In this test session A Scandialogic SL 5500 frequency converter was used. From now on, only the shaft voltage and the output from the DA have been monitored.

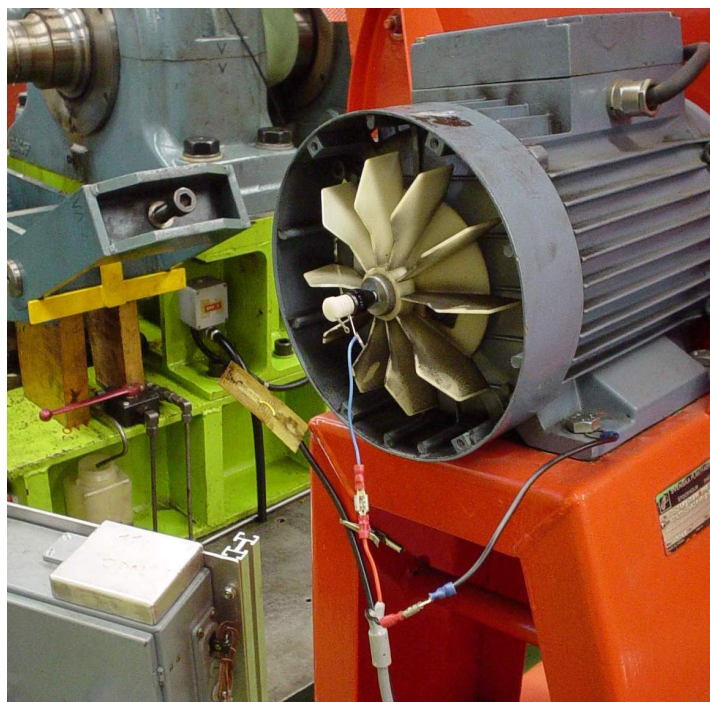


Fig.7.31 Fan motor ASEA test configuration

Surprisingly, when the motor runs in steady state, there is no indication for any discharges in the motor bearings. This can be explained with the low power consumption and not enough magnitude of common mode voltage on the motor shaft. It is well known that the motor start up current can be times bigger than the steady state one. In the starting mode of operation, the probability of having discharges in the motor bearing increases.

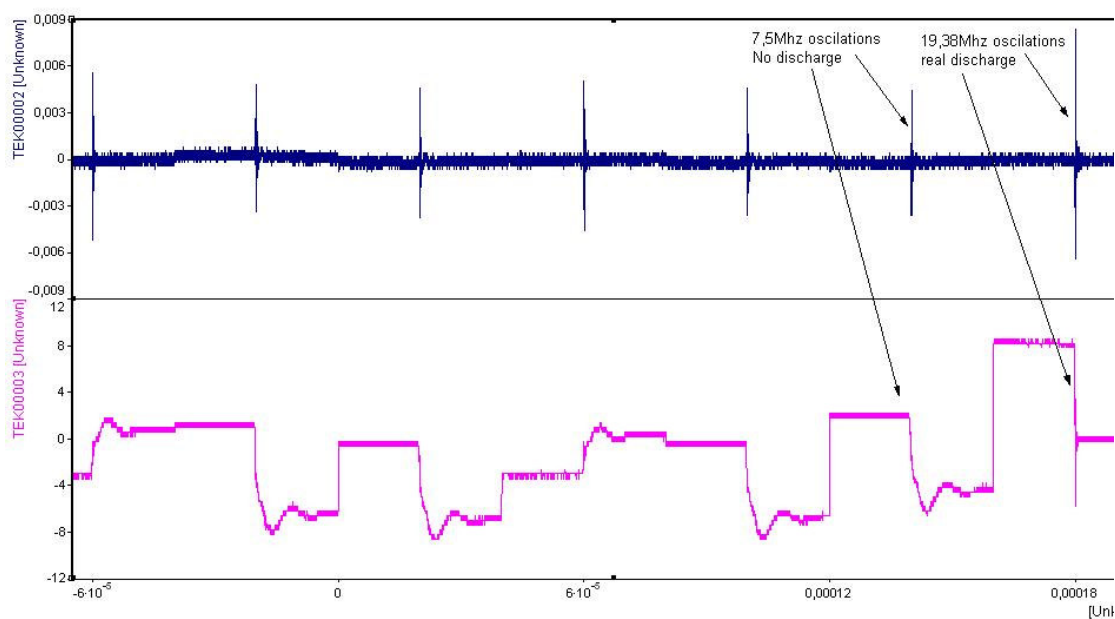


Fig.7.32 DA output signal (upper) and motor shaft voltage (bottom), motor start-up. Seven FF events

Fig.7.32 shows the impulses received with DA and the motor shaft voltage. The captured signals confirm our discovery. There are two type of impulses, one with ringing frequency of 7,5 and another, with a frequency of 19,38 MHz. Only the second one, correspond to a steep voltage drop. This can be considered as a clear indication that discharge is taking place at the same time when the DA receive a 19,38MHz signal. Only one of all seven impulses can be connected to the discharge phenomena. The first six impulses have a ringing frequency of approximately 7,5MHz. Also, it can be observed that the "19,38MHz" has a higher magnitude compared to all other. The "7.5MHz" impulses are present due to the Csr and Cb charging currents. It is mainly due to the converter switching time and high dV/dt levels.

The signals obtained using FastFrame mode and 400uV/div, during motor start-up to 1400 RPM are presented on Fig.7.33

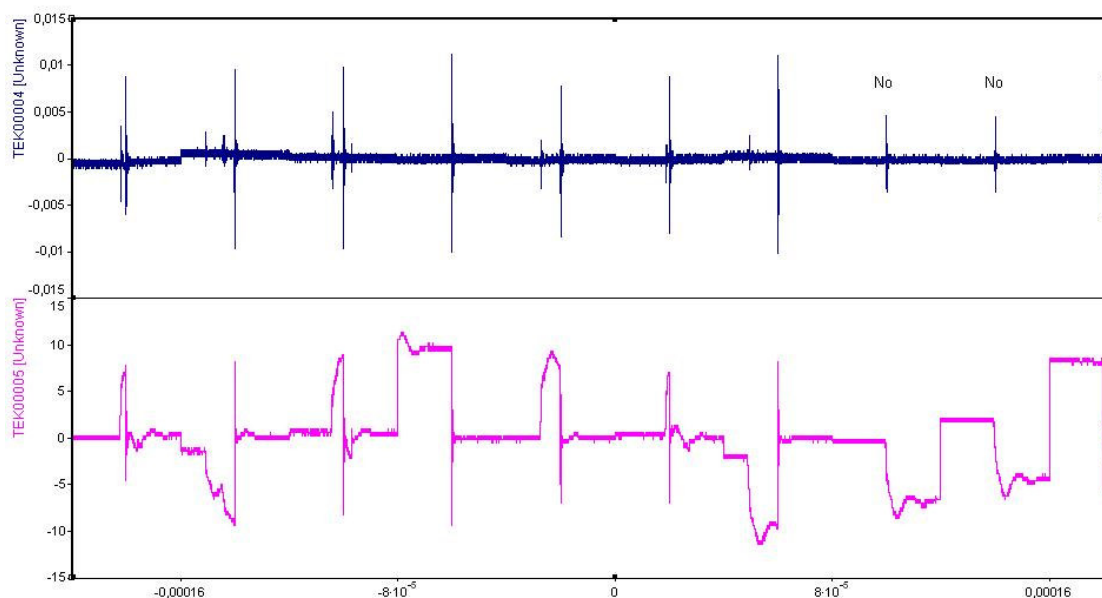


Fig.7.33 DA output signal (upper) and motor shaft voltage (bottom), motor start-up to 1400RPM. FF is used

On Fig.7.34 the DA received signal and the motor shaft voltage (MSV) are shown more in details.

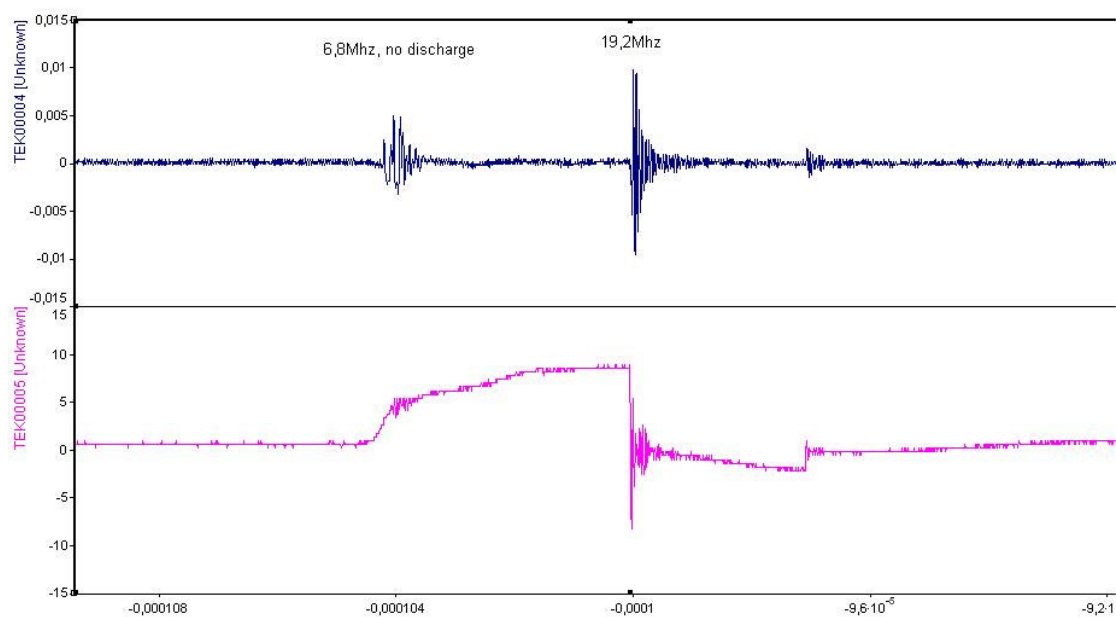
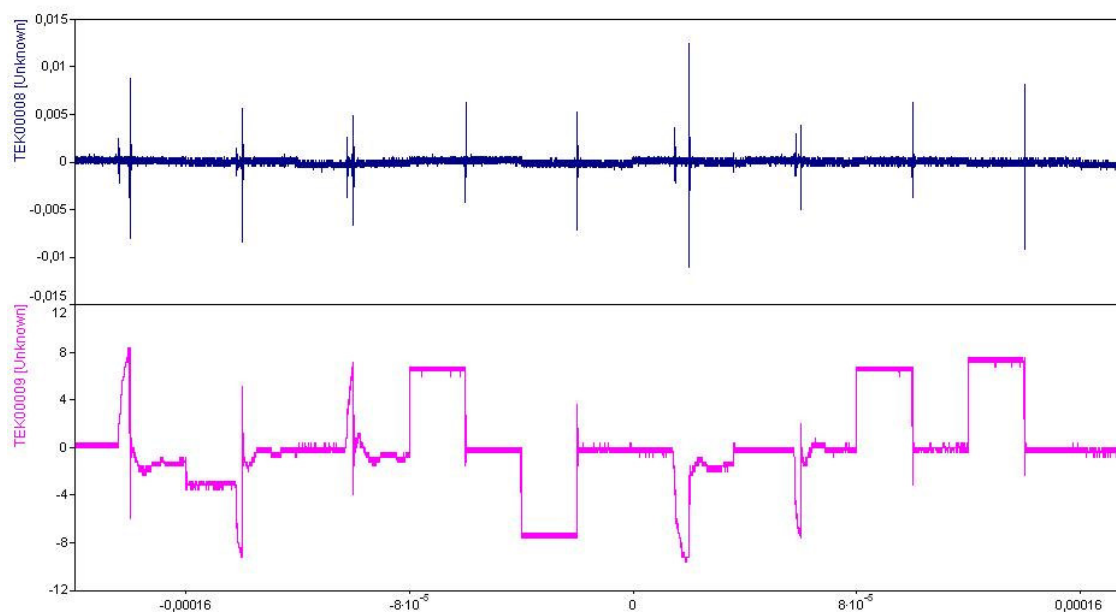


Fig.7.34 Closest look on DA output signal and motor shaft voltage. Third event

Again, when the motor shaft voltage is forming, (Csr and Cb charging), the received impulse from the DA has a frequency of 6.8MHz.

Several attempts for discharge finding during steady state was done. In Fig.7.35 and Fig.7.36, the captured events are presented. The first try is made with 1800RPM, and in the second one, a 2400RPM motor shaft speed is used.



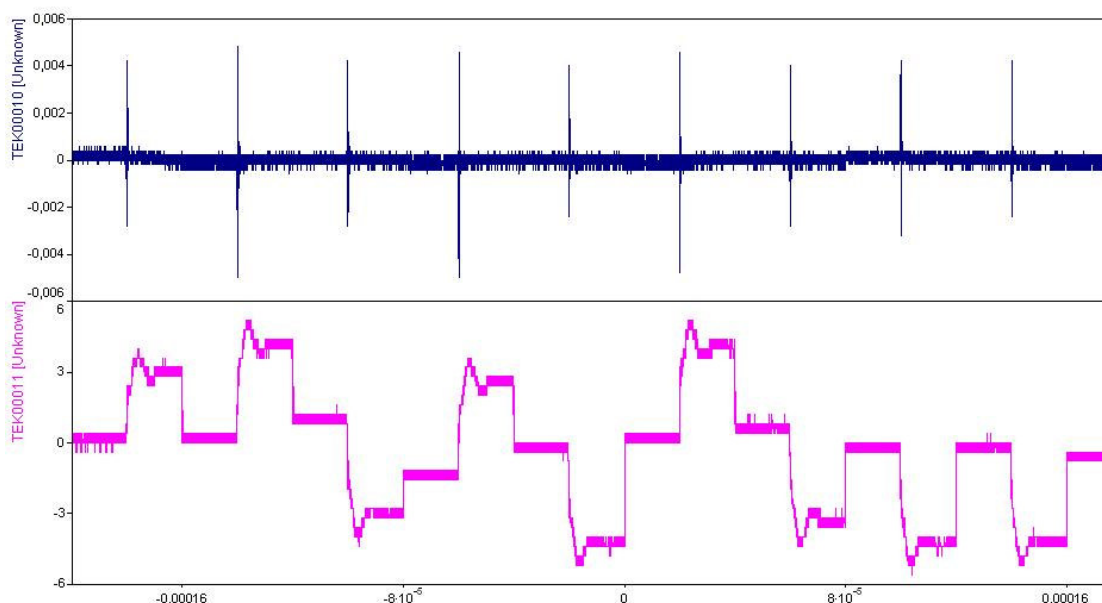


Fig.7.35 and 7.36 The discharges disappear with the speed increase. OBS. magnitudes. DA output signal (upper) and motor shaft voltage (bottom). FF mode.

With the increase of the shaft speed, the common mode voltage magnitude goes down, which leads to a decrease and even disappearance of the early-observed discharges.

There are still impulses received from the DA, but they have a low ringing frequency and magnitude. Considering the rise of consumed power from the fan, when the speed increases, we have to expect more discharges, due to the high common mode voltage and an oil film thickness increase. The obtained results from the last two measurements shows the opposite.

Also several tests with small changes in the speed have been done. The motor was running at 500RPM and the speed was changed with  $\pm 50$ RPM. The obtained waveforms are presented in Fig.7.37

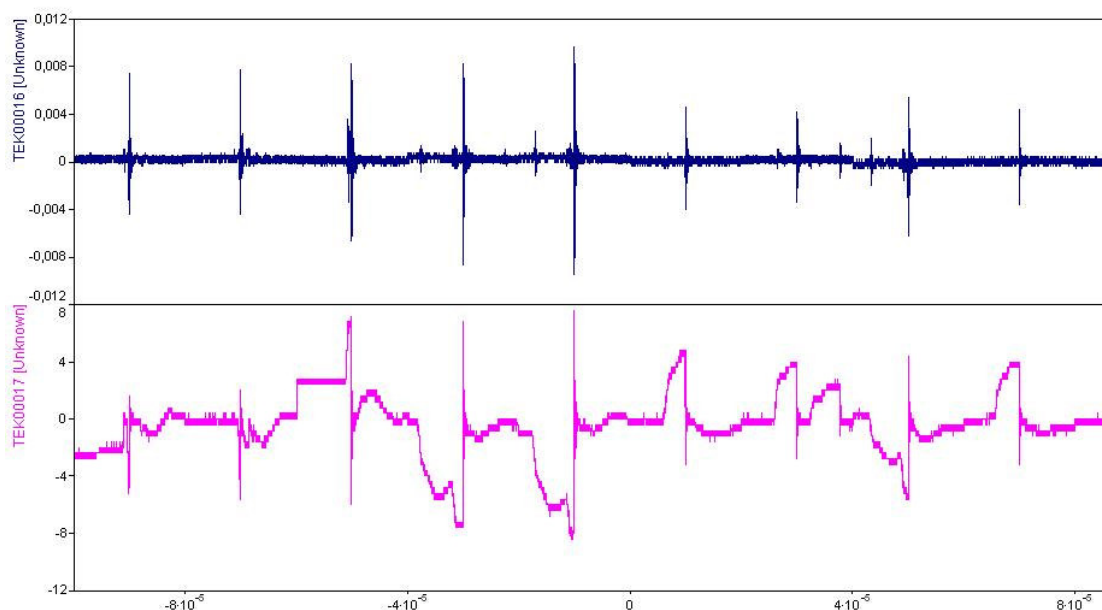


Fig. 7.37 DA output signal (upper) and motor shaft voltage (bottom), 500+/-50 RPM. Fast Frame mode.

Despite the small speed variation, there are a couple of discharges that immediately takes place.

The fifth impulse can be seen more in detail from Fig.7.38

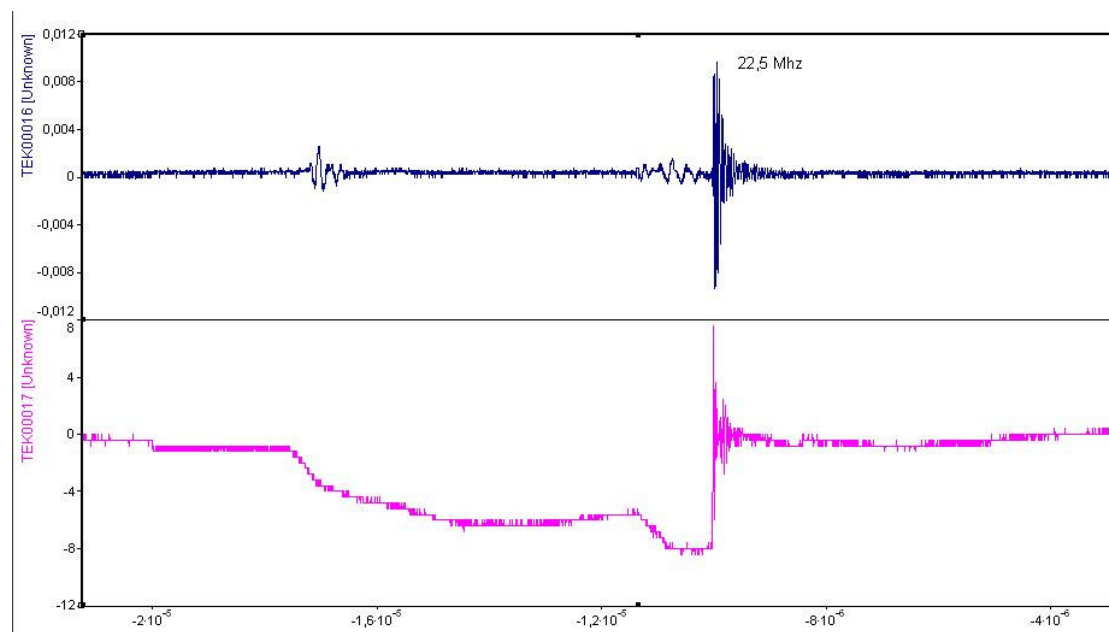


Fig. 7.38 Fifth impulse, more detail view. Time resolution  $10^{-6}$ s

The ringing frequency of the impulse, which corresponds to a steep voltage drop, now is 22,5 MHz. There is one more received impulse, which have a very small magnitude and low frequency. It appears during the high  $dV/dt$  in motor shaft voltage.

Fig.7.39 presents one better example of discharge, taking place in motor bearing. It was captured during start-up.

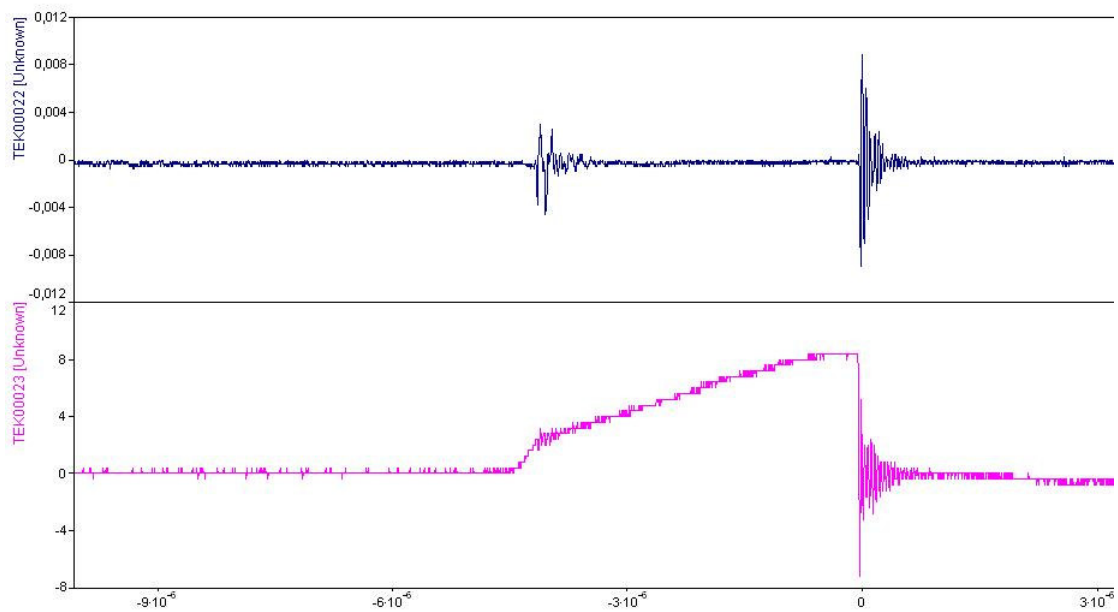


Fig.7.39 Closest look on DA output signal and motor shaft voltage. Time resolution  $10^{-6}$ s

The corresponding DA spectrum using FlexPro spectral estimator function can be seen from Fig.7.40. This function was applied for the signal between  $-6 \cdot 10^{-6}$  to  $3 \cdot 10^{-6}$  s.

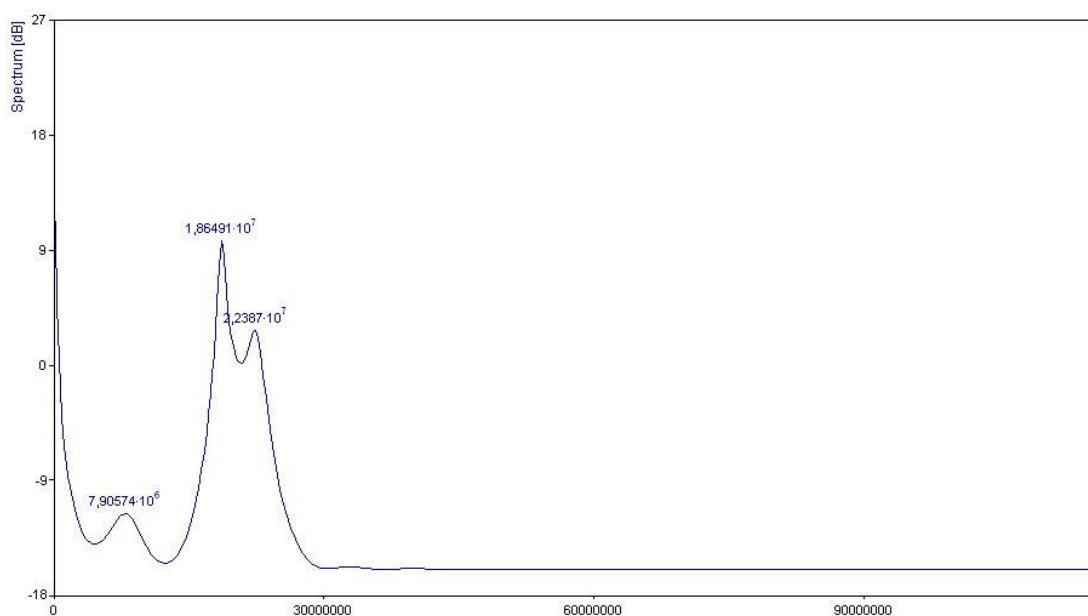


Fig.7.40 Spectral estimation of the DA signal

The first impulse has a frequency of 7,9 MHz and the second one has frequencies of - 18,6 and 22,4 MHz. The motor shaft voltage shows the exact moment, where discharge occurs. It matches exactly to the 18,6 MHz impulse, received with the DA. This can be considered as a good confirmation of the discovery, made on the 7,5kW motor. Despite the fact, that the motor has only half of the rated power on the first motor, the impulse frequency is always the same.

### 7.5.5 Fan motor ASEA MT100L28-2 3kW investigation with 16Mhz DA

The same test has been done using the new DA having a 16MHz resonance frequency

Fig.7.41 presents the captured events using FastFrame, 200ns/div time resolution during the time when motor starts-up. The final speed was to 800 RPM.

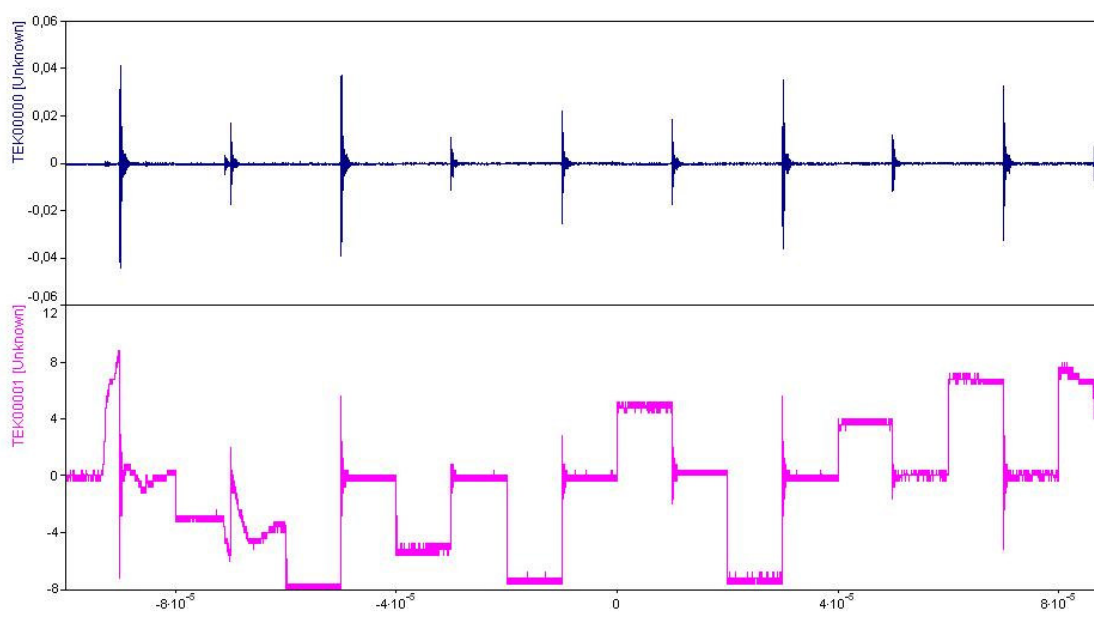


Fig.7.41 16MHz DA output signal and motor shaft voltage during start-up. FF mode

Due to the DA new resonance frequency, the received high frequency impulses have higher magnitude.

Fig.7.42 and 7.43 show the frequency spectrum of the first and sixth impulse. Both of them can be considered as a true indication for bearing discharge. They were chosen due to the different magnitudes.

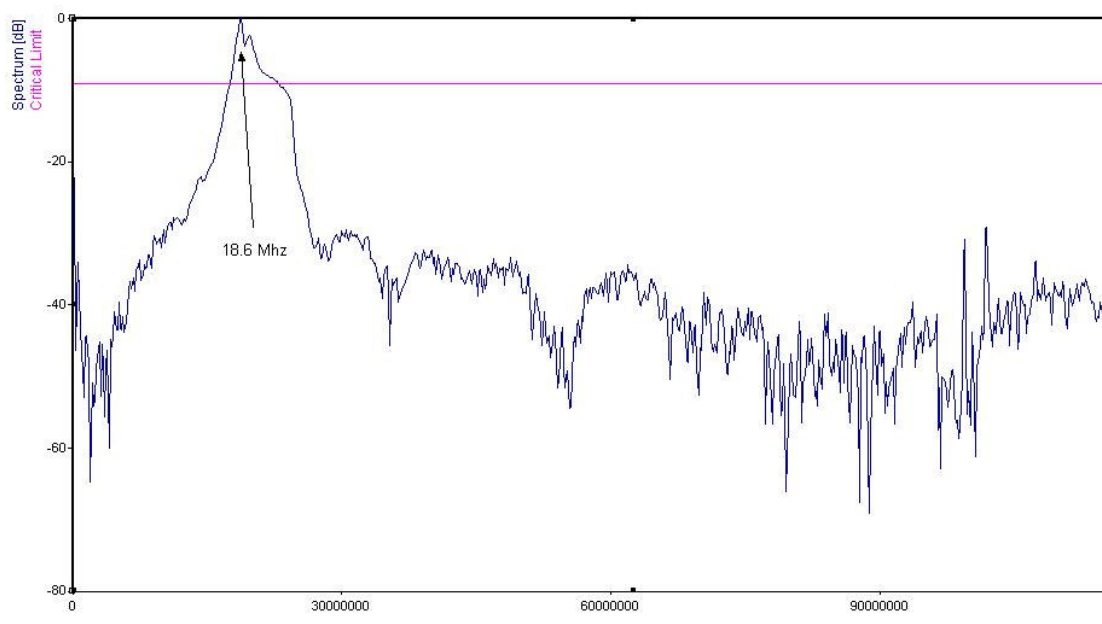


Fig.7.42 FFT first impulse, DA

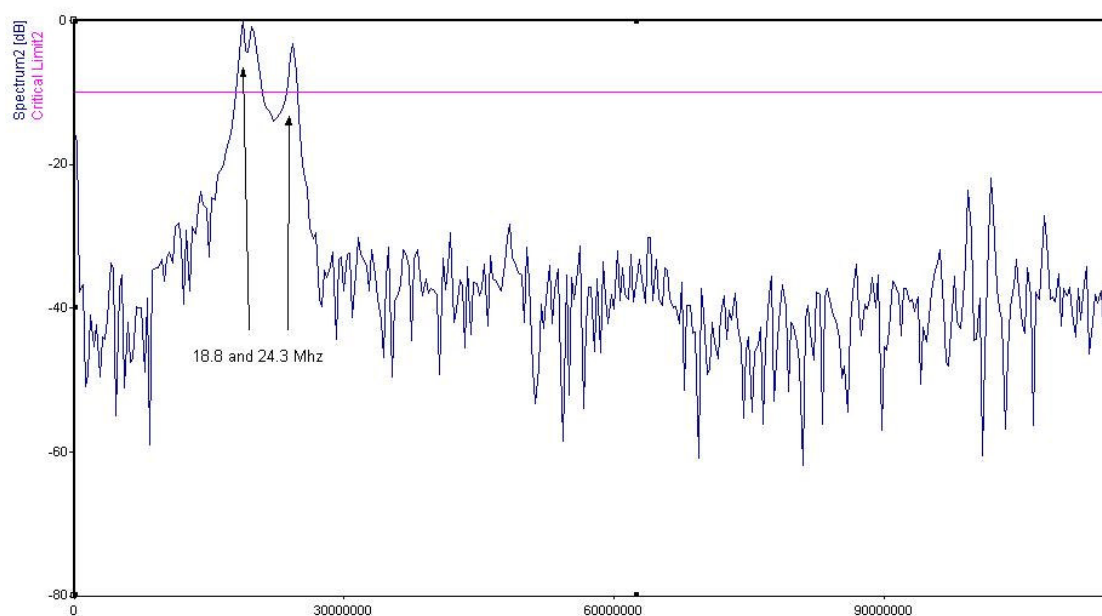


Fig. 7.43 FFT sixth impulse, DA

They have very similar frequency spectra, despite the two times higher magnitude of the first one.

From the tests performed up until now, it can be concluded that the ringing frequency of the captured events is independent of the antenna resonance frequency. Only the received signal magnitude is affected due to the different antenna sensitivity for different frequencies.

The last two tests have been performed using Fast Frame mode. Fig.7.44 presents the events obtained during small changes in the motor shaft speed. The next one is captured during motor start-up. For both cases, FFT was done for all the ten events including the background noise between them. The frequency spectra can be seen on Fig.7.45 and Fig.7.47.

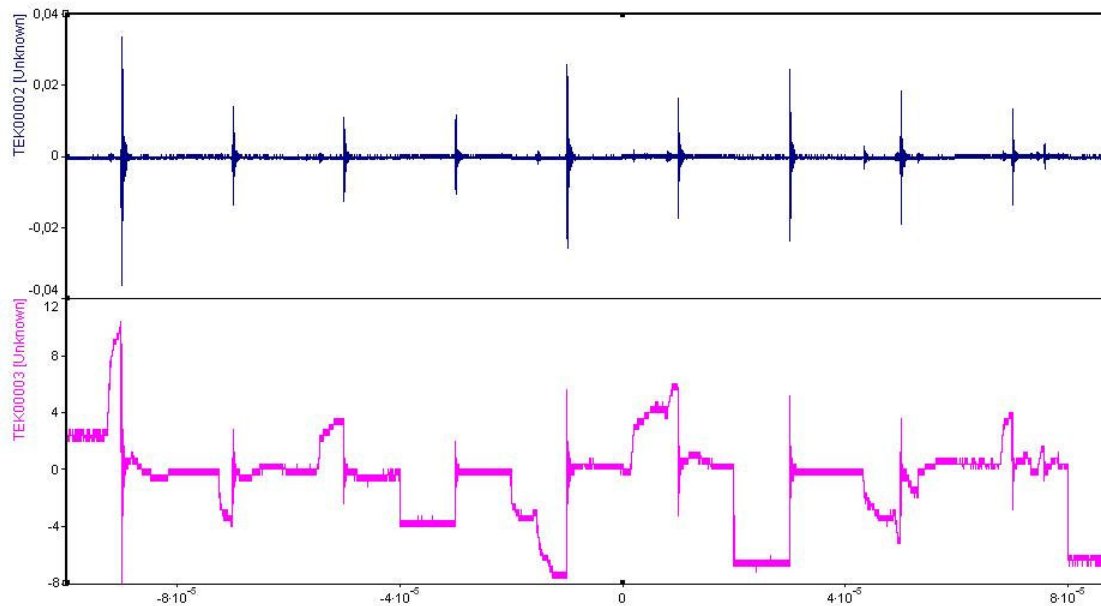


Fig.7.44 DA output signal (upper) and motor shaft voltage (bottom), small speed change, 800RPM.FF mode

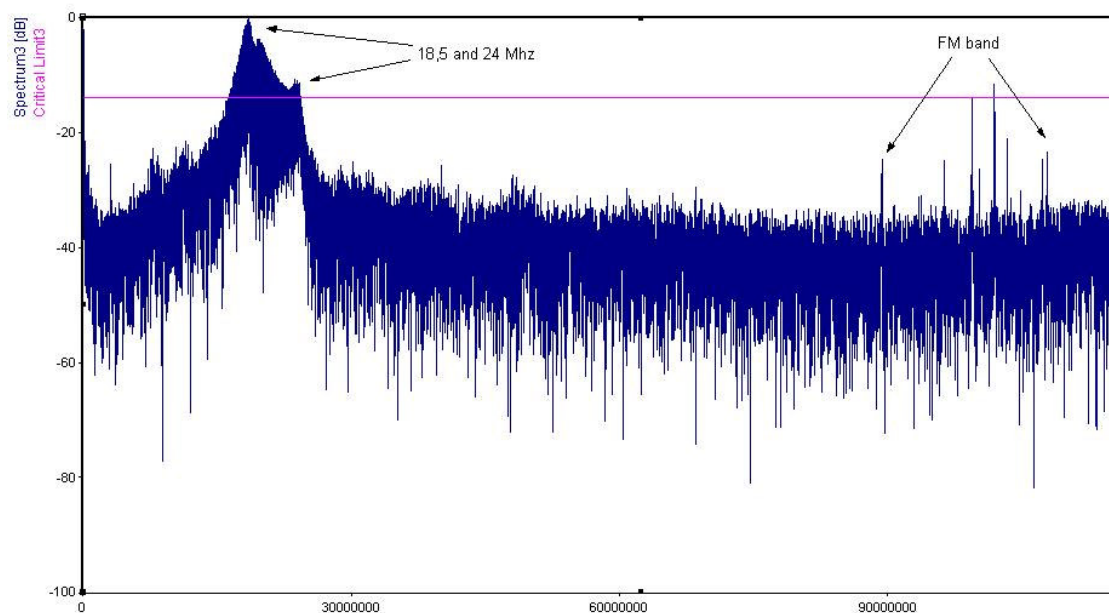


Fig.7.45 FFT of all data length of fig.7.44, small speed change, 800RPM

The dominant frequency is between 18,5 and 24 MHz. At the same time almost the entire shaft voltage event indicates discharges. The radio FM band station signals are

also present. They have no effect on our measurements, but are a good indication of the capability of our receiving equipment.

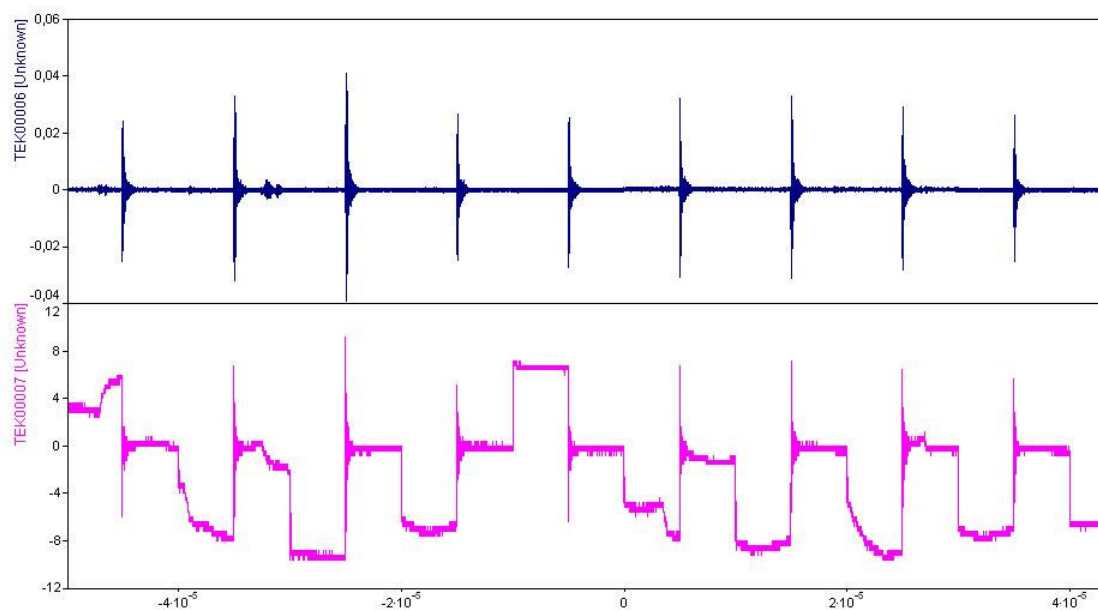


Fig.7.46 DA output signal (upper) and motor shaft voltage (bottom), rev-up 500-900RPM. FF mode

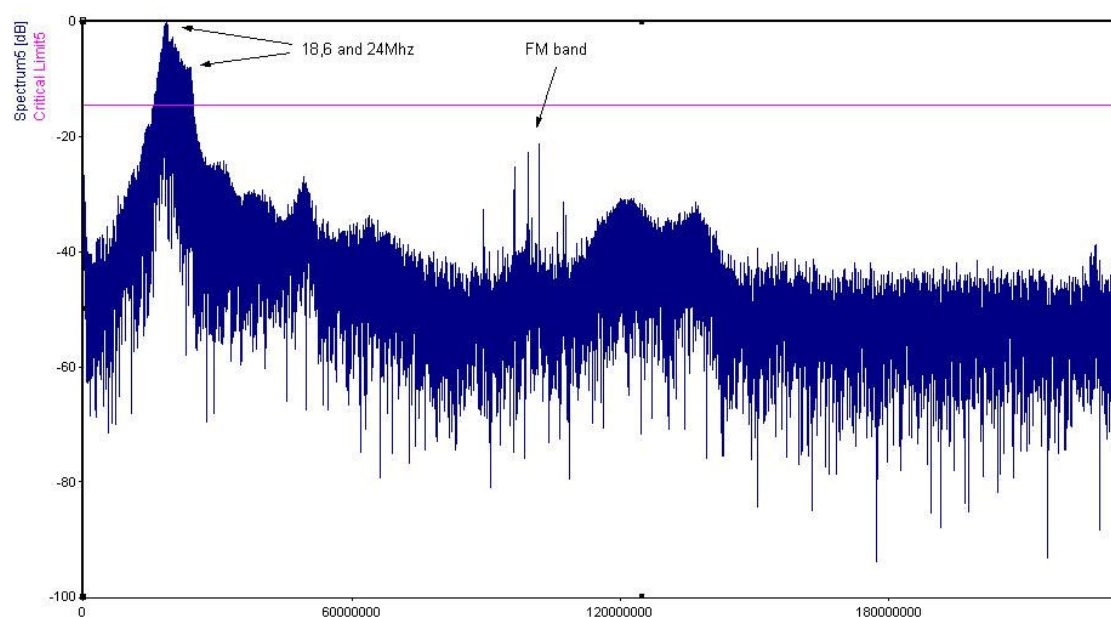


Fig.7.47 FFT of all data length of fig.7.46, rev-up 500-900RPM

Exactly the same results were obtained using 100ns/div and different motor operation conditions. To all impulses, received from the DA, there is a corresponding MSV slope with high  $dv/dt$ . According to previous authors, investigating bearing discharges, this can be considered as a true EDM discharge inside the motor bearings. [37,41,44]

From now on, we just connect the received "20MHz" pulses to this phenomenon. When discharge takes place inside the bearing, a "20MHz" is always received.

### 7.5.6 7.5kW motor driven by Scandialogic SL 5500 frequency converter investigation using 16Mhz DA

Now the bearing discharges can be connected to the "20Mhz" impulses received from the DA. Still it is not known what the impulse frequency will be when a different motor, driven by other frequency converter is used. The only way to clear the situation was to investigate all the available motors in the lab using the available converters. In this section the results obtained from 7,5kW motor driven by two different frequency converters will be presented.

The tests were performed with two different motor speeds, equal for both of them. FastFrame as well as real time mode was used to collect as much as possible events for further investigation.

In Fig.7.48 the first nine events are presented. All of them are believed to be due to discharges inside the motor bearing. In Fig.7.49 the first event is displayed and Fig.7.50 shows the corresponding frequency spectrum. The shaft voltage rises up till -9V and suddenly, the discharge take place. As can be observed from the FFT, the DA impulse ringing frequency is 21,8 MHz.

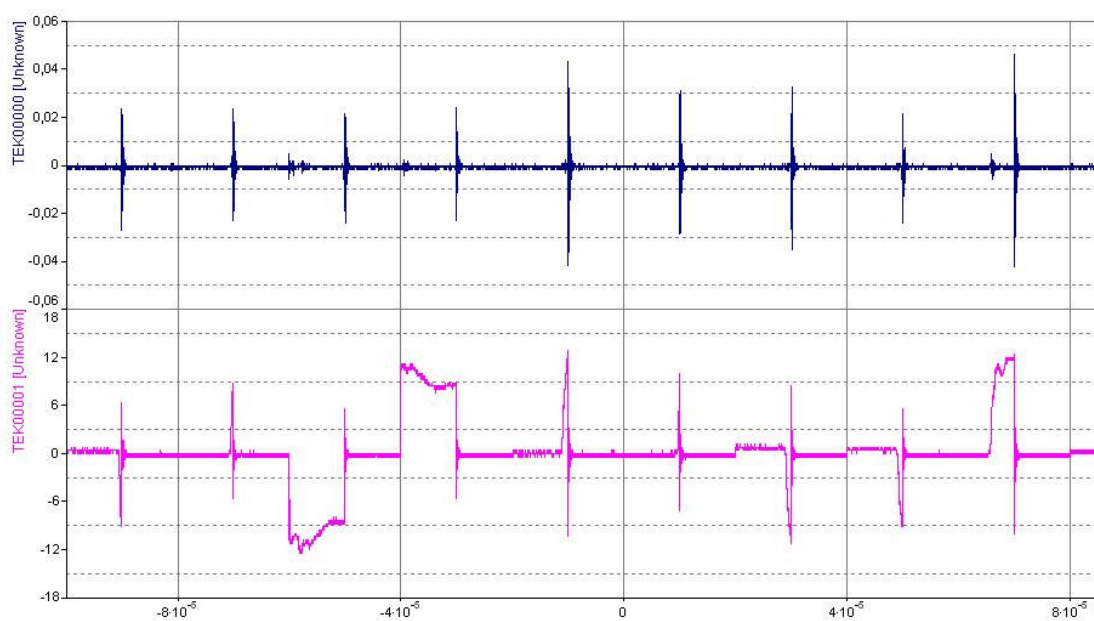


Fig.7.48 Nine events captured using FastFrame mode, DA (upper) and motor shaft voltage (bottom)

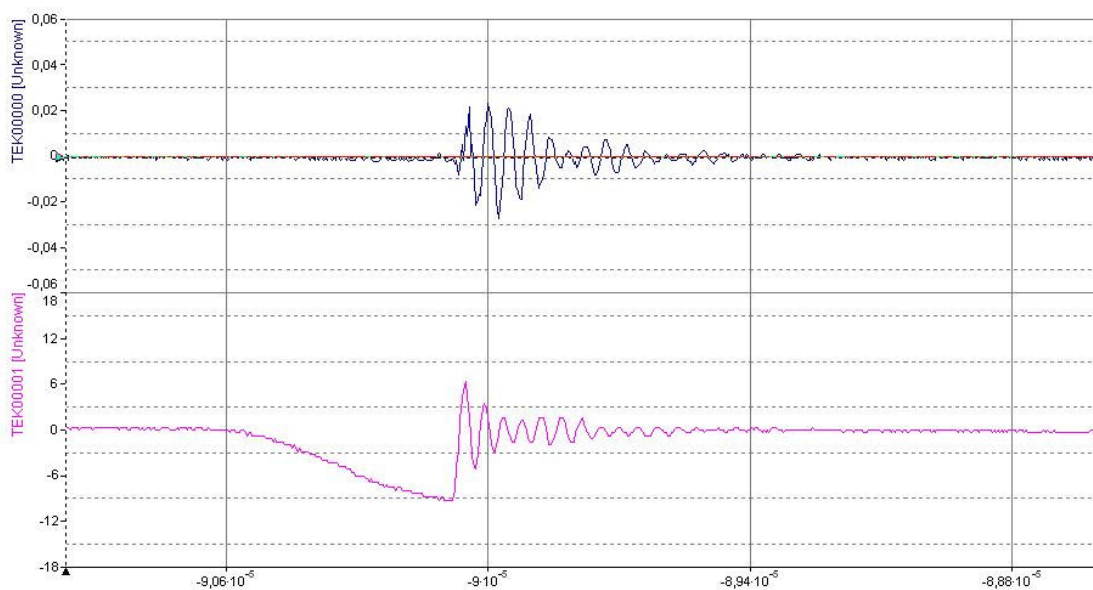


Fig.7.49 First impulse from Fig.7.48 more in detail. Timing resolution  $10^{-5}$ s

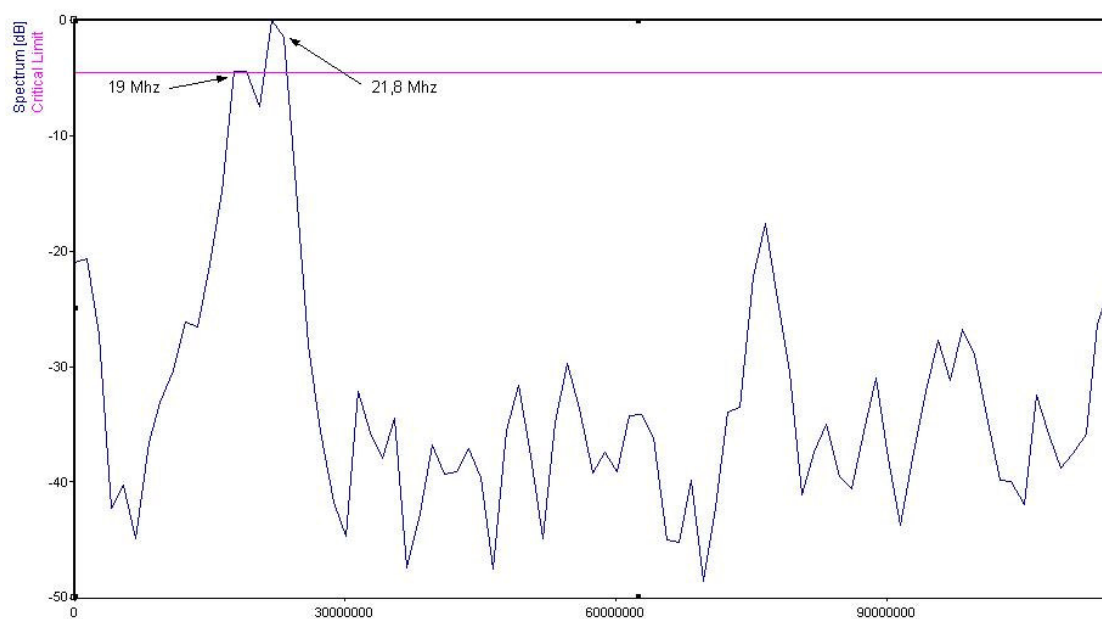


Fig.7.50 The frequency spectrum of the DA signal from Fig.7.49

In Fig.7.51 the next nine captured events are shown. At this time the second impulse were chosen due to the highest magnitude, different shape and pre-discharge voltage, compared to the previous one.

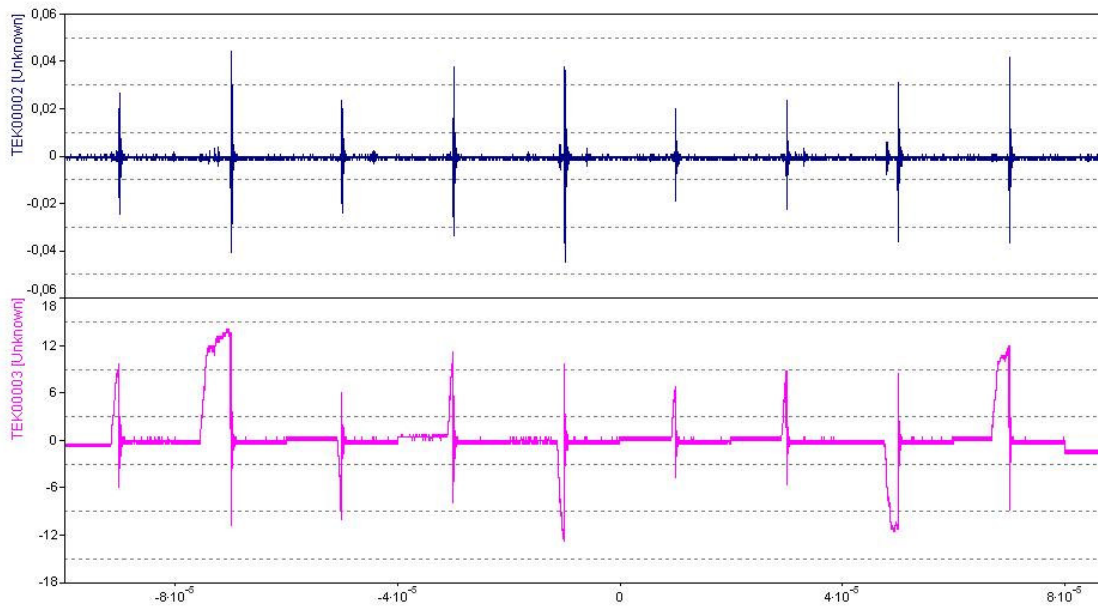


Fig.7.51 Nine events captured using Fast Frame mode, DA (upper) and motor shaft voltage (bottom)

In Fig.7.52 and Fig.7.53 the second event is displayed and the corresponding frequency spectrum. The shaft voltage rises up till 14V and the discharge take place. Using FFT, the impulse ringing frequency was find to be 22,6 MHz.

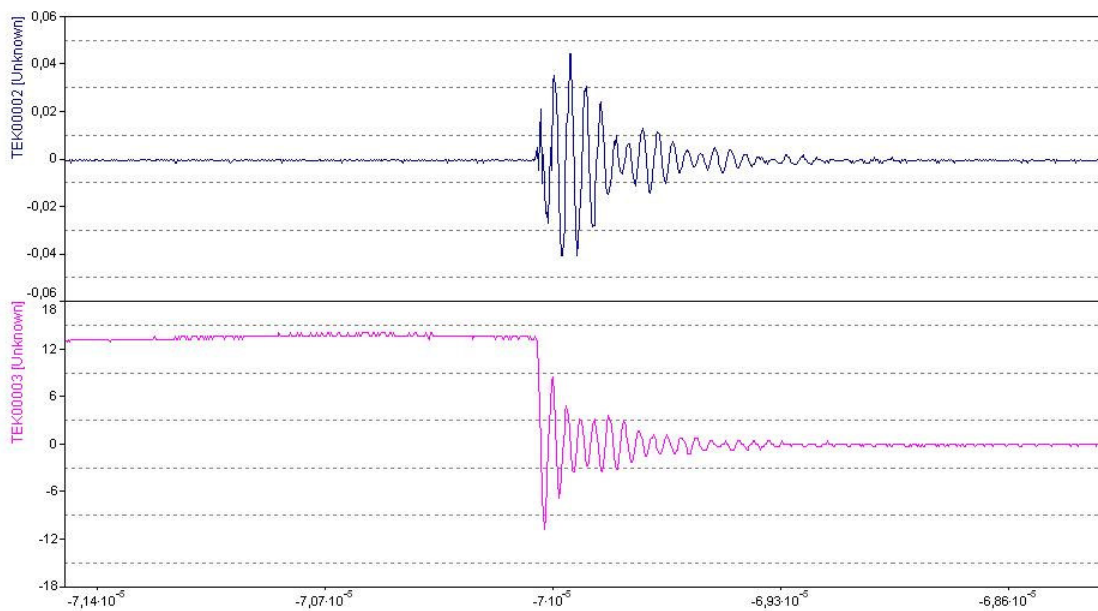


Fig.7.52 Second impulse from Fig.7.51 more in detail. Time resolution  $10^{-5}$ s

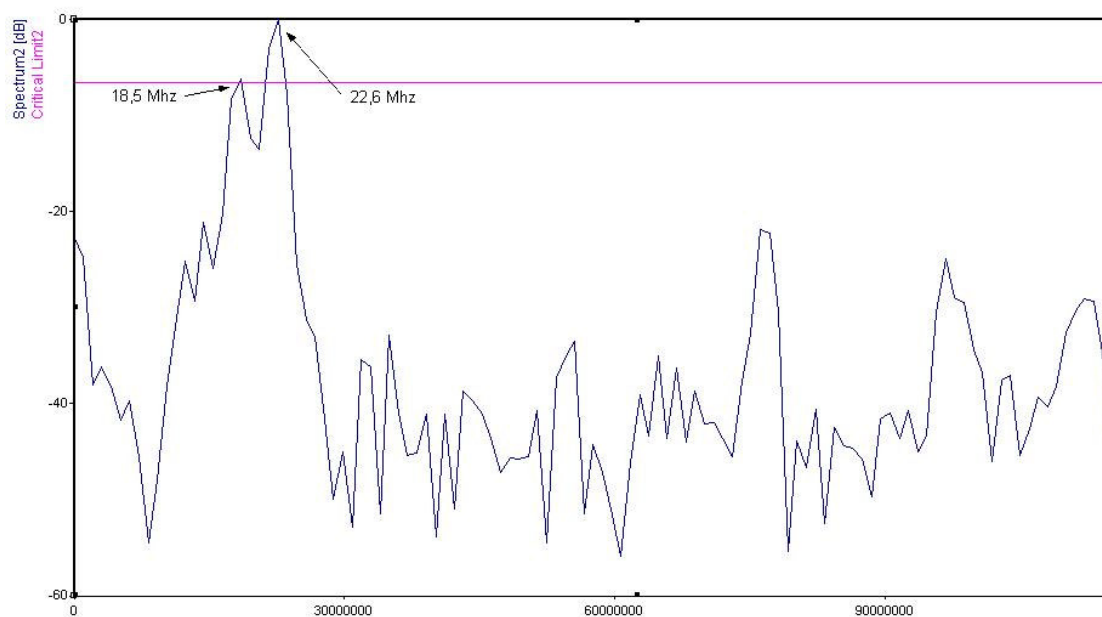


Fig.7.53 The frequency spectrum of the DA signal from Fig.7.51

Despite the different pre-discharge voltage polarity and magnitude, and also, different shaft charging slopes, the second impulse frequency is extremely close to the first one. The difference of 0,8MHz is a negligible variation, taking into account the antenna wide bandwidth.

In Fig.7.54 the next series of nine impulses is shown. Fig.7.55 presents the frequency spectrum for the whole time interval from Fig.7.54.

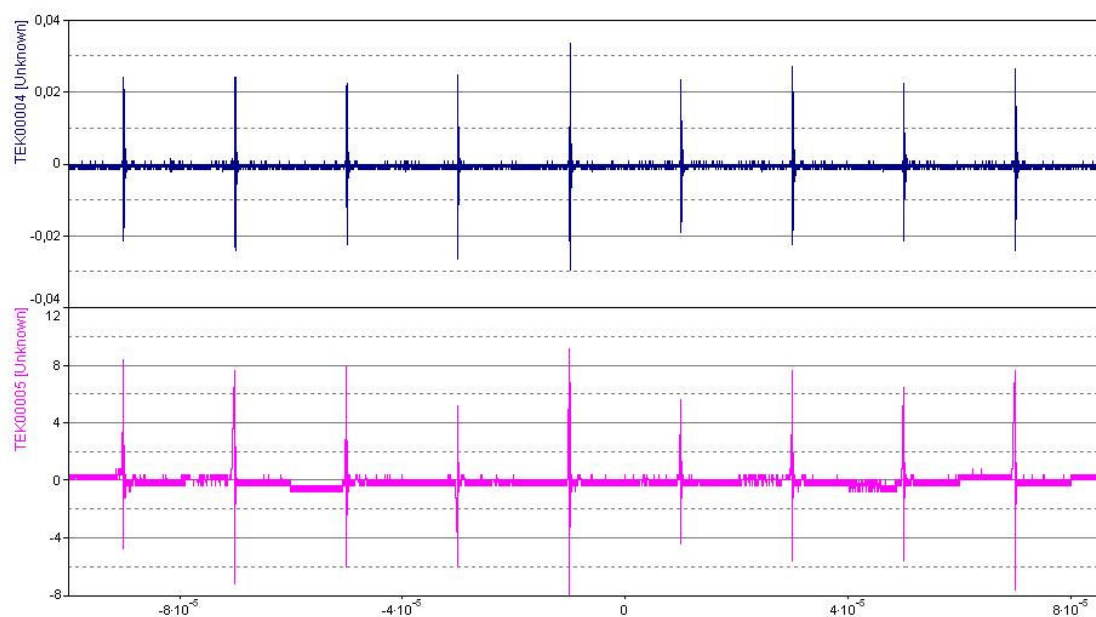


Fig.7.54 Next series of nine impulses. Fast Frame mode

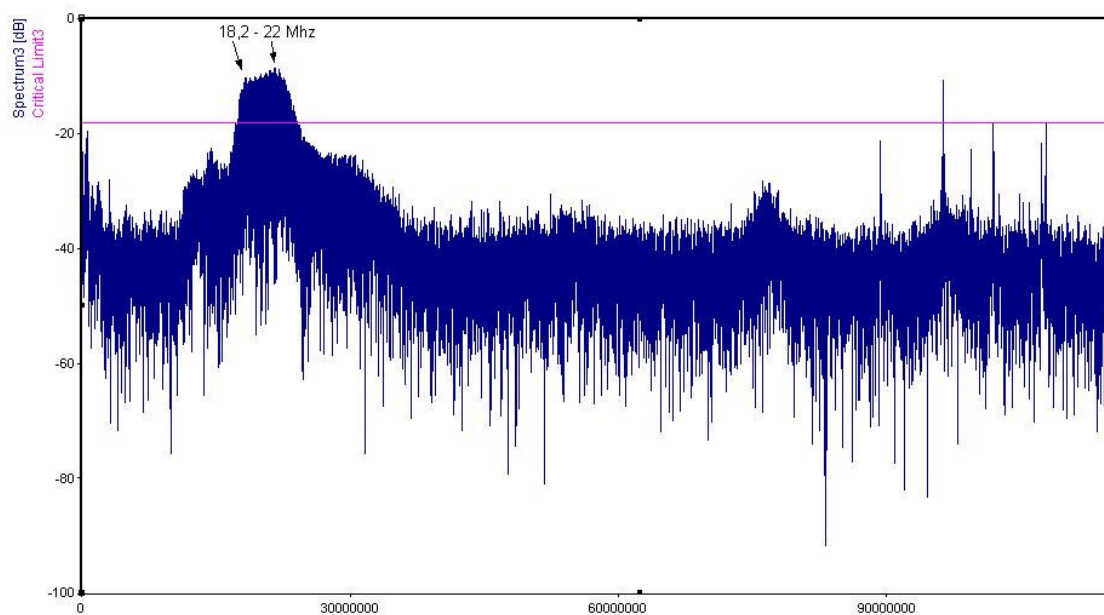


Fig.7.55 FFT of all data length of fig.7.54

Now it is easier to compare the FFT results with the one obtained from the ASEA MT100L28-2 3kW in the foregoing investigation.

Before, the dominant frequencies were between 18,6 and 24 MHz and now they are 18,2 and 22 MHz. Almost the same frequencies are obtained from the two different motors installed in totally different places. In both cases, only the frequency converter is the same.

Maybe the impulse frequencies are so close due to the use of same converter, or maybe not. The next test will clarify this.

Before we continue, let us take a look on one more figure, Fig.7.56. It shows the real time signals received from DA compared with the motor shaft voltage.

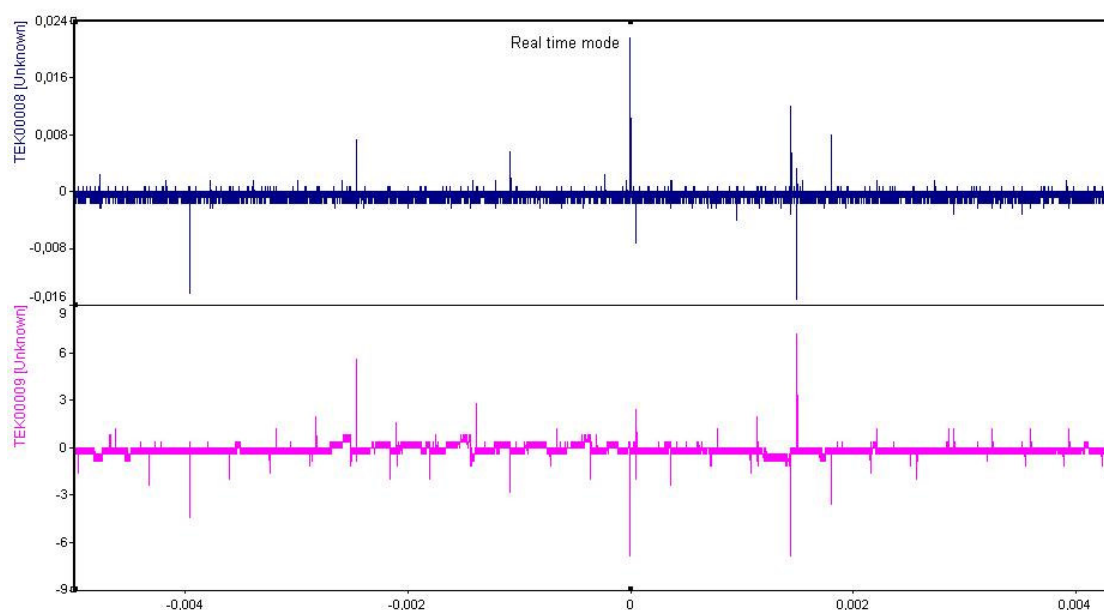


Fig.7.56 Real time signals received from the DA and the motor shaft. Approximately 600 Hz discharges repetition.

A large number of voltage variations can be seen, only for a few of them, there is a corresponding signal received with the DA. For the events with a magnitude below 3V there is no corresponding impulses from the DA. For the others, which have magnitude higher than 3V, impulses from the DA are received. This observation can be supported with information from the technical papers [42] for a typical threshold of about 3V. This voltage can vary in a wide range. Mainly it depends on the oil film thickness, dielectric strength and oil contamination concentration.

### 7.5.7 7.5kW motor driven by ABB 5.5kW Sami GS ACS501 frequency converter investigation using 16Mhz DA

In this section, the obtained results using 7.5kW motor with ABB 5.5kW Sami GS ACS501 frequency converter will be presented. It is done in order to discover the dependency of the impulses frequency of the used converter. Everything else is kept the same except the frequency converter.

In Fig.7.57 the nine captured events are shown.

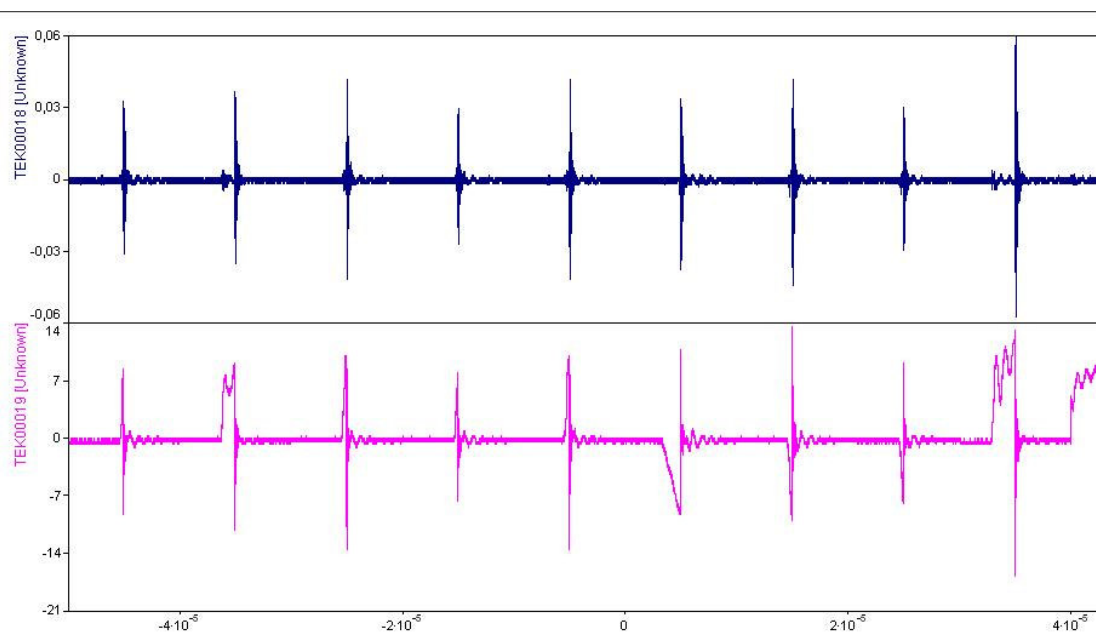


Fig.7.57 Nine events captured using Fast Frame mode, DA (upper) and motor shaft voltage (bottom)

Fig.7.58 is showing one event as an example of the zoom of one of the pulses.

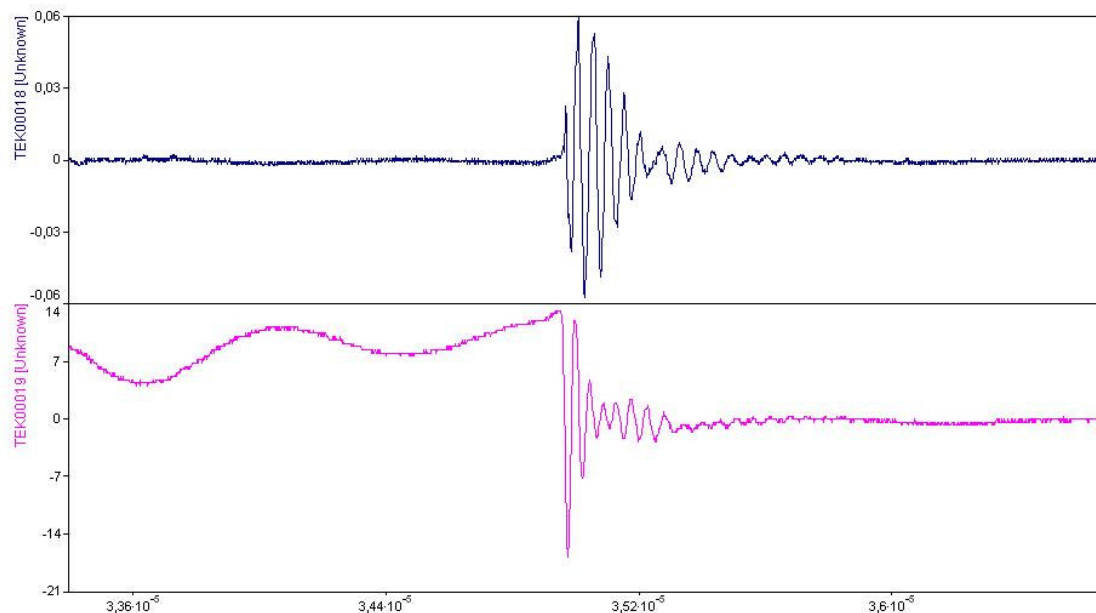


Fig.7.58 Ninth impulse from Fig.7.57 more in detail. Timing resolution  $10^{-5}$ s

And finally, the frequency spectrum of the whole data range is presented on Fig.7.59.

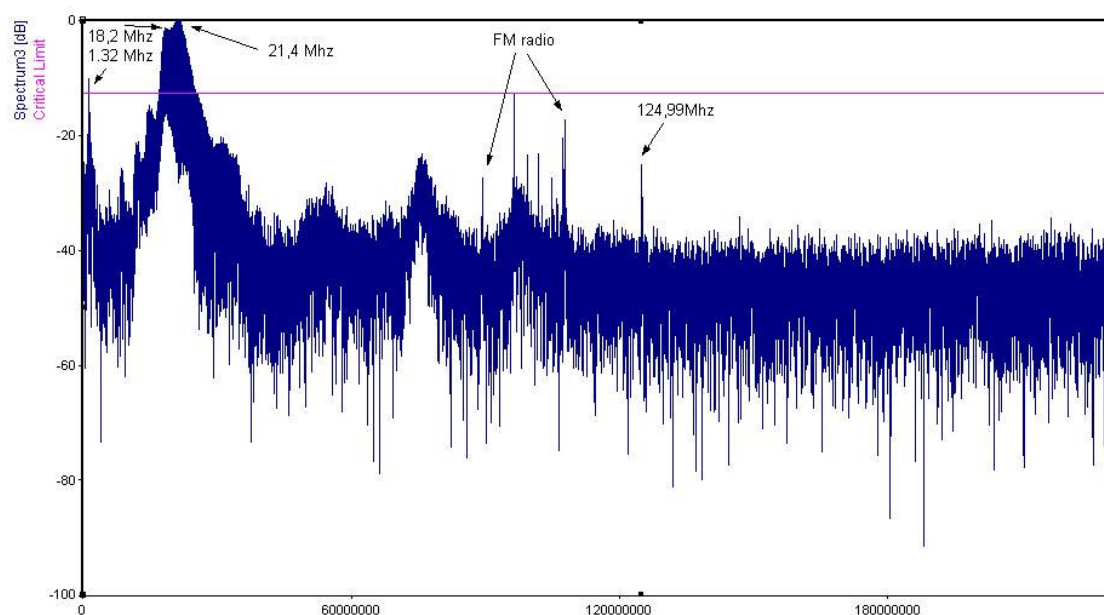


Fig.7.59 FFT of all data length of fig.7.57

Now the dominant frequencies are 18,2 and 21,4 MHz. They are the same as in all the cases reviewed before. There is also a 1,32 MHz signal of 10dB below the first two.

After the performed test, we are more convinced in the statement, that the "20 MHz" impulses can be used as an indication of discharge in the motor bearings. They show no dependency of the used frequency converter, induction motor and antenna resonance frequency.

### 7.5.8 132kW motor driven by Siemens frequency converter investigation using 16Mhz DA

Till now the results were more than promising. The remaining question is if the motor is several times bigger than the investigated before. What impulse frequencies can we expecting in this case? Probably answer for these questions can be found below.

In this section, the results obtained from the 132kW motor will be presented. The only difference compared to the previous measurements is the shaft voltage probe connection. Due to the covered shaft end, the contact method is used. This can provoke some disturbances in the obtained data. In order to obtain oil film thickness enough for keeping common voltage high, the motor speed was set to 750RPM

In Fig.7.60 the first viable nine events are shown.

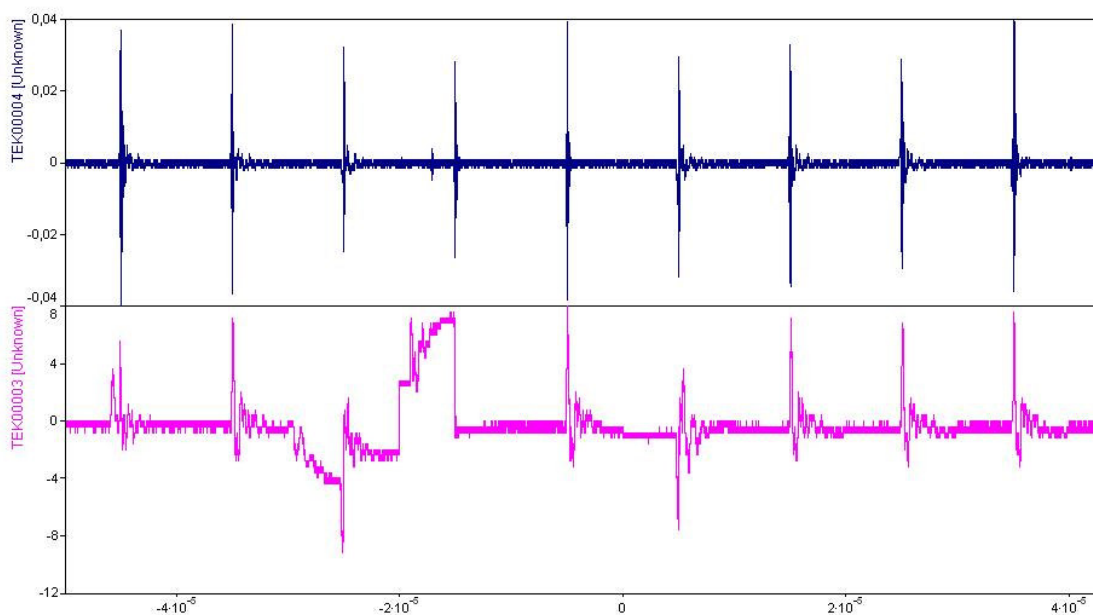


Fig.7.60 Nine events captured using Fast Frame mode, DA (upper) and 132kW motor shaft voltage (bottom).

The shaft voltage rises up to approximately 8V and down drop to zero. In all events except one, there is a strong oscillation caused by a voltage falling slope. Only one is clear. The fourth impulse was chosen for a close look. It is presented in Fig.7.61

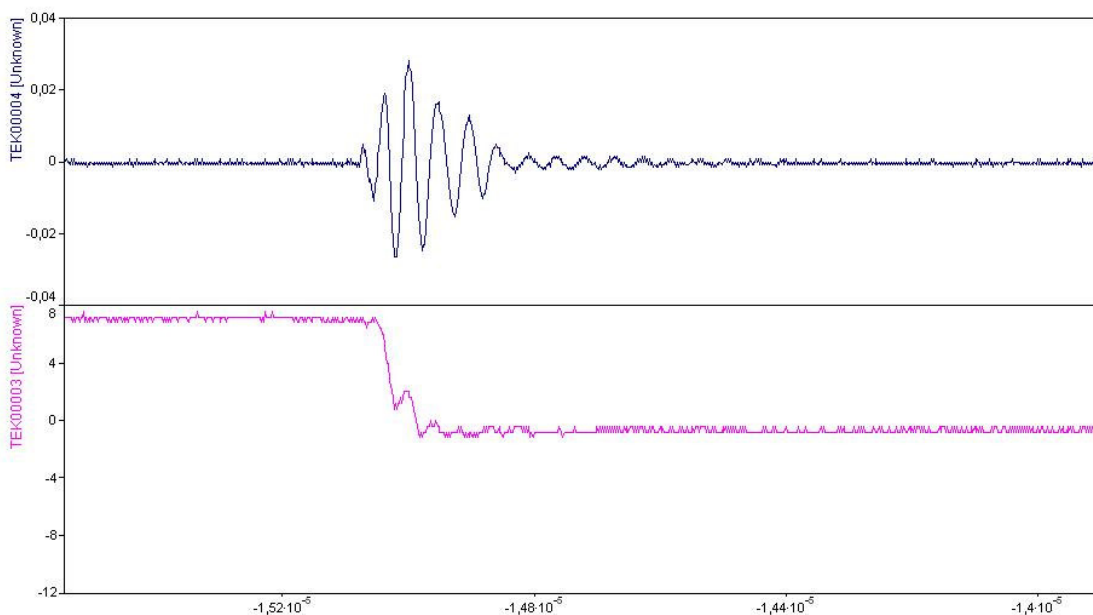


Fig.7.61 Fourth impulse from Fig.7.60 more in detail. Time resolution  $10^{-5}$ s

From this event it is clearly visible that the DA impulse oscillations are not related to any motor shaft voltage ones.

Fig.7.62 shows the frequency spectrum of the chosen impulse. Its maximum appears to be at 21,7MHz. This is an extremely good result, keeping in mind that the investigated motor has 132kW rated power and shows the same frequencies as the 3 and 7,5kW motors.

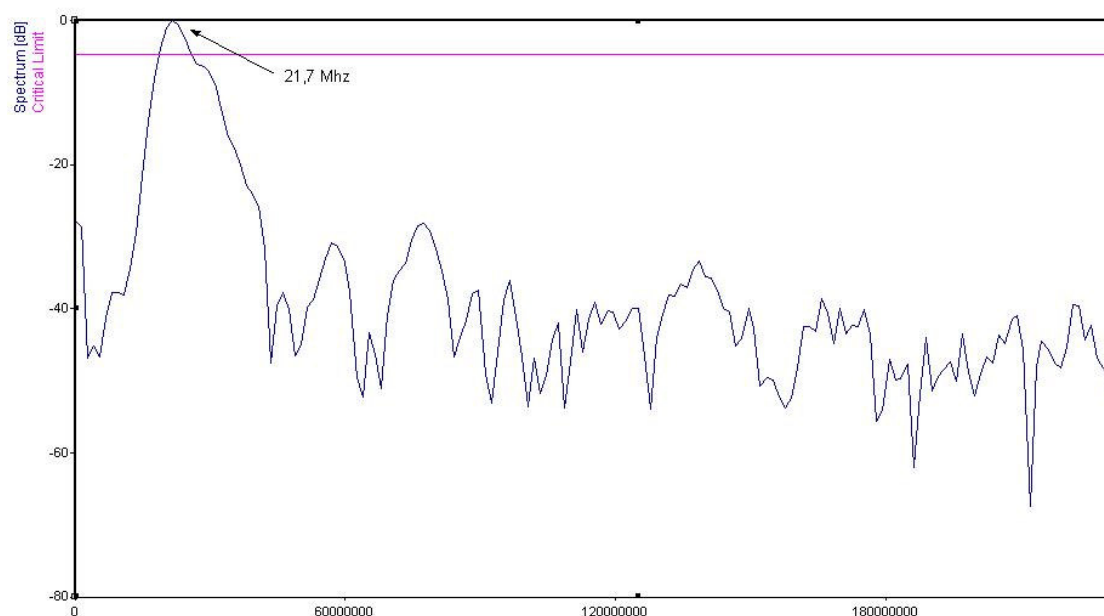


Fig.7.62 The frequency spectrum of the DA signal from Fig.7.61

This event is the only one, which does not have oscillations in the shaft voltage. Let us check what the frequency spectrum for all the captured events. In Fig.7.63 the frequency spectrum of the whole data range is shown on Fig.7.60

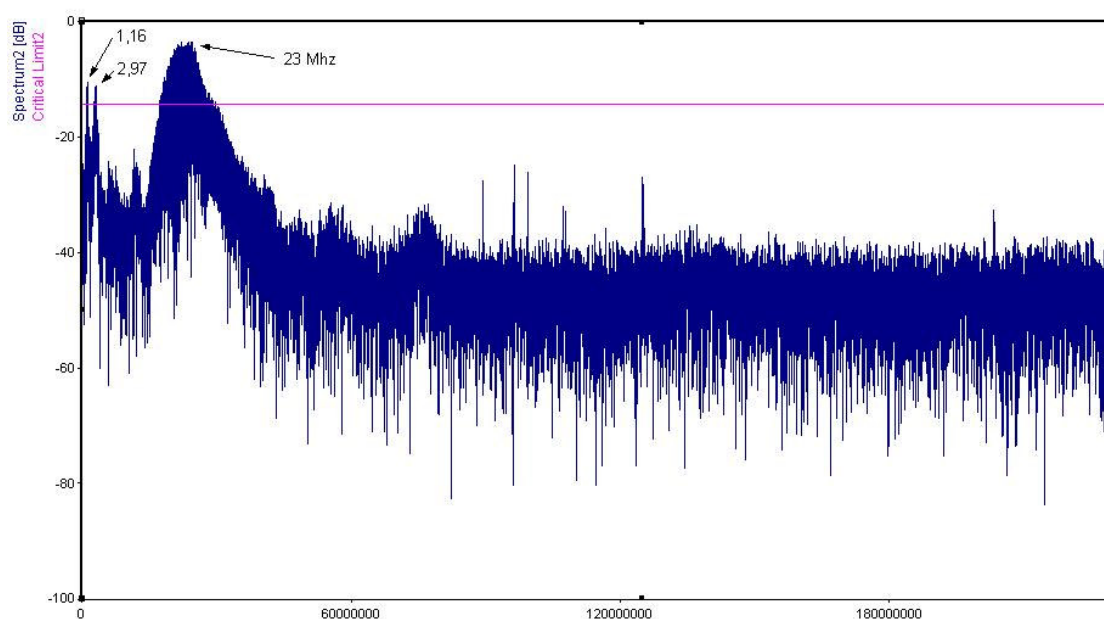


Fig.7.63 FFT of all data length of fig.7.60

The obtained plot from the FFT shows the same frequency pattern as the other, obtained from the 3 and 7,5kW motors. The only difference is that the maximum here is around 23MHz.

All the results obtained from the 132kW motor only confirm our "20MHz" discovery. In contrast with the big difference in the motors sizes, the frequency of the pulses corresponds to the discharges in the range of 18-23MHz. This is not an exact value, due to the fact that the impulse frequencies vary from impulse to impulse.

Now, lets take look on one real time event. An 180us time interval is presented in Fig.7.64.

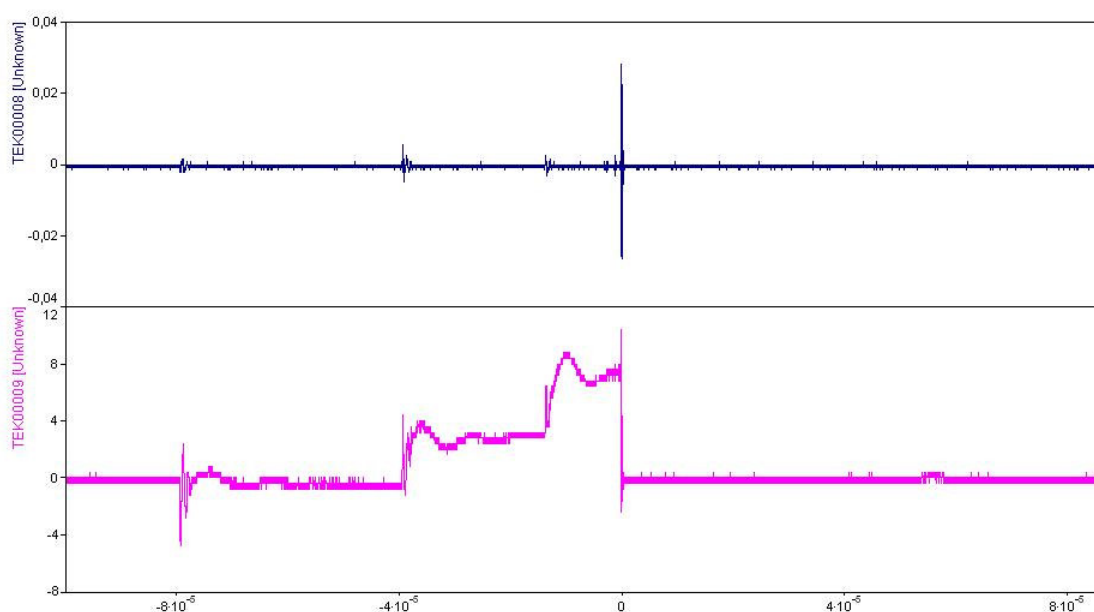


Fig.7.64 Real time signals received from the DA (upper) and the motor shaft (bottom). Time resolution  $10^{-5}$ s

It is easy to see the relations between the DA output and the motor shaft voltage variations. In contrast to the dipole antenna, the DA signal is obtained only when the shaft voltage falls down rapidly.

Let us take a closer look on the time when the shaft voltage falls down. The same waveform as in most of the previous sections can be observed in Fig.7.65.

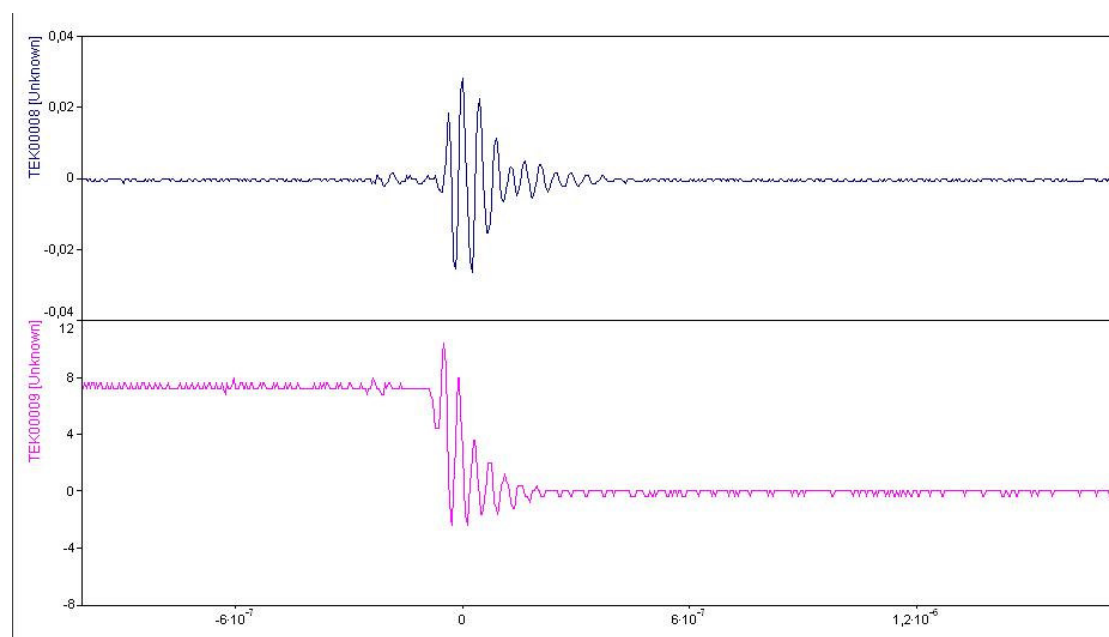


Fig.7.65 DA output and falling shaft voltage. Time resolution  $10^{-5}$ s

Fig.7.66 presents the frequency spectrum of the DA signal from Fig.7.65

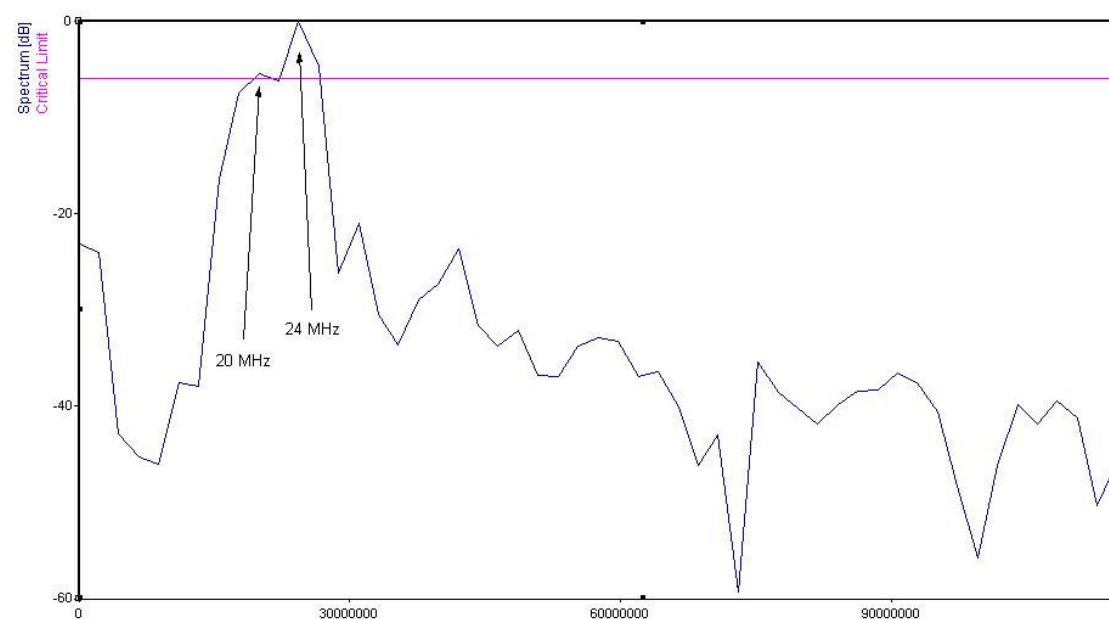


Fig.7.66 The frequency spectrum of the DA signal from Fig.7.65

The ringing frequency according to the FFT is 24MHz. It is slightly higher compared to the observations made before. The time resolution in this event is a bit low, which decrease the FFT accuracy. The obtained 24MHz should be considered as an approximately value.

Despite this difference, the frequency of the antenna signal can be considered still in the "20MHz" range. (15-30MHz)

## 7.6 Using at the Rogowski coil CWT1 in bearing currents detection

### 7.6.1 Synthetic test configuration

In order to measure the true bearing currents and compare them with the shaft voltage and DA readings, The Rogowski coil will be used in the synthetic test bench and on the already investigated motors. All possible ways of current flow will be checked.

The Rogowski coil parameters can be found in table 7.1

Table 7.1

Type	Sensitivity [mV/A]	LF bandwidth -3dB [Hz]	HF bandwidth -3dB [MHz]
CWT1	20	50	10

As a starting point the synthetic test bench was used. The coil was installed between housings one and two. The shaft was charged by the slip ring installed on the left side, and the shaft voltage was measured from the right shaft side using slip ring. Housings numbers one and two are insulated from the ground. Housing three was grounded. The DA was placed in front of the shaft right side, on the table. The whole measurement configuration can be seen on Fig.7.67



Fig.7.67 Synthetic test bench configuration

The signals obtained from the CWT1 show a current flow with a  $2A_{rms}$  value. These current flow correspond to a rapid shaft voltage drop. It also starts at the same time as

the signal received from the DA. Observing the upper and middle plots in Fig.7.68, a difference in the oscillations frequency can be noticed.

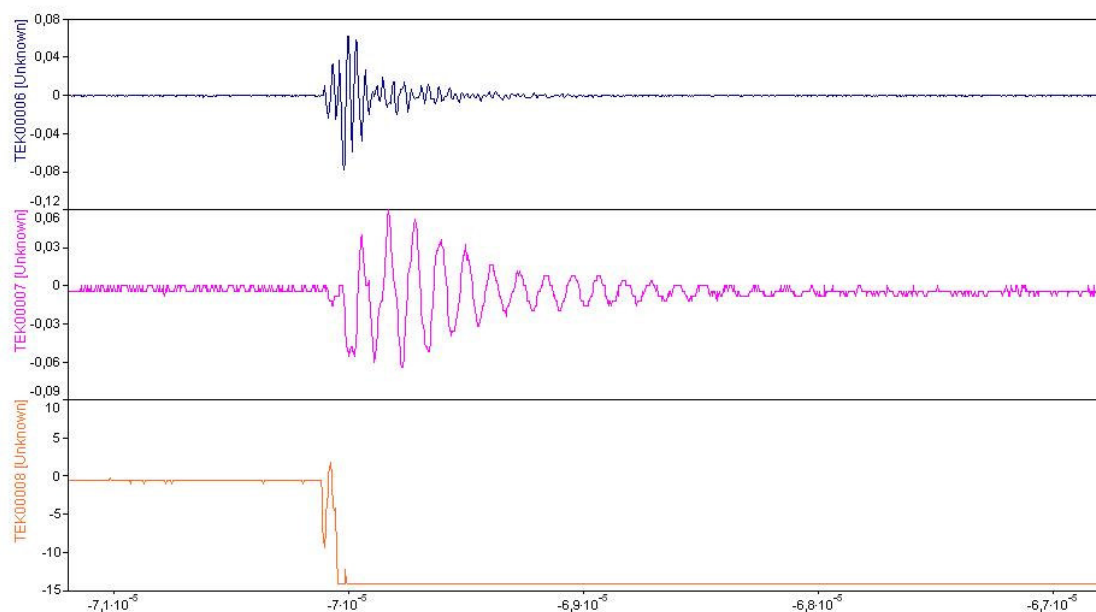


Fig.7.68 DA output (upper), CWT1 output (middle) and shaft voltage (bottom). Time resolution  $10^{-5}$ s

As in the interesting cases before, FFT on these signals have been done. The obtained result can be seen on Fig.7.69 and Fig.7.70

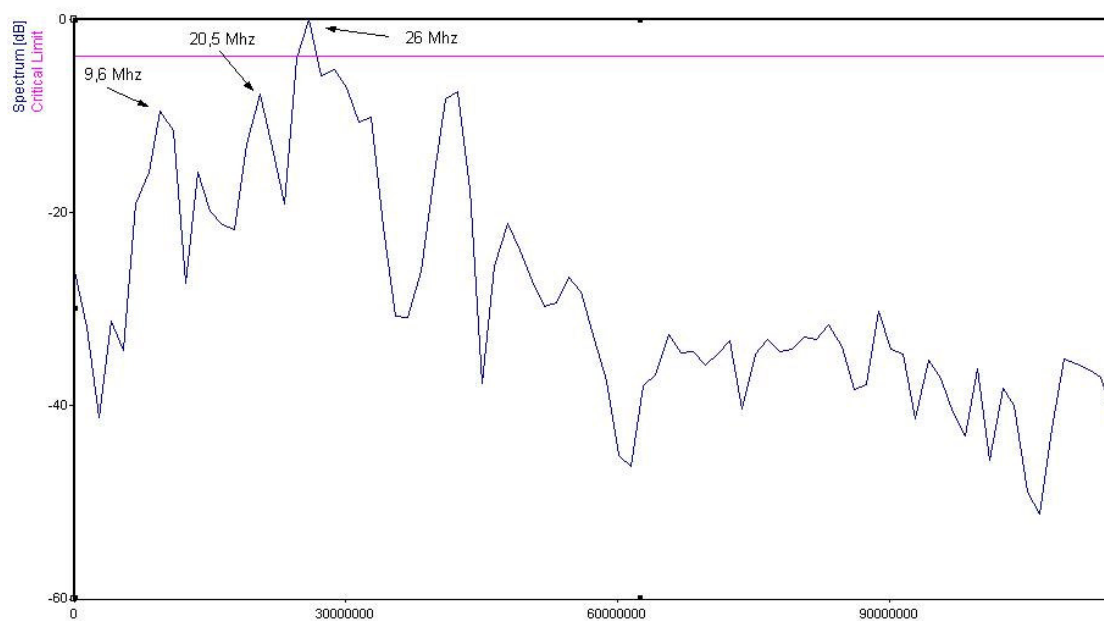


Fig.7.69 The frequency spectrum of the DA signal from Fig.7.68

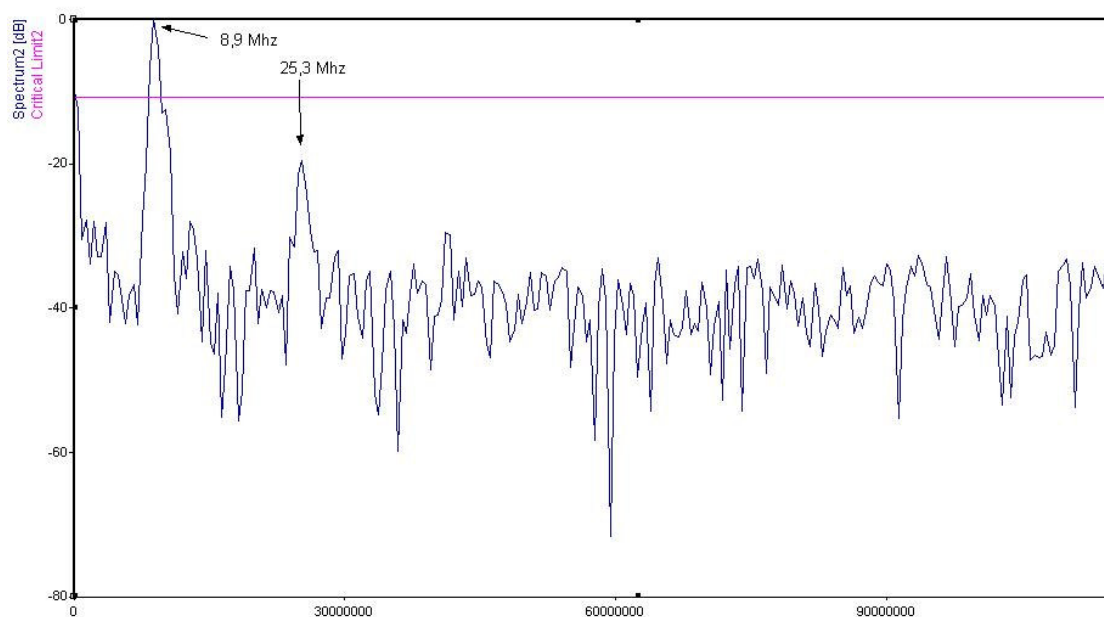


Fig.7.70 The frequency spectrum of the CWT1 signal from Fig.7.68

The dominant frequency of the CWT1 signal is 8,9MHz. There is one more frequency, which is 20dB below the first one. If they are compared to the DA signal spectrum, a similarity can be found. In both cases, the frequencies 9 and 26MHz are present. The magnitudes differ due to the CWT1 cut-off frequency of 10MHz.

Due to the absence of any other currents involved, it can be concluded that the current flow during the discharge inside the bearing three is the cause for the received signals from CWT1 and DA.

Now lets move to the real world.

## 7.6.2 7.5kW motor driven by Danffos converter

The tests described in this section have been performed using 7.5kW motor driven by the old VLT20 Danfoss converter. The main goal was to compare the CWT1 output with the DA and the shaft voltage when CWT1 is put in several different locations. In the best case it can help us to trace the unwanted current paths.

### 7.6.2.1 CWT1 around the power cable

For the first measurement, the CWT1 was placed around the motor cable. Fig.7.71 shows the obtained signals.

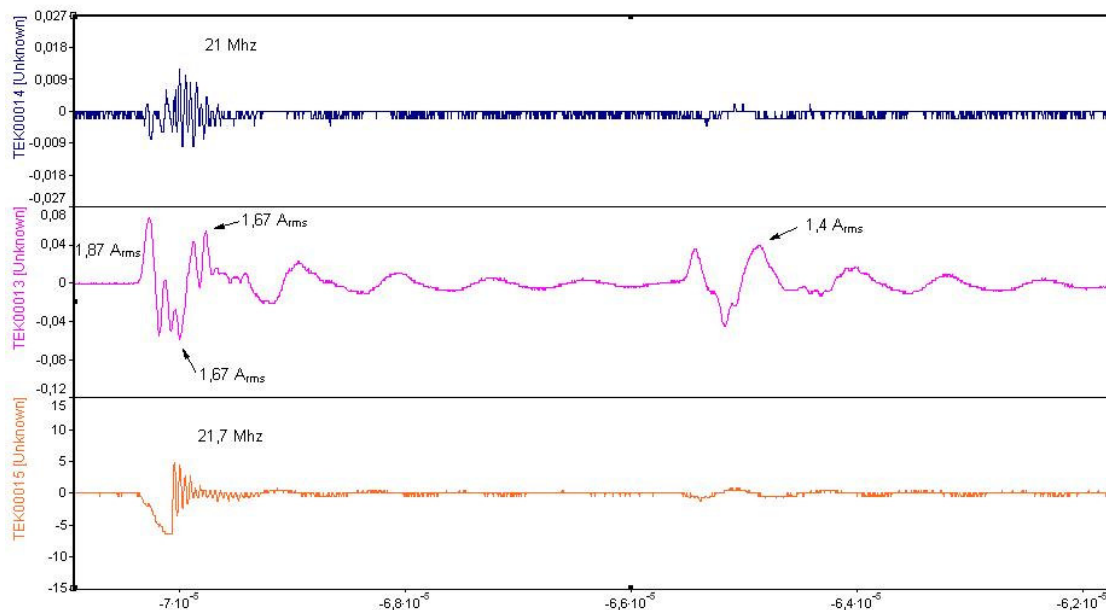


Fig.7.71 DA output (upper), CWT1 output (middle) and motor shaft voltage (bottom). Time resolution  $10^{-5}$ s

Surprisingly the highest current peak is detected before the discharge takes place. There is another current pulse in the power cable for which, the shaft voltage change is very small. A strange point is that the first CWT1 impulse and the shaft voltage rising point match in time. There is also a low frequency oscillation in the antenna signal just before the discharge takes place. Now lets take one other event and check the frequency of the DA, the CWT1 and the motor shaft voltage. Fig.7.72

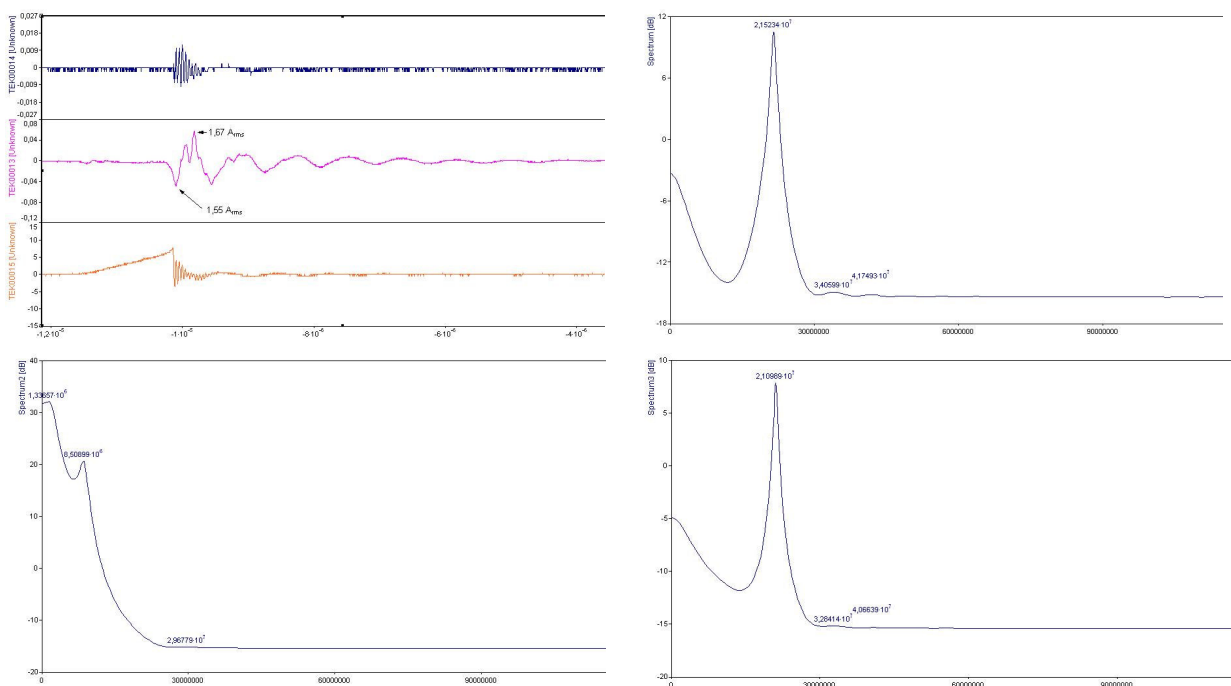


Fig.7.72 The event, DA, CWT1 and motor shaft voltage frequency spectrum

In Fig.7.72, the recorded signals are presented as well as the corresponding frequency. One of the special functions of FlexPro was used in order to estimate the signal frequencies. The values are as follow, 21,5MHz for the DA, 21,1MHz for the shaft voltage and 1,34 and 8,5MHz for CWT1. There is an indication that current pulses, coming through the power cable increase the common mode voltage and provoke the discharge. Based only on a few captured events, it is too early for any conclusions. Let's continue.

One more event will be presented before the CWT1 is moved to the new place.

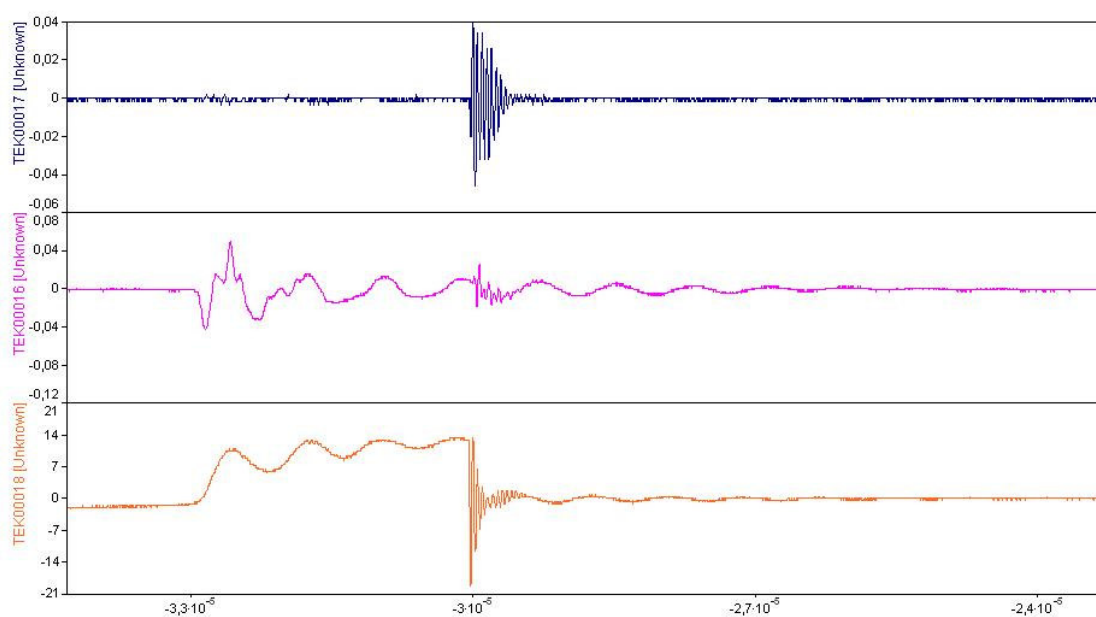


Fig.7.73 DA output (upper), CWT1 output (middle) and motor shaft voltage (bottom). Time resolution  $10^{-5}$ s

Now, lets take a look on the CWT1 output from Fig.7.73. The major current flow is during the shaft voltage formation and only a small HF oscillation is detected during the discharge. Is it an indication of bearing current? Looking only at CWT1 output, definitely not. The last figure just confirms the previously made observation about the motor shaft voltage formation.

### 7.6.2.2 CWT1 around the motor base

In order to monitor the motor frame-to-ground currents, the CWT1 have been installed around the motor base. In this setup, the plastic bushes are removed and two M8 bolts connect the motor plate to the ground. The current, which will flow trough these bolts, is going to be monitored. Fig.7.74 presents the test setup configuration.



Fig.7.74 Measurement devices placement

Now, let's take a look at the signals obtained from the new set-up. In fig.7.75 presents the one event-taking place when the motor is started-up. The final speed was set to 1300RPM but the presented results are obtained with a speed, much lower than that.

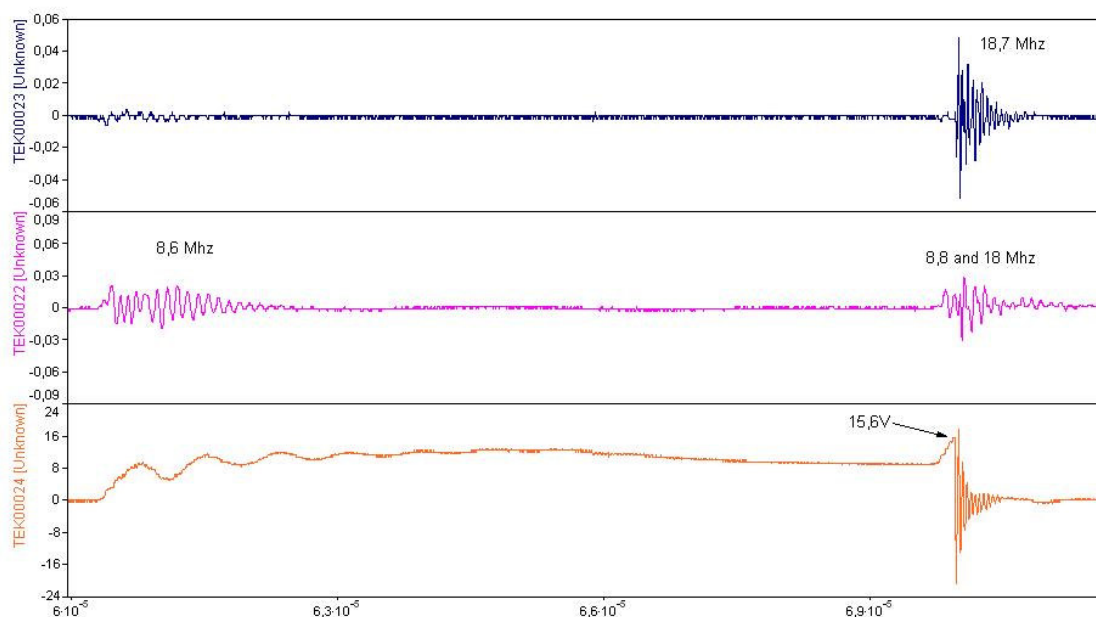


Fig.7.75 DA output (upper), CWT1 output (middle) and motor shaft voltage (bottom). Time resolution  $10^{-5}$ s

Now, instead of 1,34MHz during the shaft charge-up, the ringing frequency of the CWT1 signal is 8,6MHz. In addition, a signal with the same frequency is detected during the discharge. In the CWT1 output, an 18MHz signal is also presented due to the electrostatic coupling (no shielding). If the second CWT1 impulse is observed closely, a pre-discharge oscillation can be found. Comparing it with the configuration when the CWT1 is around the power cable, probably this can be the part of the shaft charge-up current.

Before making any conclusions, let's take a look at a couple of collected events.

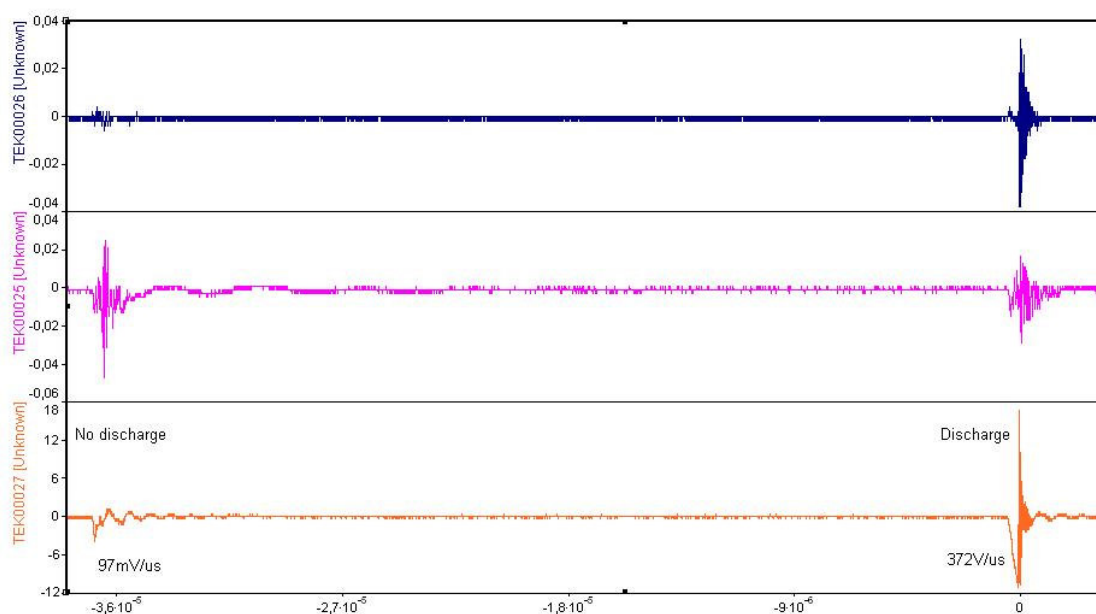


Fig.7.76 DA output, CWT1 output and motor shaft voltage. Time resolution  $10^{-5}$ s

Observing the signals shown in Fig.7.76, especially the CWT1 one, it can be calculated that in both cases there is a discharge taking place. In reality, in both cases there is a real current flow between motor frame and ground. In such a case, the shaft voltage can clear the unknowns. (Also the DA) The first voltage falling-front has a steepness of 97mV/us, which definitely is not discharge. The second event shows 372V/us steepness, which is a good indication for real discharge. At this time, the DA can confirm these observations.

The event shown in Fig.7.77 can be closely compared to the one obtained from the power cable and is shown in Fig.7.71

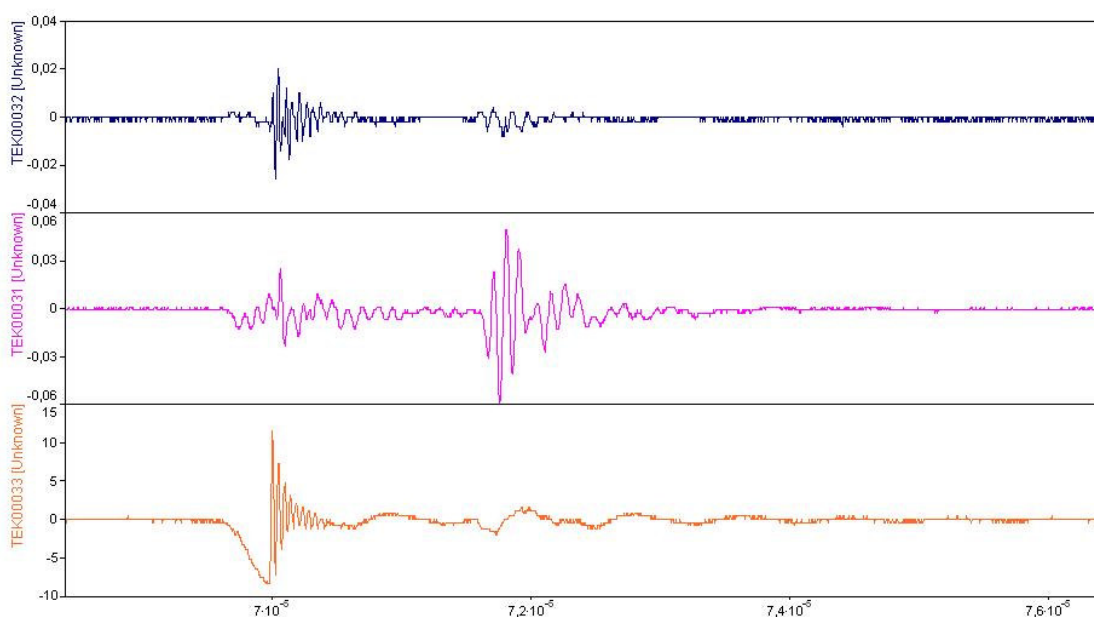


Fig.7.77 DA output (upper), CWT1 output (middle) and motor shaft voltage (bottom). Time resolution  $10^{-5}$ s

Is the second CWT1 impulse from Fig.7.77 a bearing current or it is due to inductive or capacitive coupling between the stator windings and the stator? For sure, at this time there is no discharge taking place inside the bearings.

One interesting event can be seen on Fig.7.78. There is a 1.2A current pulse flowing between the motor frame and the ground. The shaft voltage has an oscillatory behavior. The signal received with the DA has 10 times lower magnitude compared to the received signal when the discharge takes place. This can be qualified as a  $dv/dt$  current. The capacitive coupling between the stator windings and the stator can be considered as a possible cause.

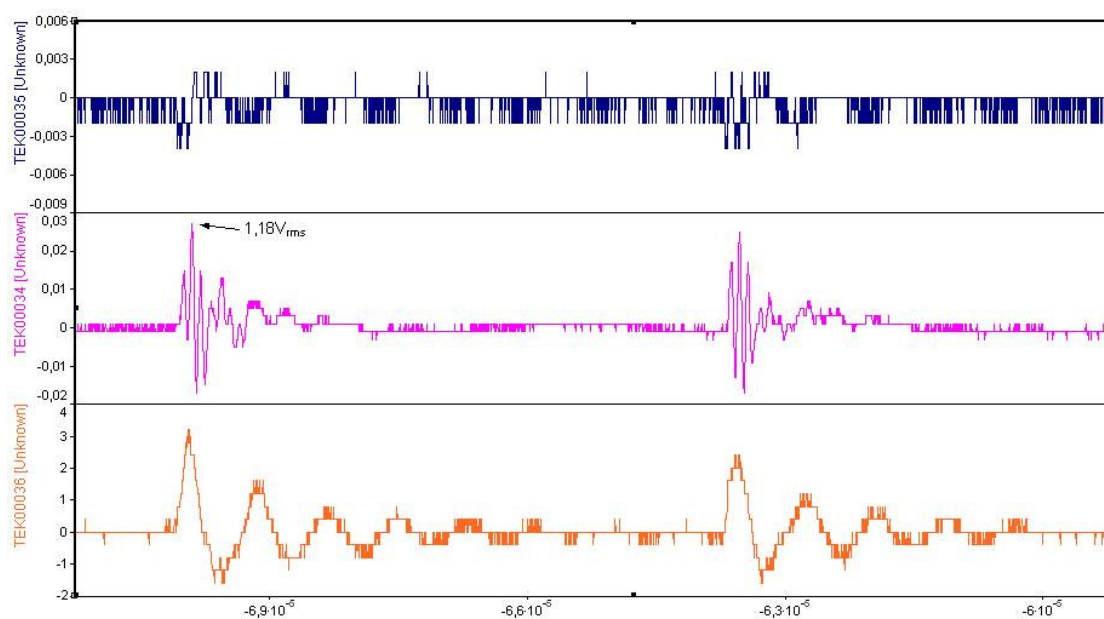


Fig.7.78. DA output (upper), CWT1 output (middle) and motor shaft voltage (bottom). Can be  $dv/dt$  current. Time resolution  $10^{-5}$ s

The last measurement was done, connecting the motor shaft to ground and putting the CWT1 around this connection. The DA and CWT outputs were monitored. A selected events is presented in Fig.7.79

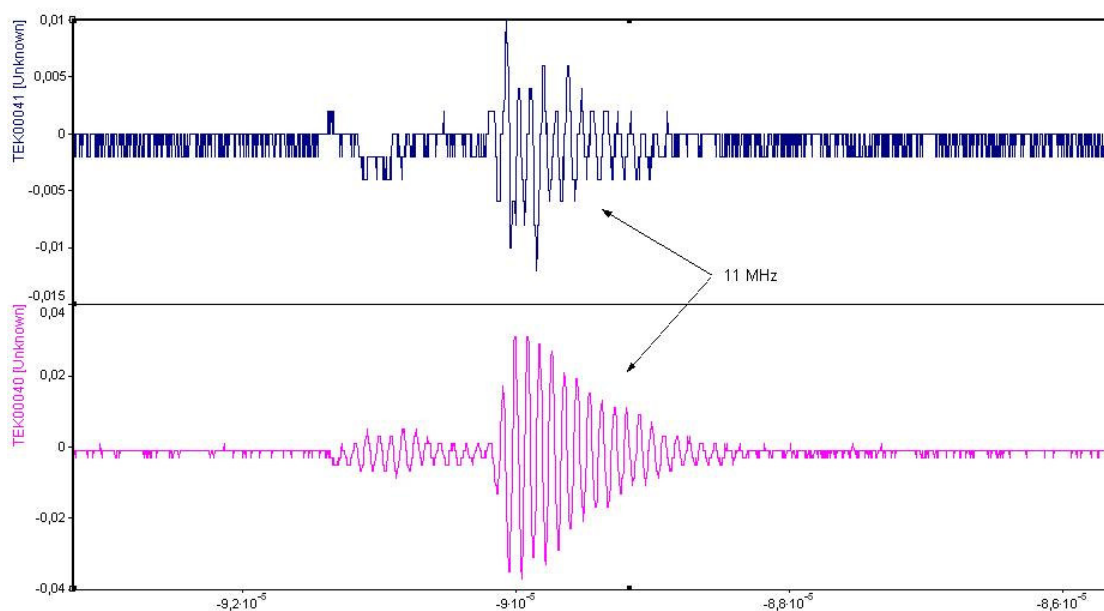


Fig.7.79 DA (upper) and CWT1 (bottom) output when the motor shaft is connected to ground. Time resolution  $10^{-5}$ s

There is 1Arms current flowing in the shaft grounding cable. The signal received with the DA has a 3-4 times smaller magnitude and a frequency of 11 MHz. The current signal has the same frequency as the one observed by the DA. This can be considered

as part of the circulating bearing currents or current due to the shaft-to-stator winding inductive and capacitive coupling. The signal frequency is expected to be dependent of the grounding cable impedance (length).

### 7.6.3 132kW motor driven by Siemens converter

The 132kW motor was used as an object of our tests. The data will be captured when the motor is running with a speed of 900RPM and also, during the start up. The most valuable data is expected from the start-up. As in the tests before, the signals from the DA, CWT and shaft voltage will be recorded.

#### 7.6.3.1 CWT1 placed around the motor shaft

The test setup configuration is presented in Fig.7.80

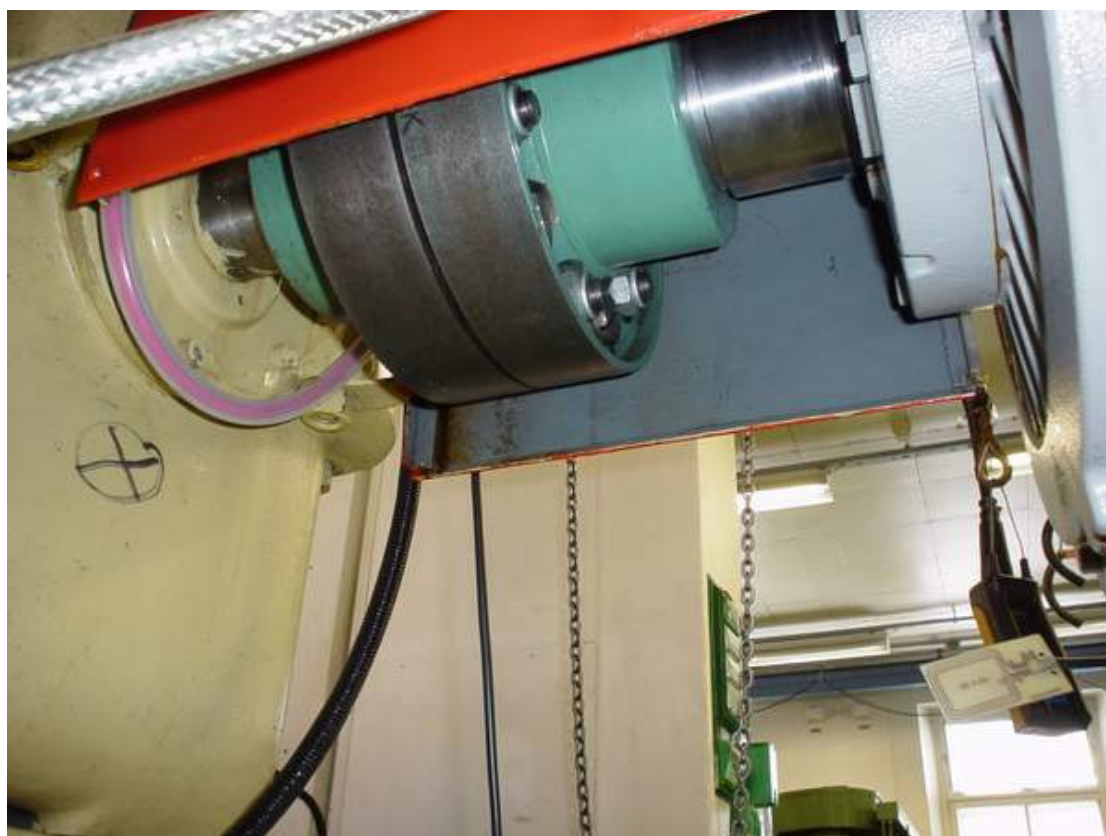


Fig.7.80 Test setup configuration

The antenna was placed approximately 300mm away from the motor shaft. The Rogowski coil was placed around the shaft between motor and gearbox. A steel wire was used as a brush, in order to monitor the shaft voltage.

Fig.7.81 present the first couple of events. At this time the motor was running with 900RPM.

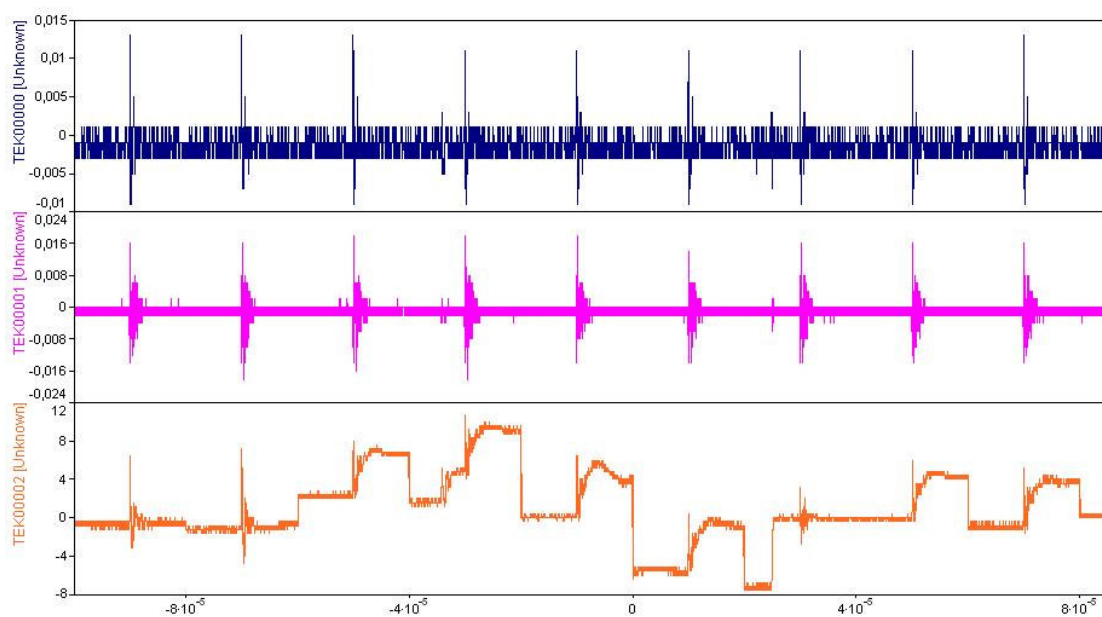


Fig.7.81 DA output (upper), CWT1 output (middle) and motor shaft voltage (bottom). 900RPM. FF mode

In order to obtain a more clear view and to study what happens in reality, let's take a closer look on two selected events. The first one can be seen on Fig.7.82

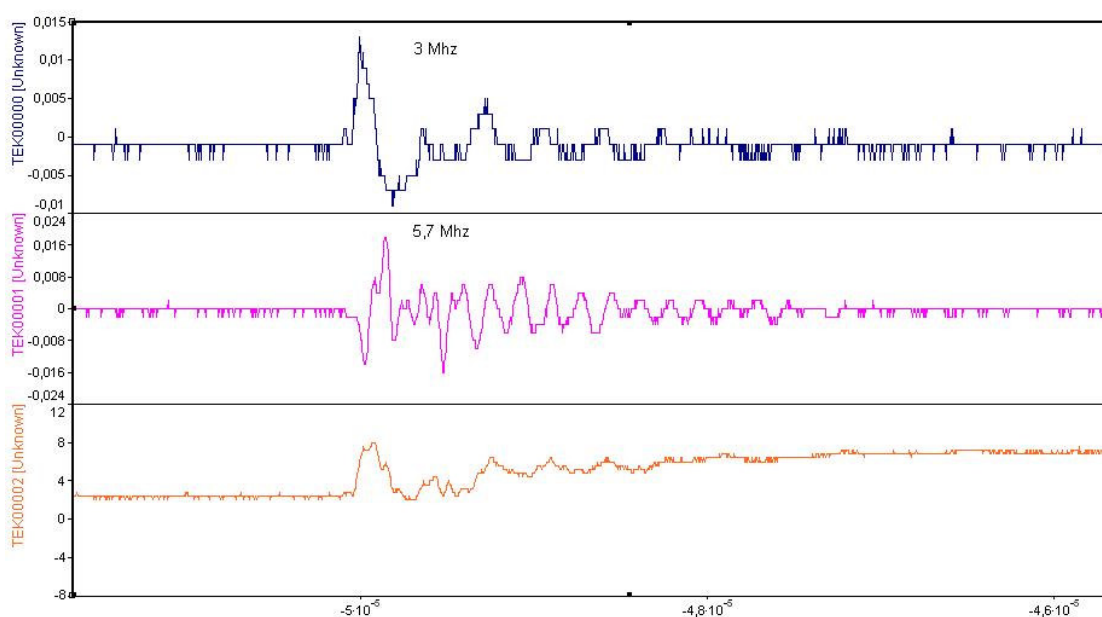


Fig.7.82 First event from Fig.7.81 Time resolution  $10^{-5}$ s

There is a shaft voltage change, a signal from the DA and current in the gearbox shaft. All start at the same time. Keeping in mind the signal frequencies and the signal shapes from the previous measurements, it is hard to classify this as a bearing discharge current. It seems to be related more to the shaft voltage formation.

Lets take a look on the next figure. The event shown, happens only once in this data length.

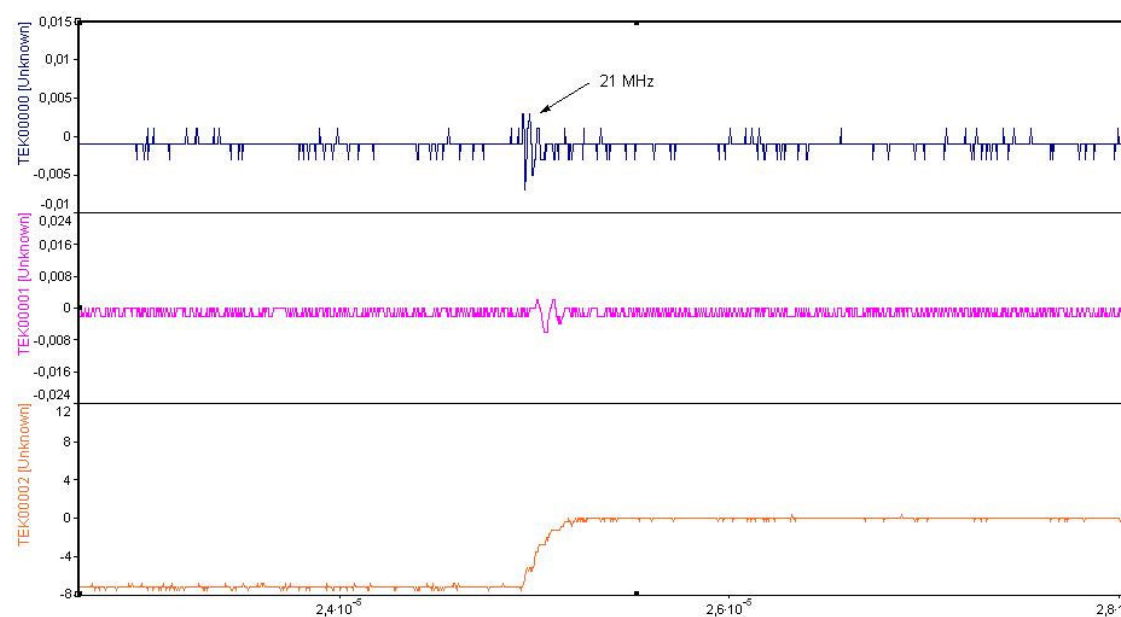


Fig.7.83 DA (upper), CWT1 output (middle) and motor shaft voltage (bottom). Probably discharge current. Time resolution  $10^{-5}$

This event matches more closely the "requirements" for a discharge current. The shaft voltage drops from -7.2V to zero, the antenna signal has a 21MHz oscillation. According to the CWT, the shaft current is  $0,2A_{rms}$ . Probably the discharge current flows from the bearing outer race, trough the motor frame and to ground.

In the second Fastframe data set, only two events can be classified as bearing discharge current. Fig.7.84 shows the first one.

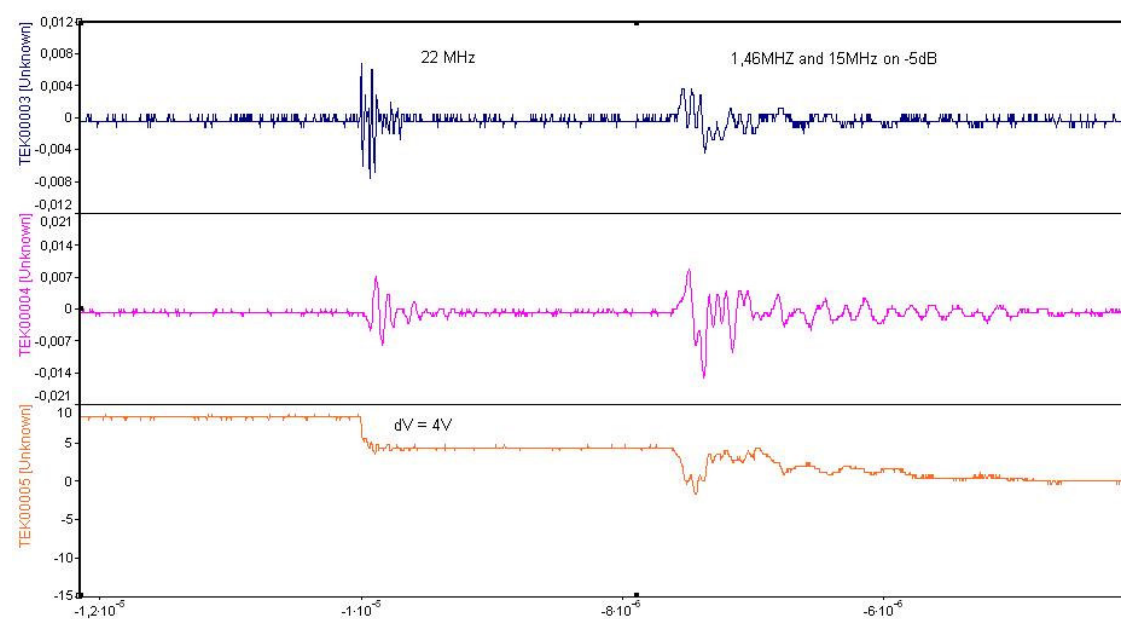


Fig.7.84 DA, CWT1 output and motor shaft voltage.

The CWT current was  $0,25A_{\text{rms}}$  and the voltage drop - 4V. In order to obtain more valuable data for comparison and investigation, several start-ups were performed and the data were saved.

Fig.7.85 present the captured data length.

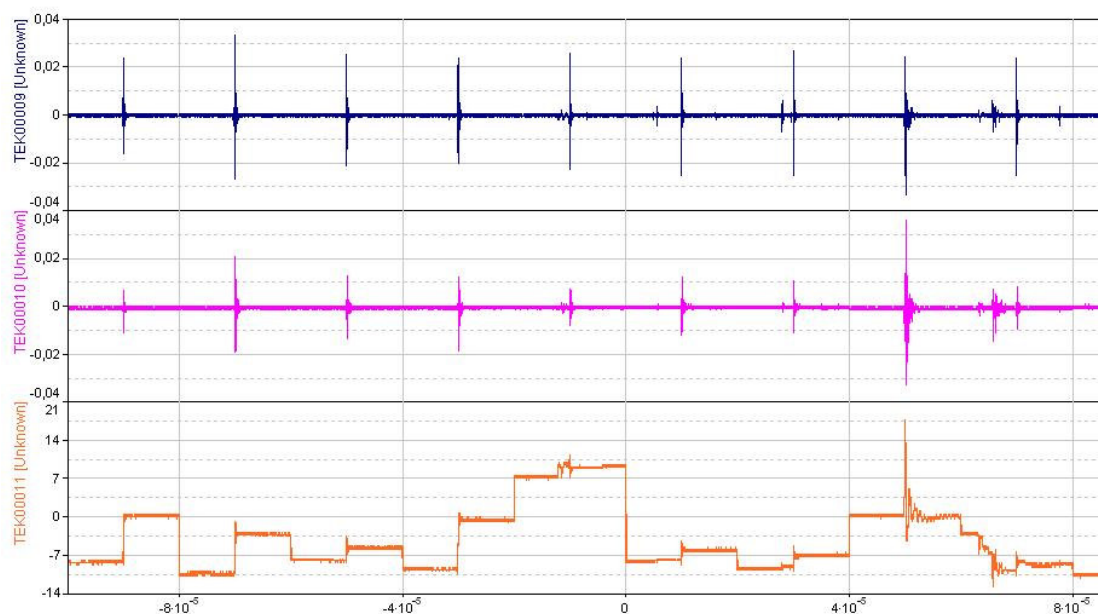


Fig.7.85 DA (upper), CWT1 output (middle) and motor shaft voltage (bottom) during start-up. FF mode

A simple comparison between the shaft voltage changes and the signal received with the DA suggests the presence of many bearing current discharges. Let us take a closer look on the first impulse from fig.7.85. The DA signal frequency is a little bit lower than our expectation.

Despite of this observation, as a combination together with the shaft voltage variation, it can be believed to be a good indication for bearing discharge currents.

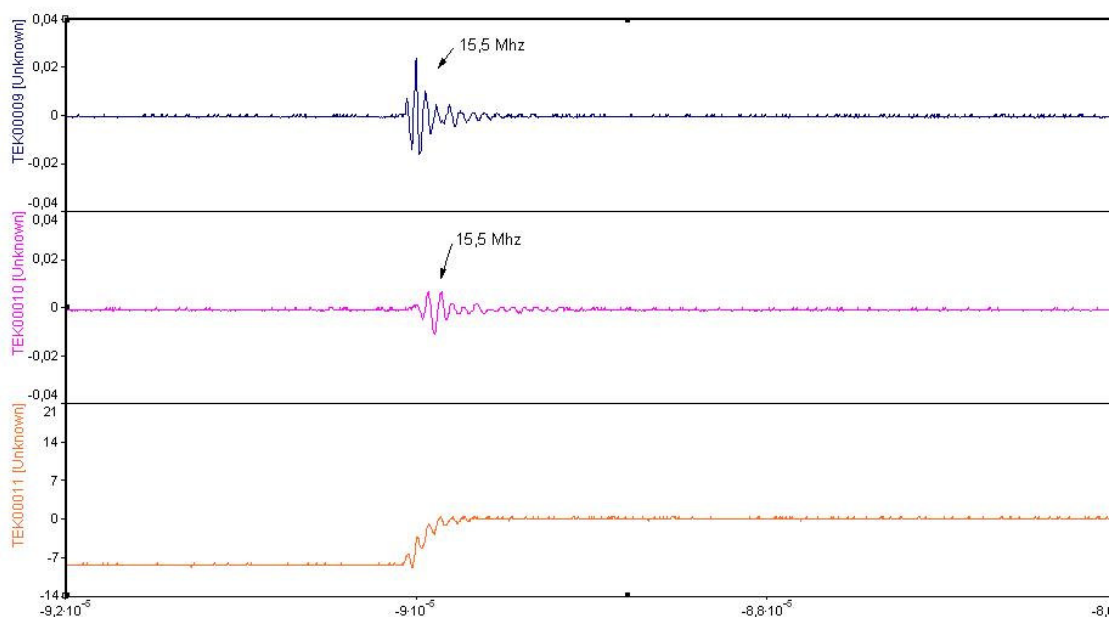


Fig.7.86 First event from Fig.7.85. DA (upper), CWT1 output (middle) and motor shaft voltage (bottom). Probably discharge current. Time resolution  $10^{-5}$

To make the situation clearer, let's take a closer look on the second impulse. As it can be seen in Fig.7.87, all three signals look similar as the one presented in the previous case.

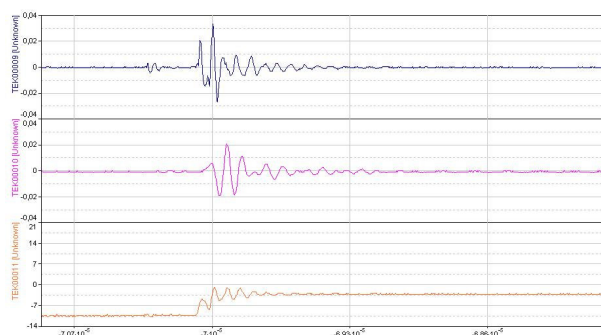


Fig.7.87 Second event from Fig.7.85

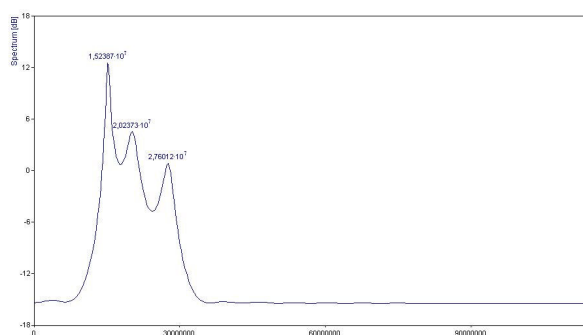


Fig.7.88 Frequency specter, Eigen estimation

The signal received with the DA has the same frequency. This is the lowest value obtained from all of the investigated motors. The result of an FFT of the whole data length is shown in fig 7.88. The dominant frequency is 15MHz, followed by a 21 and a 25MHz signals.

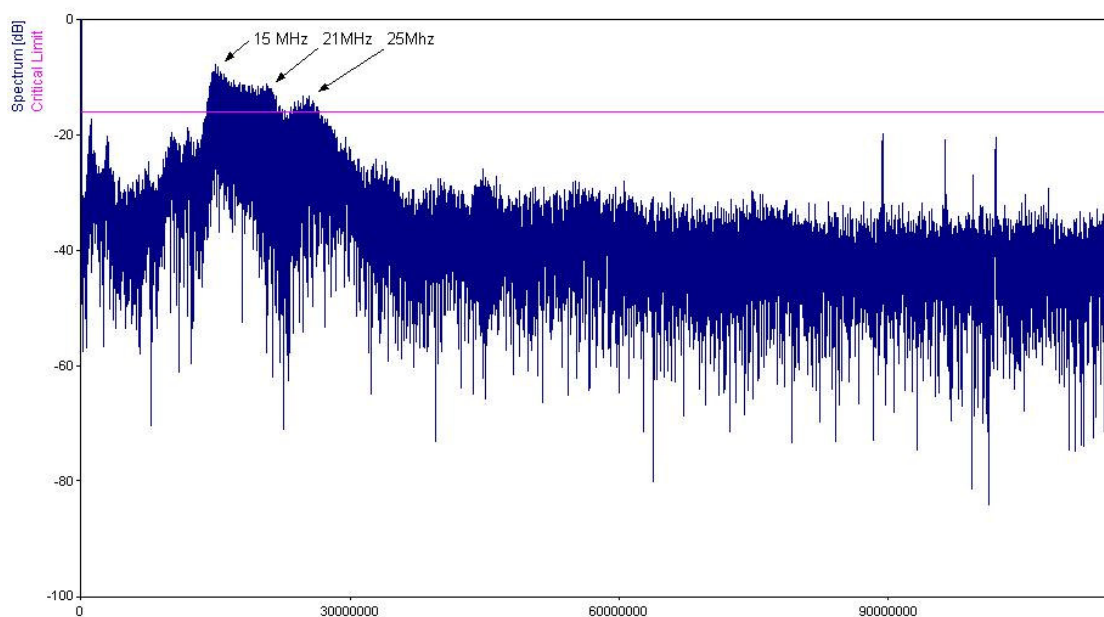


Fig.7.89 FFT of all data length of Fig.7.85

The frequency range is slightly different from the one, shown in chapter "7.5.8 132kW motor driven by Siemens frequency converter investigation using 16Mhz DA". It can be due to the different test conditions or some other still unknown factors. It has to be mentioned that the motor is running with no load.

The good news is that, still the frequency range is same.

### 7.6.3.2 CWT1 placed around the motor power cables

The test setup configuration is shown on Fig.7.90



Fig.7.90 Part of the test setup configuration

The antenna was placed approximately 600mm away from the motor shaft. The Rogowski coil was placed around the two power cables. As in the previous tests, a steel wire was used as a brush, in order to monitor the shaft voltage.

Finding pulses, which fit the "concept" for bearing discharge, was more difficult. The whole data length, consisting of more than ten events is shown on Fig.7.91

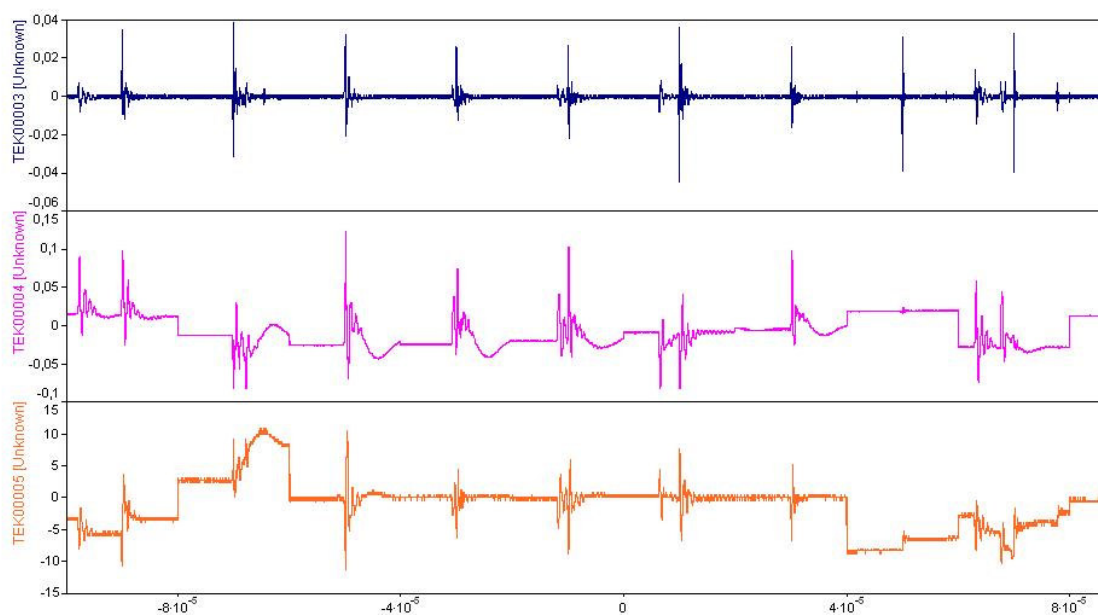


Fig.7.91 DA (upper), CWT1 output (middle) and motor shaft voltage (bottom) during

start-up. FF mode

In most of the time, the motor shaft voltage follows the CWT1 output (current like). This is not valid for the cases, where a "25 MHz" DA impulse is present. At this time, the shaft voltage changes and reach values, close or exactly 0.

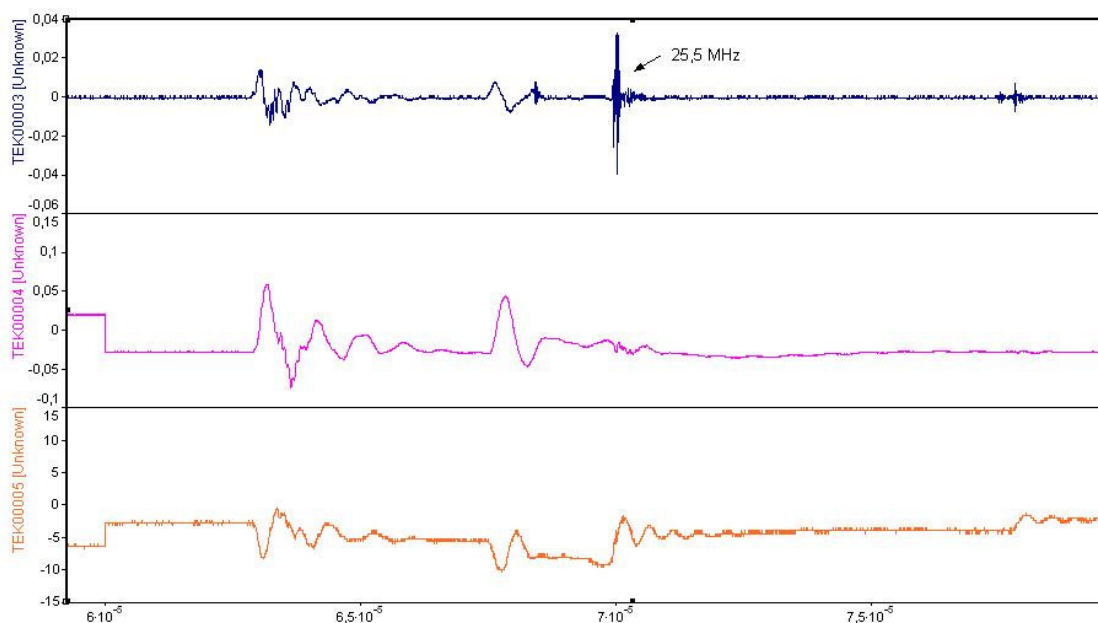


Fig.7.92 Two different DA impulses. Time resolution  $10^{-5}$ s

In the above-presented data, and especially from the CWT1 output it is hard to find a clear indication for bearing discharge currents. Using the power cables as a source of information does not give satisfactory results.

## 7.7 Summary

Using three bearings mounted on one shaft, a simple impulse circuit, an dipole antenna and a coaxial shunt, the detecting of EDM currents were investigated. The antenna voltage pulses were proportional to the current pulses. They started at the same time. The current pulse had 5 MHz oscillations. The coaxial shunt connection cable impedance should be taken into account when this frequency is mentioned.

After several performed test with the dipole antenna and the Pearson current monitor, it was concluded that the OLA output is more related to motor shaft voltage and the disturbances emitted from the current carrying cables.

The first antenna showed good results on a synthetic test configuration but failed in a noisy environment.

The performed tests using a closed loop antenna showed a good relation between the DA output and the steep slopes in the shaft voltage. It can be concluded that the discharges can be counted easily. With the antenna placed 600mm away from the housing we still receive a strong signal. When the shaft voltage goes down, the corresponding impulse is received with the antenna. This impulse has a ringing frequency of 8MHz. The shaft voltage has a very steep slope that is clear indication for bearing current.

The performed tests using the DA on a 7.5kW motor demonstrate the impulse separation capability of the DA. Fig.7.20. The impulses obtained by DA corresponds to voltage drops in the motor shaft. The number of received signals from the DA depends of it placement.

The measurement of the motor frame to ground current cannot give bearing discharge information that is clear enough. Such a measurement can only be helpful when it is combined with other signals.

Using the DA on a 7.5kW motor two type of impulses occurred. One had a dominant ringing frequency of 20 MHz, and the other - a frequency of 3.8 MHz. The 20 MHz impulses correspond to motor shaft voltage drops, for the 3.8 MHz ones, there is no shaft voltage changes observed.

A 3.5kW motor for a fan application shows no discharges when it operates in steady state. However, during the start-up, using the DA, two types of impulses were captured. They have a ringing frequency of 7,5MHz and 19,38 MHz, respectively. The 19,38MHz impulse can be connected to the discharge phenomena.

The "7.5MHz" impulses are present due to the Csr and Cb charging currents. This component is mainly present due to the converter switching times and high  $dV/dt$  levels.

With the increase of the shaft speed, the common voltage magnitude goes down, which leads to a decrease and even a disappearance of the observed discharges. It was noted that small variations of only 50rpm could trigger EDM currents

The same result was obtained using a 16MHz antenna instead of an 8MHz antenna. The impulse frequency shows no dependency of the antenna resonance frequency. Only the received signal magnitude is affected due to the different antenna sensitivity for different frequencies.

To all impulses, received from the DA, there is a corresponding MSV slope with high  $dV/dt$ . This can be considered as a true EDM discharge inside the motor bearings.

The frequency of the events, captured from 3kW and 7.5kW motors are very similar. The two motors are installed in totally different places. In both cases, only the frequency converter is the same. For the first motor, the dominant frequency is around 18,5MHz and for second one it is located around 22MHz.

For the events with a magnitude of below 3V there is no corresponding impulses from the DA. For the others, which have a magnitude higher than 3V, impulses from the DA were received. This observation can be supported with information from technical papers, which describe a minimal threshold of about 3V. This voltage can vary in a wide range. Mainly it depends on oil film thickness, dielectric strength and oil contamination concentration. The repetition of the discharges is approximately 500Hz.

The performed tests using a 7.5kW motor and two different frequency converters show no dependency between the events frequency, the used converter and antenna resonance frequency. (Fig.7.55 and Fig.7.59). The received signals from the DA remain in the expected frequency range of 18-22MHz.

It was found that there is no relation between the DA impulse oscillations and the motor shaft voltage.

The frequency of the captured events remains the same for the 3kW, 7.5kW and 132kW motors driven by different frequency converters.

In contrast with the large differences in the motors sizes, the frequencies of the pulses, correspondent to the discharges, are in the range of 18-23MHz. This is not an exact value, even for the same motor and converter, due to the fact that the impulse frequency varies from impulse to impulse.

Using a Rogowski coil CWT1 mounted around the motor power cable, the highest current peak is detected before the discharge takes place. There is another current pulse in the power cable for which, the shaft voltage change is very small. There is also a low frequency oscillation in the antenna signal just before the discharge takes place.

There is an indication, that first current pulse, coming trough the power cable increase the common mode voltage and provoke a bearing discharge.

The major current flow is during the shaft voltage formation and only small HF oscillations are detected during the discharge. Looking only at the CWT1 output, it is hard to detect the presence of a discharge.

Using the CWT1 mounted around the motor base, the currents flowing between the motor frame and ground could be measured. They can have different origins. Based only on the CWT1 output information, it is hard to separate them. The presence of HF (20MHz range) oscillations in the CWT1 output can be used as an indication for the presence of a discharge current.

The currents flowing through the connection joint between the motor and the gearbox can be measured with a CWT1. The frequency of the captured events is typically in the coil bandwidth. The impulse frequency can go up to the frequency of the impulse, received by the DA.

From the performed tests it can be concluded that the Rogowski coil cannot give a reading of discharge currents due to the low HF bandwidth. It is possible to use it in a common mode current formation detection.

It is also suitable to use a CWT1 for circulating, common mode, shaft grounding and protection earth currents detections and also for the detection of different unwanted current paths.

## 8 Suggested set-up

To give advice for the staff, which will try to evaluate the antenna EDM detection method, the information obtained from all performed tests have to be considered. There is not a single solution for antenna placement and shaft voltage detection. It differs from motor to motor and place to place. Based on the tests, performed on different motor installed in different places, we can give a couple of guiding notes.

- The DA should be pointed to the suspected place.
- When looking for EDM inside the motor bearings, the antenna should be placed far away from the motor feeding cables.
- Monitoring of the shaft voltage if possible using a slip ring or an OLA.
- Short coaxial connection cables should be used.
- Always check the background noise, before starting the investigated motor.
- Try different antenna placement in order to find the strongest signal.
- If gearbox or other conductive equipment is connected to the motor, use a Rogowski coil placed around the shaft.
- When using a Tektronix 544 try to use the highest triggering level on the DA signal.
- The Tektronix Fast Frame mode is very useful when event with random nature have to be collected.
- Restrict channel bandwidth to 100MHz in order to minimize the unwanted noises.

## 9 Characterization

Using the new antenna method, different devices can be constructed for early bearing discharges detection. Starting from the simplest one and ending with microcomputer based characterization equipment. At this time the technology is no limiting factor.

Fig.9.1 presents the block diagram of a possible device configuration.

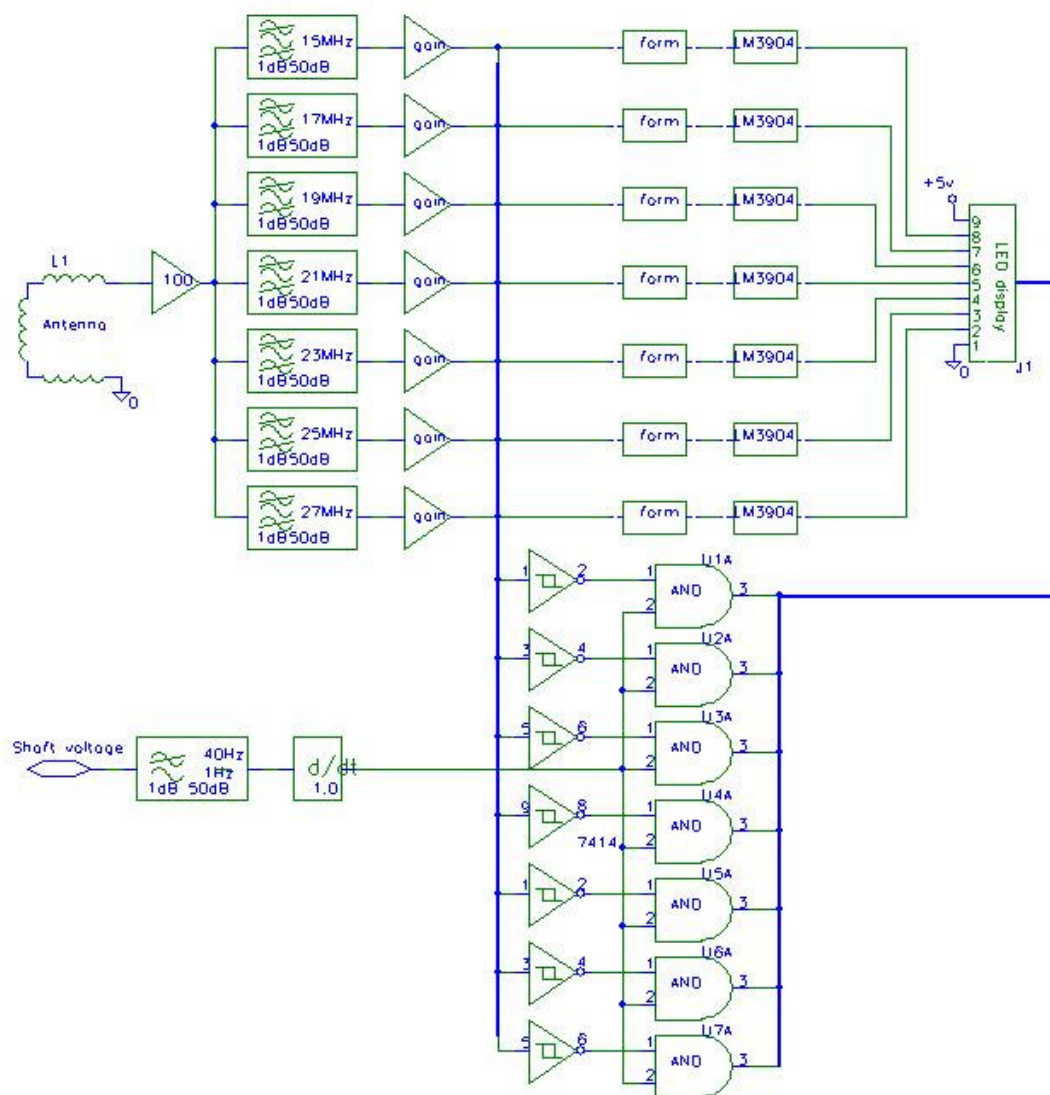


Fig.9.1 Simple characterization device block diagram

This is only a block diagram aimed to show the principle of work of the device. It can be realized with discrete components. The easiest way is to implement it in MatLab. As an input, a file with collected data from the DA and OLA or shaft voltage has to be provided. Using mathematical algorithms, the needed information easily can be visualized. The purpose of using two input signals is to improve the authenticity of the displayed information. Based on the information, obtained from different motor tests, the combination of a "20MHz" antenna signal and steep negative shaft voltage slope

can be considered as a true discharge indication. In the same way, using the powerful calculative methods of MatLab. The discharge energy can be calculated. It simply can be done using the motor and bearing capacitance estimation and the pre-discharge shaft voltage.

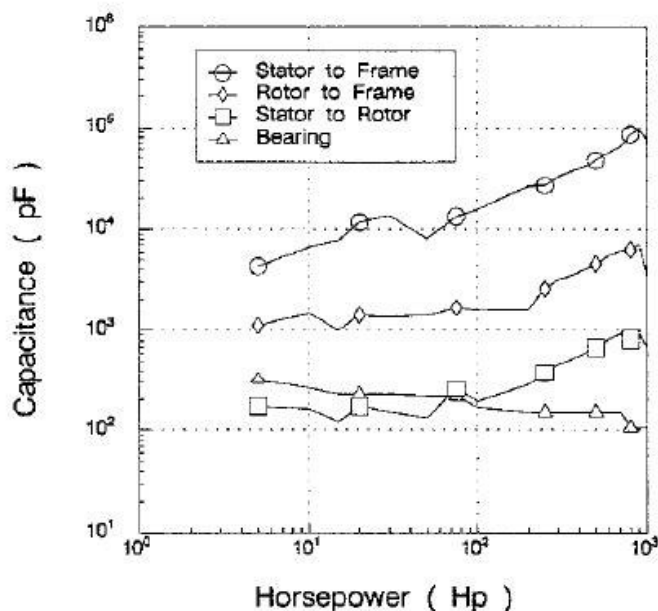


Fig.9.2 Motor and bearing capacitances

Already calculated values for discharge energy with combination with the repetition of the discharges can be used for bearing life estimation.

Another proposed circuit topology is presented in Fig.9.3.

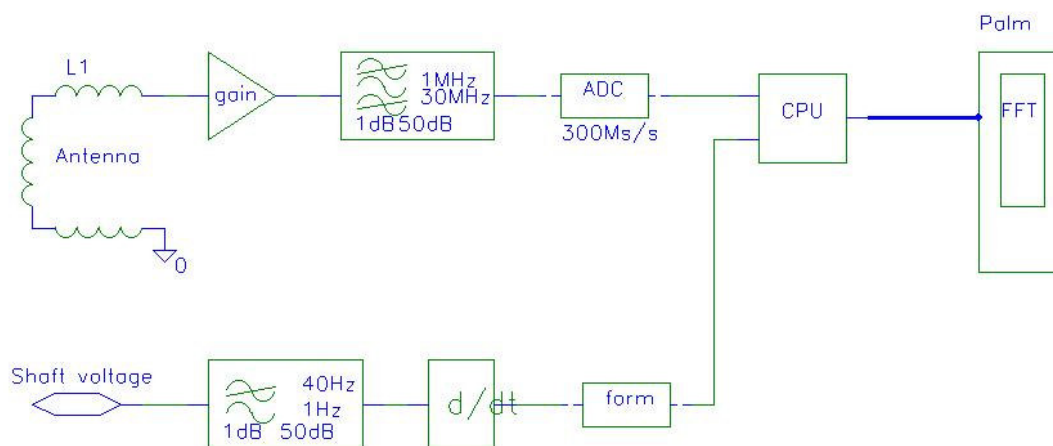


Fig.9.3 ADC and microcontroller based characterization device

The same principle of the DA output and shaft voltage monitoring can be used. When this circuit is realized as a standalone handheld device, it will provide the test personal with information for the DA signal spectra, event repetition, and discharge energy. Using the capability of the new handheld device for memory expansion, it also can be used for long period data logging and further signal investigation.

## 10 Conclusion

Bearing currents in electric motors are not new. Internally sourced currents within the motor have been known to exist in sine wave driven motors at least 80 years. Externally sourced bearing currents are new and present new challenges. When and where bearing currents will become a problem is still unpredictable.

The main objective of this thesis was to investigate the discharge characteristics phenomenon of bearing currents for inverter driven motors. No standard test methods exist, that can evaluate bearing current problems and one of the key aspects associated with that is the inability to directly measure bearing currents.

This thesis proposes a new approach for the measuring & detection of bearing currents in inverter driven motors. The results are promising due to the fact, that the test was successful to identify the presence of shaft currents and hence discharge of bearing currents.

The theory is based on the identification of high frequency bearing currents existing inside the motor. Experiments have been performed on different types of motors to verify the discharge currents in induction motors. The existence of bearing discharge currents have been predicted both theoretically and verified experimentally.

The obtained results shows that it is also a promising and convenient way of analysis in this field. There is no standard, well-known direct relationship between bearing voltage magnitude and bearing damage.

The result of this report can be applied in research and development. This thesis may gives guidelines for research in the area of bearing failure analysis and hopefully may give some ideas for developers.

## 11 Future work

Hardware software for remote detection and analysis has to be developed. The "20MHz" signal presence has to be proved in as much as possible different induction motor sizes. The obtained information will be used for discovering the reasons of having relatively narrow frequency band of the transmitted signals.

The early diagnostic will provide the possibility to minimize or fully eliminate the discharge currents and save the bearings.

In contrast to the present diagnostic "after fault" study, the proposed antenna method will provide the chance to detect the problem before any surface changes takes place in the bearing races and rollers.

Bearing currents with pre-programmed magnitude and repetition can be used to investigate and even to destroy a couple of bearing and create a database with the most common damages. This database can be used later on by the qualified service engineers for easy troubleshooting and problem solving.

The bearing discharge detection techniques described in this thesis can be developed further. The most interesting aspect is probably the potential to use it as an automatic early warning system and continuous monitoring. It will provide the possibility to act before the irreversible processes takes place in the motor bearings.

Finally, it will be of interest to study the emitted signal frequency dependency from the motor type, converter type of operation and the surrounding environment. Remote detection and measurement of bearing currents is certainly a challenging task where non-traditional methods can be discovered and investigated further.

---

## References

- [1]. S.Chen and T.A.Lipo, "Bearing currents and shaft voltages of an induction motor under hard and soft switching inverter excitation", Industry applications, IEEE transaction on Volume: 34 Issue: 5, Sept.-oct.1998, pp: 1042-1048.
- [2]. P.J. Link, P.E. "Minimizing Electric bearing currents in adjustable speed drive systems" ABB industrial systems Inc.
- [3]. M.J.Costello,"Shaft voltages and Rotating Machinery", Industry applications, IEEE Transactions on, Volume: 29 Issue: 2, March-April 1993,pp: 419-426.
- [4]. A.von Jounne and H.Zhang, " Bearing currents: A major source of mechanical failure for motors in adjustable speed drive applications", Turning point, September 1998.
- [5]. H.E.Boyanton," Bearing damage due to electric discharge", 23July 1995.
- [6]. D McDonalds and W.Gray," A practical guide to understanding bearing damage related to PWM drives", Pulp and paper Industry Technical conference, 1998, Conference record of 1998 Annual, 21-26 June 1998,pp: 159-165
- [7]. Steve Barker, "Avoiding premature bearing failure with inverter-fed induction motors", Power Engineering Journal August 2000.
- [8]. A.Muetze, A Binder, " Experimental evaluation of mitigation techniques for bearing currents in inverter supplied drive systems-Investigations on induction motors up to 500kW".
- [9]. "Bearing currents in modern AC drive systems", Technical guide no.5, ABB industry Oy, Finland.
- [10]. Steven W Saylor's, P.E, "Motor bearing failure from VFD induced shaft to ground voltages in HVAC applications".
- [11]. "Greenheck product application articles", A technical bulletin for engineers, contractors and students in the air movement and control industry, P.O. Box 41; Schofield, WI54476.
- [12]. "Motor shaft voltages and bearing currents under PWM inverter operation", A Gambica/Rema Technical report no.2 first edition.

---

[13]. S.Chen and T.A.lipo and Donald W.Novotny," Circulating type motor bearing current in inverter drives".

[14]. EDM process mechanism,  
<http://www.unl.edu/nmrc/Processmech/Processmech.htm>

[15]. "Inverter-driven induction motors shaft and bearing current solution, industry white paper" Rockwell automation.

[16]. D. A. Ward and J. La T. Exon, "Using Rogowski coils for transient current Measurements", Engineering Science and Education Journal, Volume: 2 Issue: 3, June 1993, pp: 105 –113.

[17]. Tuomo Lindh "On the condition monitoring of induction machines" PhD paper of Lappeenranta University of Technology, Finland.

[18]. Adam Kempinski, Ryszard Strzelecki, Robert Smolenski, Zbigniew Fedyczak" Bearing current path and pulse rate in PWM-inverter-fed induction motor".

[19]. Dick Buddulph G8DPS, VHF/UHF Handbook ISBN 1 872309429

[20]. Harry's Homebrew Homepages

[21]. HF Antenna Design Notes, Technical Application Report, Texas Instruments

[22]. HF Antenna Cookbook, Technical Application Report, Texas Instruments

[23]. Antenna Circuit Design for RFID Applications, Microchip, AN710

[24]. High Performance Rogowski Current Transducers W.F.Ray

[25]. High Frequency Improvements in Wide Bandwidth Rogowski current transducers W.F.Ray

[26]. RF Inductor Design, <http://www.lancs.ac.uk/ug/simmw/inductors.html>

[27]. Rogowski transducers for measuring large magnitude short duration pulses.

[28]. Exon Electrical Engineering Consultancy "Rogowski Coils and Current Transformers" Dr John Exon BSc PhD MIEE C Eng, online material.

- 
- [29]. HyperPhysics, <http://hyperphysics.phy-astr.gsu.edu/hbase/hframe.html>
- [30]. An alternative low-cost current-sensing scheme for high-current power electronics circuits, Arthur Radun. IEEE 1995
- [31]. Mercotac, application information sheet.
- [32]. A method of lowering bearing current with embedded circular comb-like coil, Jun-seok Kim, IEEE 2000
- [33]. Using Rogowski coils for transient current measurements, D.A.Ward, Engineering Science and education Journal June 1993.
- [34]. S.Chen, T.A.Lipo and D.Fitzgerald "Source of induction motor bearing currents caused by PWM inverters", IEEE transaction on energy conversion, Volume: 11, No.1, March-1996.
- [35]. A. Muetze, A. Binder, H. Vogel and J. Hering "Experimental evaluation of the endangerment of ball bearings due to inverter-induced bearing currents".
- [36]. M. J. Costello, "Shaft Voltages and Rotating Machinery", Industry Applications, IEEE Transactions on, Volume: 29 Issue: 2, March-April 1993, pp: 419 –426.
- [37]. "Shaft currents and grounding brush applications in rotating machinery". Panel session, presented at the Oct. 1986, Joint Power Conference, Portland, Oregon.
- [38]. D. Macdonald and W. Gray, "A practical guide to understanding bearing damage related to PWM drives", Pulp and Paper Industry Technical Conference, 1998, Conference Record of 1998 Annual, 21-26 June 1998, pp: 159 –165.
- [39]. V. Hausberg, H.O. Seinsch, "Kapazitive Lagerspannungen und Stroeme bei umrichtergespeisten induktionsmaschinen", Electrical engineering(82), pp153-162,2000
- [40]. Tektronix TDS544A user guide.
- [41]. IEEE motor reliability working group "Report on large motor reliability survey of industrial and commercial installations", IEEE trans. on Industry Application, vol.IA-21, No.4, July-august 1985, pp.853-872,1985

---

[42]. Doyle Busse, "Bearing Currents and Their Relationship to PWM Drives" Allen Bradley Drives Division, 1995 IEEE

[43]. Measurement of phase difference, measurement of current and voltage  
Lecture\_5\_XE38EMB-C.pdf

[44]. CWT specifications, CWT.PDF

---

## List of symbols

a	area
ASDs / VFD	Adjustable Speed Drive / Variable Frequency Drive
B	magnetic field
C	capacitance
C <sub>b</sub>	bearing capacitance
DA	dipole antenna
CMV	common mode voltage
C <sub>rf</sub>	rotor to frame capacitance
C <sub>s</sub>	shunt capacitance
C <sub>sf</sub>	stator to frame capacitance
C <sub>sr</sub>	stator to rotor capacitance
CWT1	Rogowski coil
D	diameter
d	original design dimension
D	scaled dimension
DIY	do it yourself
E	field intensity
EDM	Electric Discharge Machining
EMF	electromotive force or simply
f <sub>1</sub>	original design frequency
f <sub>2</sub>	scaled frequency (frequency of intended operation)
<i>f<sub>b</sub></i>	coil bandwidth
FF	Fast Frame
FFT	Fast Furier transformation
<i>f<sub>h</sub></i>	high frequency at -3dB
<i>f<sub>l</sub></i>	low frequency at -3dB
<i>f<sub>res</sub></i>	resonance frequency
GTO	gate-turn-off thyristor
H	coil sensitivity (Vs/A)
I	current
IGBT	Insulated gate bipolar transistor
l	coil length
L	inductance
M	mutual inductance
MSV	motor shaft voltage
MSV	motor shaft voltage
DA	dipole antenna
PET	polyetilen
PWM	Pulse wave modulation

---

Q	quality factor
R	resistance
$R_d$	Damping resistance
RFID	Radio frequency identification tag
$R_{par}$	parallel resistance
s	side length
S	surface area of the coil
T	number of turns
$U_{bd}$	breakdown voltage
$U_{in}$	input voltage
$U_{out}$	output voltage
$V_{th}$	threshold voltage
$V_u, V_v, U_w$	phase voltages
$Z_0$	Characteristic coil impedance
$Z_b$	bearing impedance
$Z_{cable}$	coaxial cable characteristic impedance
$\epsilon_0$	permittivity
$\epsilon_r$	relative permittivity
$\lambda$	wavelength
$\pi$	constant 3.141528
$\Psi$	magnetic flux through each turn
$\omega_A$	low frequency bandwidth
$\omega_B$	upper frequency bandwidth